Investigating the Role of Cellular Polarity in the Causation of Superior Coloboma

by

Melissa Wilson

A thesis submitted in partial fulfillment of the requirements for the degree of

Master of Science

in

Molecular Biology and Genetics

Department of Biological Sciences

University of Alberta

© Melissa Wilson, 2020

Abstract

Ocular coloboma is a congenital disorder that presents as an ocular malformation in the inferior aspect of the eye and may result in blindness. Recently, our lab characterized a novel disorder, superior coloboma, which presents as a coloboma affecting the superior portion of the eye. We discovered a transient groove in the superior eye during development, termed the superior ocular sulcus (SOS), and hypothesized that superior coloboma results from failed closure of the SOS. Research in our lab has focused on identifying genetic factors that regulate closure of the SOS. We performed whole exome sequencing on five superior coloboma patients to identify potentially disease causing variants that result in failed SOS closure. After analysing variant data, several variants were found in genes involved in planar cell polarity (PCP). Through the course of the current project, evidence was collected to support the hypothesis that PCP is required during eye development to ensure proper timing of SOS closure. Through MO knockdown of the PCP core components, *scrib* and *vangl2*, and use of fish carrying a loss of function *vangl2* allele, significant SOS closure delays were observed in zebrafish embryos. The Wnt receptor, Fzd4, was also investigated through MO knockdown and morphant embryos were not found to have SOS closure delays, suggesting that Fzd4 does not regulate PCP during eye development. Likewise, the apicobasal component, Shroom3, was investigated in regulation of SOS closure but no significant closure delays were observed in morphant embryos. To investigate the mechanism of PCP-related SOS closure defects, GFP-tagged Prickle was used to indicate planar polarization in live and fixed embryos, with the intent of determining if and when cells within the eye field, optic vesicle and optic cup are planar polarized. While initial results of this experiment are

promising, further testing is necessary to determine the dynamics of planar polarization in ocular development. Overall, the research outlined in this work provides a foundation for future studies investigating the role of cellular polarity in ocular development and causation of superior coloboma.

Preface

This thesis is an original work by Melissa M. Wilson. The study, of which this thesis is a part, has received research ethics approval from the University of Alberta Animal Policy and Welfare Committee. The author has met the Canadian Council on Animal Care mandatory training requirements for animal users on the Care and Use of Animals in Research, Teaching, and Testing. The protocols used in this study were approved by the University of Alberta's Animal Care and Use Committee.

A version of Chapter 4 was published:

Yoon K, Widen S, Wilson M, Hocking JC, Waskiewicz AJ. 2019. Visualization of the Superior Ocular Sulcus during *Danio rerio* Embryogenesis. Journal of Visualized Experiments 145: e59259. doi:10.3791/59259

In this work, I wrote the protocol for synthesis and injection of GFP-caax mRNA, provided GFP-caax mRNA for embryo injection, optimized the laminin immunostaining protocol, and provided edits towards the final manuscript.

Acknowledgment

I would like to express my gratitude to my supervisor, Dr. Andrew Waskiewicz, for providing me with this opportunity through which I experienced tremendous personal growth. I would like to further thank Dr. Waskiewicz and my committee members, Drs. Jennifer Hocking and Heather McDermid, for their guidance and support throughout the completion of this work.

I am grateful for sharing this experience with the members of the Waskiewicz lab, Dr. Sonya Widen, Kevin Yoon, Kacey Mackowetzky, Renee Dicipulo, Jens Herzog, and Sabrina Fox who were instrumental in the completion of this degree. Special thanks are given to my friend Matthew Arkinstall, who has been by my side since undergrad and spent many late nights keeping me motivated while writing this thesis.

Finally, I would to thank my family and friends who have encouraged me through life and the completion of this degree. I could not have finished without them.

Table of Contents

List of Tables

List of Figures

Glossary of Terms

AB	Apicobasal
Alcam	Activated leukocyte cell adhesion molecule
aldh1a2	*aldehyde dehydrogenase 1a2*
AP	Anterior/posterior
ASD	Apx/shroom domain
ATF2	Cyclic AMP-dependent transcription factor
AV	Animal/vegetal
bambi	*BMP and activin membrane-bound inhibitor homologue*
BCIP	5-bromo-4-chloro-3-indolyl phosphate
BME	β-mercaptoethanol
BMP	Bone morphogenic protein
BMPR1A	*Bone Morphogenic Protein Receptor 1A*
BSA	Bovine serum albumin
CE	Convergent extension
CELSR	*Cadherin EGF LAG seven-pass G-type receptor*
CNS	Central nervous system
CRD	Cysteine-rich domain
CYP1B1	*Cytochrome P450, Family 1, Subfamily B, Polypeptide 1*
Daam	Dishevelled-associated activator of morphogenesis
DEPC	Diethyl pyrocarbonate
DIC	Differential interference contrast
DIG	Digoxigenin
dlg	*discs large*
dpf	Days post-fertilization
Dpp	Decapentaplegic
dRok	*Drosophila* rho-associated kinase
DRV	Dorsal radial vessel

ds	*dachsous*
dsh	*Dishevelled*
DV	Dorsal/ventral
EAF2	*RNA polymerase II elongation factor-associated factor 2*
Eph	Erythropoietin-producing human hepatocellular receptors
Ephrin	Eph receptor-interacting protein
EC	Endothelial cells
ExAC	Exome Aggregation Consortium
F-actin	Filamentous actin
FEVR	Familial exudative vitreoretinopathy
FGF	Fibroblast growth factor
fj	*four-jointed*
fmi	*flamingo*
ft	*fat*
fz	*frizzled*
fzd4	*frizzled class receptor 4*
Gdf6a	Growth differentiation factor 6a
GEF	Guanine nucleotide exchange factor
hpf	Hours post-fertilization
IHC	Immunohistochemistry
JNK	c-Jun N-terminal kinase
Lgl	*Lethal giant larvae*
LRP6	Low density lipoprotein receptor-related protein 6
LRR	Leucine-rich repeat
MAC	Microphthalmia, anophthalmia and coloboma
MAPK	Mitogen activate protein kinase
mitf	*melanocyte inducing transcription factor*
MO	Morpholino oligonucleotide
MT	Microtubule

NBT	Nitro-blue tetrazolium chloride
Nlcam	Neurolin-like cell adhesion molecule
NRV	Nasal radial vessel
Otx2	*Orthodenticle homeobox 2*
Pard	Partition defective homologue
Pax6	*Paired box 6*
PBST	Phosphate-buffered saline+0.1% Tween-20
PCP	Planar cell polarity
PD	Proximal/distal
PFA	Paraformaldehyde
pk	*prickle*
PTU	Phenylthiourea
RA	Retinoic acid
Rax/rx	*Retinal homeobox*
RBC	Red blood cells
RhoA	Ras-homologue family member A
Rock	Rho-associated kinase
ROR2	Retinoic acid-related orphan receptor 2
RPE	Retinal pigmented epithelium
SNV	Single nucleotide variant
scrib	*scribble planar cell polarity protein*
Shh	Sonic hedgehog
Sift	Sorting intolerant from tolerant
SOS	Superior ocular sulcus
ss	Somite stage
SSC	Saline-sodium citrate buffer
stan	*starry night*
tbx5a	*T-box transcription factor 5a*
Vang	*Van gogh*

vangl2	*van gogh-like 2*
WES	Whole exome sequencing
wg	*wingless*
Wnt	Wingless (vertebrate)
WT	Wildtype

Chapter 1: Introduction

1.1 Vertebrate Eye Development

1.1.1 Early eye development

Eye development begins during late gastrulation, when a group of cells in the forebrain located between the telencephalon and diencephalon differentiates into retinal precursor cells called the eye field. This specification occurs through the regulation of eye-specific transcription factors that endow the eye field cells with a retinal precursor identity. These factors were elucidated by Zuber et al. (2003) through investigating *Xenopus* eye development. Epistasis experiments show that *Orthodenticle homeobox 2* (*Otx2*) expression is required to inhibit Noggin signalling that represses eye field specification (Zuber et al. 2003). Otx2 also initiates expression of the core eye-specification genes, *Retinal homeobox* (*Rax*; *rx*) and *Paired box 6* (*Pax6*), and mutations in human *OTX2* are associated with bilateral anophthalmia due to failure to initiate eye specification (Deml et al. 2016). Zebrafish *rx3* mutants present with anophthalmia due to failure to specify retinal precursor cells (Loosli et al. 2003). These *rx3* mutant embryos do not show expression of *pax6a*, indicating that Rx3 regulates *pax6a* expression. Loss of *Pax6* in *Xenopus* embryos causes subtle changes in *Rx* expression, indicating a feedback mechanism between these genes (Chow et al. 1999). As with Rax, Pax6 is required for eye formation, and in *Xenopus*, overexpression of *Pax6* is sufficient for ectopic eye formation (Chow et al. 1999). The *Pax6* function of regulating eye development is conserved in *Planaria*, *Drosophila* and vertebrate models, and *Pax6* has sequence and functional conservation with the ancestral *Cnidarian PaxB*, indicating an evolutionarily conserved mechanism of eye induction (reviewed in Kozmik 2005). Pax6 regulates further expression of eye field-specific genes, such as *Sineoculis homeobox homolog 3* and *Lin11/Isl1/Mec3 homeobox 2*. Expression of *Pax6* and downstream targets differentiates the anterior neural plate cells into retinal precursors and maintains boundaries between the eye field and surrounding telencephalon/diencephalon cells. Once cells gain eye field identity, this patch of neural cells is maintained through intercellular binding of erythropoietin-producing human hepatocellular receptors (Eph) by Eph receptor-interacting protein (Ephrin) (Cavodeassi et al. 2013). Eph/Ephrin binding creates cohesion and repulsion interactions at the boundary between the eye field and surrounding forebrain tissue. In

zebrafish, Rx3 initiates expression of Ephrin genes in the eye field and inhibits expression of Eph genes, so that intercellular Eph-Ephrin binding at the margins of the eye field prevent intermixing (Cavodeassi et al. 2013).

After eye field specification in zebrafish, each side of the eye field migrates laterally away from the midline. Cells at the edge of the eye field gain apicobasal (AB) polarity and elongate to initiate evagination and formation of the optic vesicle, with core eye field cells filling in behind while maintaining mesenchymal morphology (Ivanovitch et al. 2013). These core cells eventually elongate and intercalate with marginal cells at the leading edge of the forming optic vesicle. Differences in cell adhesion between the eye-field cells and the surrounding tissue are thought to aid in the lateral eye field movement. Rx3 inhibits expression of *neurolin-like cell adhesion molecule* (*Nlcam*) in the zebrafish eye field (Brown et al. 2010). This downregulation of adhesion prevents the eye field cells from participating in convergent extension (CE) movements, while the surrounding tissue converges rapidly on the midline. If *rx3* is disrupted, Nlcam in the eye field results in eye field cells converging towards the midline with the surrounding forebrain tissue and causes microphthalmia (Brown et al. 2010). The lateral movement of the retinal precursors may also result from the prechordal plate, which is placed at the ventral midline and migrates in an anterior direction. This forward movement is hypothesized to displace eye field cells to either side of the midline (Woo and Fraser 1995). The lateral movement of eye field requires intricate and coordinated migration of retinal progenitor cells, which was characterized through cell tracking experiments (Rembold 2006). As the surrounding neural plate converges toward the midline, the bulk of the eye field does not participate. However, retinal progenitors at the lateral edges of the eye field migrate dorsally and medially, folding over the eye field. Then, coordinated lateral migration of the eye field results in evagination to form the optic vesicle, which will migrate laterally until coming in contact with the overlying ectoderm. Signalling from the optic vesicle induces lens placode formation in the ectoderm (Huang et al. 2011). Cells of the lens placode apically constrict and lens-facing cells of the optic vesicle constrict basally, causing invagination and formation of the optic cup and lens vesicle (Huang et al. 2011). Formation of the zebrafish optic cup relies on further coordinated cellular movements, with

retinal progenitor cells on the lens-apposing side of the optic cup migrating around the nasal and temporal sides of the cup, increasing the surface area on the lens facing side of the optic cup (Heermann et al. 2015). The lens-facing layer of the optic cup will further develop to form the neural retina while the outer layer of the optic cup will form the retinal pigmented epithelium (RPE). The optic stalk will eventually house vasculature and axons from the retinal neurons and form the optic nerve.

Tissue patterning is a crucial part of eye development as it controls differentiation of ocular structures to ensure proper formation of the eye. Patterning includes signalling through the bone morphogenic protein (BMP), sonic hedgehog (Shh) and Wingless (Wnt) signalling pathways. These pathways ensure expression of transcription factors that regulate tissue specific gene expression. For example, patterning is necessary to ensure proper differentiation of retinal precursors into either the neural retina or the RPE. Specification of the RPE begins as the optic vesicle comes in contact with the overlaying epithelium. In mice, the optic vesicle has ubiquitous expression of *melanocyte inducing transcription factor* (*Mitf*), but fibroblast growth factor (FGF) signalling from the epithelium inhibits *Mitf* in the distal optic vesicle so that its expression is restricted to the presumptive RPE cells (Nguyen and Arnheiter 2000). Additionally, canonical Wnt signalling in the dorsal RPE maintains expression of *Mitf* and *Optx*, and loss of this signalling in mice disrupts formation of RPE, resulting in a thickening of the tissue and ocular malformation (Fujimura et al. 2009). Expression of *Mitf* and *Optx* increases in the RPE as the optic cup forms, controlling further differentiation and pigmentation.

Dorsal/ventral (DV) patterning of the optic vesicle begins around 12 hours post-fertilization (hpf) in zebrafish, establishing identities prior to evagination and optic cup formation. At this time, the diencephalon at the ventral midline of the embryos induces ventral identity in the optic vesicle through Shh signalling and promotes expression of the transcription factor *vax2* (Take-uchi et al. 2003). Growth differentiation factor 6a (Gdf6a) initiates dorsal identity through phosphorylation of Smad1/5/8 that upregulate expression of dorsal marker genes such as *bmp4*, T-*box transcription factor 5a* (*tbx5a*), *aldehyde dehydrogenase 1a2* (*aldh1a2*), and *BMP and activin membrane-bound inhibitor homologue*

(*bambi*) (French et al. 2009). Bmp2b appears to mediate Gdf6a-regulated dorsal expression as *bmp2b* zebrafish embryos have little or no expression of the dorsal marker genes, but have normal *gdf6a* expression (Kruse-Bend et al. 2012). Canonical Wnt signalling from the presumptive dorsal RPE regulates *bmp4* and *tbx5* expression in the early optic cup to maintain dorsal identity after initiation by Gdf6a (Veien et al. 2008). Mice with conditional knockout of *Shh* have increased expression of *Tbx5* that extends into the ventral dorsal cup (Zhao et al. 2010), while *vax2* expression domains are expanded dorsally in *gdf6a*$^{-/-}$ zebrafish embryos (French et al. 2009), indicating that antagonistic interactions between dorsal and ventral markers maintains regional identity in the optic cup.

As the optic cup forms, vascularization of the eye begins. The ocular vasculature arises from mesenchyme cells surrounding the developing eye, through the process of vasculogenesis, where mesodermal cells differentiate into endothelial progenitors and aggregate to form blood vessels (Saint-Geniez and D'Amore 2004). Vascularization progresses through angiogenesis, where new blood vessels form by branching off existing vasculature (Kaufman et al. 2015; Kolte et al. 2016). The eye has three main blood supplies - the choroidal, hyaloid, and superficial vasculature. The choroidal vasculature forms a network of blood vessels around the back of the eye, providing blood to the retina, RPE, and optic nerve. Mice that express dominant negative FGF receptor in the RPE have reduced choroidal vascularization indicating that choroidal vasculature depends on FGF signalling in the RPE to produce angiogenic signals (Rousseau et al. 2003). The hyaloid vasculature enters the ventral portion of the optic cup and forms vessel networks around the lens. This network serves to vascularize the developing eye, but eventually regresses as sufficient blood supply is obtained from the other ocular vasculatures. The mechanism of hyaloid regression is unclear, but hyaloid vessels do not regress in the mouse model that expresses a dominant negative FGF receptor in the RPE (Rousseau et al. 2003). This study indicates that FGF signalling from the RPE is responsible for inducing hyaloid regression, and indicates a system of redundancy that ensures vascularization of the eye in the case of defective choroidal vasculature. The superficial vasculature forms over the dorsal/superior portion of the optic cup, forming two vessels, the dorsal radial vessel (DRV) and the nasal radial vessel

(NRV) and wrapping around the lens (Kaufman et al. 2015). Additional vascularization occurs in the retina if the eye is large enough that diffusion from the RPE is not sufficient. As tissue become hypoxic, the cells secrete vascular endothelial growth factor that acts as an attractant for endothelial cells and can induce endothelial differentiation. Through this mechanism, blood vessels form in the retina as it develops beyond the means of the choroidal vasculature (Stone et al. 1995).

1.1.2 Ocular coloboma

Failure at any point in eye development can cause congenital ocular malformations. MAC (microphthalmia, anophthalmia and coloboma) comprises a set of related ocular malformations that are major contributors to childhood blindness. A 1996 global survey of children with congenital ocular abnormalities identified that MAC contributes to 14.3% of blinding malformations (Hornby et al. 2000). Pedigree analyses of families with MAC disorders have identified mutations in different genes involved in eye development, such as *OTX2*, *PAX6*, and *RAX*, indicating a large genetic component to these disorders (Williamson and FitzPatrick 2014). However, incidence of these ocular malformations increases with environmental stressors, such a pesticide exposure, illness and drug use (Hornby et al. 2002). Vitamin A deficiency during early pregnancy correlates with an increase in MAC, resulting in higher rates of MAC in regions that rely on a rice-based diet low in vitamin A, such as Sri Lanka and India (Hornby et al. 2000). However, in India, 43% of cases of MAC coincide with consanguinity in parental or grandparental generations (Hornby et al. 2002), so it is unclear whether the increased incidence of MAC in these regions is due to environment, fixation of deleterious mutations, or a combination of both.

Of particular interest to our lab is ocular coloboma, which is the most common of the MAC disorders (Shah et al. 2011). Coloboma presents as a gap in the inferior ocular tissue, and can affect any layer of the eye, including the cornea, iris, lens, retina, and optic stalk. As the malformations associated with coloboma range in presentation, they also range in severity and can have little effect on vision or can be completely blinding. Ocular coloboma is caused by incomplete closure of the choroid fissure. Invagination of the optic vesicle coincides with formation of a fissure along the ventral optic cup and optic stalk. This fissure, termed the

choroid fissure, guides the hyaloid vasculature into the forming eye and guides retinal ganglion cell axons out of the eye towards the brain. The choroid fissure remains open in zebrafish from 20 to 60 hpf, and after the hyaloid vasculature and the optic nerve have grown through the choroid fissure, the lobes of the fissure will fuse at the midpoint and move distally and proximally to close the entire fissure. Closure of the choroid fissure is complex and requires proper ocular patterning, signalling from adjacent cell populations, apoptosis, degradation of the extracellular matrix and fusion of the optic cup tissue lining the fissure (James et al. 2016; Cao et al. 2018).

1.1.3 Superior coloboma

Recently in our lab, with the help of collaborators, we identified five local patients with an abnormal presentation of coloboma. These patients showed coloboma-like malformations in the superior portion of the eye. Examination of these abnormal coloboma patients led to the hypothesis that there is a structure in the superior optic cup homologous to the choroid fissure, and failed closure of this structure causes this abnormal coloboma, termed "superior coloboma". Although this paper is the first to argue that superior coloboma is a distinct congenital disorder, there are several mentions of abnormal coloboma affecting the superior aspect of the eye in the literature. The first report of an atypical coloboma was in 1927, when Mann and Ross describe a macular coloboma in the superior-temporal retina. However, it is unclear if this is a case of coloboma or optic disc duplication as these conditions can have a similar appearance, as discussed in Islam et al. (2005). An infant with coloboma of the superior-nasal iris, along with various other congenital ocular defects, is described in Villarroel et al. (2008), and the disorder is linked to a missense mutation in *PAX6*. Further examples in the literature include a superior-nasal lens coloboma (Jethani et al. 2009), ten related patients that all have superior-nasal or superior-temporal iris coloboma, with one family member presenting bilateral superior-nasal iris coloboma (Abouzeid et al. 2009), and more recently a case of superior coloboma affecting the lens and retina (Jain et al. 2018).

To explore the hypothesis that superior coloboma is derived from failed closure of an unknown fissure in the superior eye during embryogenesis, our lab and collaborators

examined eye development of zebrafish, chick, mouse, and newt, and found an evolutionarily conserved developmental feature in the dorsal eye, termed the superior ocular sulcus (SOS) (Hocking et al. 2018). This feature appears as a well-defined groove in the dorsal optic cup shortly after evagination of the optic vesicle. The SOS is transient, closing soon after formation. As it was hypothesized that this feature is homologous in function to the choroid fissure, our lab investigated whether the SOS also acts to guide vascularization of the optic cup. The dorsal radial vessel of the superficial vasculature was found to migrate through the SOS and changes to sulcus morphology result in misguided or incomplete vascularization of the eye (Hocking et al. 2018). Therefore, the SOS has the important function of guiding vasculature over the top of the eye.

To explore the mechanisms that regulate morphogenesis of the SOS, and to identify the causation of superior coloboma, Hocking et al. (2018) performed whole exome sequencing (WES) of the five superior coloboma patients. The sequencing data was refined through *in silico* analysis to identify nonsynonymous rare mutations that are likely deleterious. This analysis included testing of variants through MutationTaster, Polyphen-2, and Sorting Intolerant from Tolerant (Sift) algorithms. This analysis resulted in a data set that our lab has used to form hypotheses about molecular mechanisms involved in closure of the SOS. Two variants in genes involved in cell signalling were identified in patient #2, including a mutation in *Cytochrome P450, Family 1, Subfamily B, Polypeptide 1* (*CYP1B1*), which is involved in retinoic acid (RA) signalling, and a mutation in *Bone Morphogenic Protein Receptor 1A* (*BMPR1A*), which in involved in BMP signalling. Investigations of *cyp1b1*$^{-/-}$ zebrafish showed no disturbance of SOS closure, indicating that RA signalling is not involved in this process. However, Hocking et al. show that BMP signalling is necessary for SOS closure. Zebrafish mutants that have loss of BMP signalling in the dorsal eye have disrupted SOS closure and show a low penetrance of superior coloboma in *gdf6a*$^{-/-}$ adults. As discussed above, balance between dorsal BMP signalling and ventral Shh signalling maintains optic cup regional identity, and it appears that loss of BMP and subsequent ventralization of the optic cup disrupt events that lead to SOS closure. However, the downstream targets of BMP signalling that allow for closure of the SOS are unknown and

are a current subject of research in our lab. Another superior coloboma patient also presents with tuberous sclerosis and has a corresponding deleterious mutation in *TSC2*, and the role of mTor signalling in SOS morphogenesis is also being investigated in our lab.

1.2 Cellular Polarity

Cellular polarity refers to the organization of cellular components so that a cell has distinct intracellular domains capable of specialized behaviours. Cellular polarity is particularly important during embryogenesis when cells must participate in complex morphogenic events. Organogenesis requires that cells migrate and contribute to collective cell movements. To do so, cells must have a uniform directionality. For a tissue to properly develop, the cells within the tissue must have a sense of direction, which is directed by cellular polarization. A well characterized form of cell polarity is AB polarity, in which a cell gains different composition in the tissue-apposing (apical) and tissue-facing (basal) intracellular domains (reviewed in Karner et al. 2006) (**Figure 1.3**). The vertebrate AB polarity system is established through opposing antagonistic interactions: the apical polarity complex, composed of Cdc42, Partition defective homologue 6 (Pard6), Pard3, and Atypical protein kinase C, antagonizes the activity of the basal polarity complex, composed of Scribble, Lethal giant larvae (Lgl), and Disks large (Dlg), which in turn antagonizes the apical polarity complex (Tanentzapf and Tepass 2003). These polarity complexes are separated by two scaffolding complexes, the adherens junction and tight junction, which mediate cell-cell adhesion. AB polarity allows for specialized cellular behaviour and proper orientation of cellular structures.

Similar to polarization along the AB axis, cells can be polarized along the axis of the tissue or within the plane orthogonal to the AB axis. This polarity, termed planar cell polarity (PCP), confers a sense of “front” and “back” to the cell through the subcellular asymmetric localization of core PCP proteins to either the anterior or posterior side of the cell. PCP is achieved through a noncanonical branch of the Wnt signalling pathway. Both canonical and noncanonical Wnt pathways have similar induction through Wnt ligand binding of Frizzled receptors, but diverge through separate intracellular cascades.

1.2.1 Drosophila studies of PCP

PCP was first characterized in the invertebrate model, *Drosophila*. Mutagenesis screens produced a series of flies with striking phenotypes; the bodies and wings of these flies are covered in bristles and hairs that are oriented in the same direction, and PCP defects disrupt this orientation causing the projections to form novel swirling patterns or to be oriented in random directions (Gubb and Garcia-Bellido 1982). PCP is also required for ommatidia rotation during eye development, so these mutants had obvious ocular phenotypes (Jenny 2010). These surface structures and the eye are easily examined for polarity phenotypes, making *Drosophila* an ideal model for inquiry into the PCP pathway. As such, the model of PCP is largely based on studies using the invertebrate model, *Drosophila*.

Using flies, the core components of the PCP pathway were discovered by examining mutants with loss of planar polarity phenotypes. Gubb and Garcia-Bellido (1982) described phenotypes of *frizzled* (*fz*) and *prickle* (*pk*) mutants, with both showing changes to bristle orientation on the wings. In mosaic flies, cells lacking *fz* disrupt PCP in distally neighboring cells, indicating that Fz acts in a non-cell autonomous fashion and indicating that Fz is involved in a unidirectional intercellular signalling mechanism (Gubb and Garcia-Bellido 1982). Theisen et al. (1994) characterized *dishevelled* (*dsh*) mutant flies, which were also found to have PCP defects and mosaic analysis showed a cell-autonomous pattern of polarity defects. This study also implicated the *wingless* (*wg*) morphogen in PCP, with some *wg* mutants having misoriented bristles. Previously, *wg* and *dsh* were only known to act in the *wingless* pathway that controls segmental patterning, and this study linked the Wingless and PCP pathways for the first time. However, the involvement of wg in *Drosophila* PCP is controversial as it is unclear whether the wg morphogen is required for initiating PCP. The gene *Van gogh* (*Vang)* was identified as a PCP related gene due to similar phenotypes to other PCP mutant flies. Vang was further determined to interact with previously discovered PCP components through crossing dominant *Vang* heterozygotes to *fz* and *pk* mutants and observing increased severity of PCP phenotypes (Taylor et al. 1998). As with the previous genes, *flamingo* (*fmi*, also known as *starry night, stan*; *Celsr* in vertebrates) was identified as a PCP gene by mutant phenotype. Interestingly, intracellular localization of Fmi protein

formed a zig-zag pattern along the proximal/distal (PD) edges of hexagonal cells in the *Drosophila* epidermis, indicating that the protein is localized to either one or both of the proximal or distal, but not the lateral, membrane (Usui et al. 1999). This finding of PD localization was not isolated to Fmi but was found in other PCP core components, including Fzd and Vang. The large cytoplasmic protein Scribble (Scrib) was first identified as part of AB polarity in conjunction with *lgl* and *dlg* (Bilder et al. 2000). However, Scrib was found to bind to Vang through one of its PDZ domains, linking Scrib to both AB polarity and PCP (Kallay et al. 2006). Several other genes have been implicated in *Drosophila* PCP, including *fuzzy*, *inturned*, and *multiple wing hair* amongst others. However, orthologues have not been identified in vertebrate PCP, so these genes will not be discussed here.

1.2.2 A model for establishment and regulation of PCP

The mechanism of how cells become planar polarized and how that signal is communicated uniformly across a tissue is not completely known, but a model has been formed from molecular studies along with theoretical modelling. Much that is known about PCP is derived from studies using invertebrate models, however general PCP will be discussed in terms of vertebrate genes and proteins for the purposes of this review. Planar polarization requires 1) induction through an extracellular signal; 2) intracellular segregation of polarity proteins to amplify the initial polarization signal; 3) formation of molecular bridges between neighboring cells to amplify and fortify polarity; and 4) downstream activation of signalling cascades that regulate cellular behaviour.

PCP is set up initially through signalling by Wnt ligands that bind Fzd receptors and initiate a pathway resulting in intracellular polarization of PCP complexes (**Figure 1.1**). Wnt proteins are cysteine-rich secreted morphogens that create a concentration gradient through a tissue and have a multitude of roles in animal development (Kikuchi et al. 2007). There are at least nineteen mammalian Wnts, which bind promiscuously to at least ten Fzds, making for complicated ligand-receptor interactions and diversifying the downstream effects of Wnt-Fzd binding. The non-canonical Wnts include Wnt5a and Wnt11, although Wnt ligands can have roles in both canonical and non-canonical signalling depending on the spatial and temporal context, as well as the receptor that Wnt is binding. For example, Wnt6 acts through

the non-canonical pathway to produce neural crest in chicks, as shown by expression of the downstream PCP components Ras-homologue family member A (RhoA) and c-Jun N-terminal kinase (JNK), and an absence of nuclear localization of activated β-catenin (Schmidt et al. 2007). Conversely, Wnt6 regulates heart size during *Xenopus* organogenesis through the canonical pathway (Lavery et al. 2008). The same can be said of Fzd receptors, where binding of Fzd can activate either the canonical or non-canonical pathway, also dependent on spatial and temporal context and which Wnt is binding the receptor.

Initiation of non-canonical Wnt signalling polarizes the cell so that subsets of proteins become localized to the opposite membrane, with Fzd/Dvl localized to the posterior membrane, and Vangl/Pk localized to the anterior membrane (**Figure 1.2**). This polarization is in part set up through extracellular gradients of Wnt. How Wnt signalling initiates planar polarization is not completely understood, but several hypotheses have been proposed. In mouse limb development, Wnt5a has been shown to regulate PCP through binding of the receptor tyrosine kinase, retinoic acid receptor-related orphan receptor 2 (ROR2), and subsequent phosphorylation of Vangl2 (Gao et al. 2011). Studies of *C. elegans* vulva development show that this mechanism is evolutionarily conserved, as the ROR tyrosine kinase, cell adhesion molecule-1, has been shown to interact with Vangl to initate PCP (Green et al. 2008). Vangl2 phosphorylation has been well established as being necessary for establishment of PCP, with mutations affecting *VANGL2* phosphorylation causing neural tube defects in human fetuses (Lei et al. 2010) and mutations affecting the ability of WNT5A and ROR2 to phosphorylate VANGL2 causing skeletal dysplasia due to embryonic elongation defects (Person et al. 2010). However, the mechanism of how this phosphorylation directs planar polarization is unknown. It is possible that Vangl2 must be phosphorylated to participate in the formation of molecular bridges. Wnt-directed Vangl2 activation and subsequent molecular bridging would increase Vangl2 on the cell edge proximal to the Wnt expression domain, initiating polarization of Vangl/Pk and Fzd/Dsh complexes. This polarization would be amplified by inhibitory interactions between Vangl and Fzd, biasing Fzd to localize on the opposite membrane. Vangl2 phosphorylation may also be required for

downstream signalling resulting in PCP-generated cellular behaviours, though this mechanism does not explain loss of intracellular polarization in *Vangl2* mutants.

Through *Drosophila* wing experiments, Wu et al. (2013) suggest that Wnt sets up PCP by competing with Vangl for extracellular binding of Fzd, and thus Wnt binding inhibits Fzd-Vangl interactions. This competitive inhibition would initiate polarization by preventing Fzd on the anterior membrane from forming molecular bridges. It is thought that Fzd is trafficked to the anterior membrane and, no longer bound to Wnt, it can form molecular bridges on the posterior membrane. There is evidence that Wnt binding Fzd initiates endocytosis of the ligand/receptor pair in both *Drosophila* and mammals, including mammalian endocytosis involving non-canonical Wnt5a (Strigini and Cohen 2000; Chen et al. 2003; Yamamoto et al. 2006). Mammalian endocytosis of the ligand/receptor pair is clathrin-dependent, and involves a mechanism in which Wnt binding Fzd phosphorylates Dvl through PKC, and the activated Dvl protein mediates clathrin-dependent uptake (Yamamoto et al. 2006). Ligand/receptor uptake is important for regulating Wnt-signalling because it prevents continual signalling through the receptor and modulates extracellular concentrations of the morphogen. Further, uptake of Fzd mediates intracellular polarization through endocytic trafficking. In *Drosophila* wing cells, *fz* is observed to travel distally (corresponding to posterior trafficking in vertebrate cells) after onset of Wg signalling, mediated by microtubules (MT) oriented in the proximal-distal direction, with MT positive ends pointing distally (Shimada et al. 2006).

After initiation of polarization through binding of the Wnt ligand, core PCP components reorganize in the cell to impart intracellular polarization. Both the Vangl/Pk and Fzd/Dvl PCP complexes interact with Celsr at the anterior and posterior membranes, respectively, and form intercellular connections through the formation of molecular bridges (Usui et al. 1999) (**Figure 1.2**). The molecular bridge forms from homophilic binding of Celsr on apposing membranes. The role of Vangl and Fzd in molecular bridge formation is unclear, but it is proposed that either the extracellular portions of the two proteins interact or that their binding to Celsr changes its conformation to allow for Celsr:Celsr binding. It appears that differential affinities of Celsr for Fzd and Vangl lends to intracellular feedback

that strengthens the initial polarization of Wnt signalling (Strutt and Strutt 2008). The mechanism behind this is unclear, but when considering the available pools of Fzd and Vangl, a possible mechanism is proposed. Preferential formation of Celsr:Fzd, and then endocytic trafficking to the posterior membrane would deplete Fzd at the anterior membrane. After Fzd is depleted, remaining Celsr would be able to bind Vangl, then participate in formation of molecular bridges on the anterior membrane. This mechanism is plausible if Celsr is only trafficked when bound to Fzd. The requirement of opposing Celsrs within a molecular bridge to be bound to Fzd on one side and Vangl on the other side locks Vangl/Pk and Fzd/Dvl in polarized positions. This intercellular complex coordinates polarization across a tissue and fortifies the polarization so that individual cells do not polarize incorrectly due to weak Wnt signals. Scribble is thought to act as an adapter protein, linking Vangl2 to other proteins to facilitate PCP signalling. As Scribble is shown to bind the secretory protein, Sec24b, a component of the coat protein complex II, it is thought that Scribble facilitates vesicular trafficking of Vangl2 (Wansleeben et al. 2010).

Fisher and Strutt (2019) produced a mathematical/computational model of how morphogen gradients establish planar polarization in systems similar to the core PCP module. Considering the morphogen gradient, the dosage of Wnt signalling may cause a whole cell response, affecting transcription or activation of PCP components. Alternatively, individual cells may be able to detect different Wnt concentrations at the cell edges proximal and distal to the origin of Wnt production, perhaps giving different levels of activated protein across the cell. When the morphogen gradient increases expression or activation of only one transmembrane component, without affecting the availability of the other component (either Fzd or Vangl), polarization is easily achieved. More activated Fzd is available in cells closer to the anterior Wnt signal, so Vangl accumulates on the membrane shared with the cell with more available Fzd. Celsr plays a role in the availability of Fzd as Celsr has a higher binding affinity for Fzd than Vangl. This means that when Fzd becomes activated by Wnt binding and is trafficked to the posterior membrane with Celsr, an increased amount of Fzd-bound Celsr is available for binding by Celsr-Vangl complexes on the posterior-neighboring cell.

1.2.3 Downstream effects of non-canonical Wnt signalling

After initiating planar polarization of cells and coordination of that polarity across a tissue, non-canonical Wnt signalling activates intercellular pathways that have non-transcriptional outcomes through Rho-GTPase regulation of the actin cytoskeleton or have transcriptional output through the JNK pathway (**Figure 1.1**). Activation of these downstream targets results in changes to cell shape and behaviour required for cellular functions, such as coordinate cell migration.

One output of PCP is changes to actomyosin networks through activation of Rho-GTPases, which act as molecular switches regulating activation of downstream effectors. Briefly, phosphorylation of Rho GTPases by guanine nucleotide exchange factors (GEF) allows activation of downstream effectors such as formin proteins that regulate polymerization of filamentous actin (F-actin), and Rho-associated kinase (Rock) and myosin II which causes contraction of the actin cytoskeleton when bound to two antiparallel F-actin strands. Involvement of PCP-regulated Rho-GTPase activity has been documented in both *Drosophila* and zebrafish studies. Winter et al. (2001) found that wing hair number and photoreceptor cell rearrangement leading to ommatidial rotation are reliant on PCP mediated activation of *Drosophila* Rock (dRok) by phosphorylated Rho. dRok was found to target the nonmuscle myosin II light chain to control actin dynamics. Genetic interaction between *fz*, *dsh*, and *drok* were characterized by Winter et al, but it was unknown how the signal is passed between Dsh and Rho. A yeast two hybrid screen identified Dishevelled-associated activator of morphogenesis (Daam) as a binding partner of Dvl (Habas et al. 2001). As Daam also binds RhoA as a GEF, and loss of Daam phenocopies PCP defects in *Xenopus*, it was determined that Daam confers non-canonical Wnt-derived activation from Dvl to Rho (**Figure 1.1**). In zebrafish, Rok2 controls cell elongation and orientation to drive CE during gastrulation in response to Wnt11 signalling (Marlow et al. 2002). As such, *rok2* mutant fish phenocopy other PCP mutants with elongation defects. Rac has been implicated in regulating actin cytoskeletal dynamics in neuronal axon guidance during *Drosophila* brain development (Gombos et al. 2015). Rac is thought to activate Daam, which is enriched in axonal growth cones, enabling axon migration. Directionality of cellular movements is attenuated by planar

polarization of cells. At the posterior membrane, the Fzd → Dvl → Daam pathway is active, but on the anterior membrane this pathway is inhibited in part by lower levels of Fzd, and also by sequestration of Dvl through binding by Vangl (Seo et al. 2017). This inhibition results in growth and contraction of F-actin in the posterior region of the cell to allow for proper cellular orientation, movement, and division.

Non-canonical Wnt signalling is known to activate the JNK pathway. Canonical JNK pathways work through a hierarchy of kinases (reviewed in Zeke et al. 2016), where a variety of inputs may activate the top tier kinases, known as mitogen activated protein 3 kinases (MAP3K), which in turn will phosphorylate the middle tier MAP2K. MAP2K then phosphorylate JNK which will pass the signal to activate transcription factors, like c-Jun, to achieve transcriptional output of the original cellular input. Several studies have indicated downstream activation of JNK signalling in response to non-canonical Wnt signalling. For example, non-canonical signalling by *Xenopus* Wnt5a activates JNK, and this activation was linked to regulation of gastrulation by expression of dominant-negative JNK that inhibits CE behaviours required for gastrulation (Yamanaka et al. 2002). Additionally, non-canonical Wnt signalling through Wnt7b activates JNK signalling through Dvl and Rac to regulate dendritic development in rat neurons (Rosso et al. 2005). This study indicated that dendritic development is regulated by JNK transcriptional control as Wnt7b signalling increases levels of phosphorylated c-Jun, but the transcriptional output is unknown. In fact, while non-canonical Wnt signalling is well established in its ability to active JNK signalling, little evidence exists as to the transcriptional targets of this pathway.

1.2.4 Planar cell polarity through the Fat/Dachsous pathway

A second polarity pathway, the Fat (ft)/Dachsous (ds) pathway, that works in parallel to the non-canonical Wnt pathways was characterized in *Drosophila* shortly after the components of PCP were found. *Fat* and *ds* encode large, atypical cadherins that were originally found to control cell proliferation and development of imaginal discs. Using transplant of imaginal wing discs from *fat* mutants, it was observed that extremely overgrown wings developed on the WT recipient flies due to misregulation of epithelial proliferation

(Bryant et al. 1988). The Ft and Ds cadherins regulate epithelial proliferation through the Hippo tumour suppression pathway (reviewed in Halder and Johnson 2011).

The Fat/Dachsous planar polarity pathway was discovered using a similar method of examining mutant flies with polarization defects. Mutants of *ft* and *ds* were found to have polarity defects resulting in disorganized patterning of bristles and ommatidia (Bryant et al. 1988; Adler et al. 1998). Another gene that acts in the Ft/Ds pathway is *four-jointed* (*fj*). Flies with deleterious *fj* mutations have PCP defects in wing and leg morphology, as well as mispolarized ommatidia (Zeidler et al. 1999). Fj is a transmembrane kinase that is localized to the golgi apparatus (Ishikawa et al. 2008). Like in the Fzd/Dvl pathway, or the "core" PCP pathway, Ft and Ds localize to opposite membranes, with Ft localized distally and Ds localized proximally in *Drosophila* cells (Matis and Axelrod 2013). As with Fzd and Vangl, Ft and Ds complex heterophilically across adjacent cells, forming molecular bridges that stabilize polarized localization of the cadherins. Four-jointed modulates polarity by phosphorylating the extracellular cadherin domains of Ft and Ds as they pass through the golgi network (Ishikawa et al. 2008). Phosphorylation of Ft increases its ability to bind Ds, but conversely, Ds phosphorylation inhibits its ability to bind Ft (Hale et al. 2015). Therefore, polarization is based on transcriptional levels of *fj*, as cells with higher levels of FJ-mediated Ft phosphorylation will have Ft localized towards the neighboring cell with a lower FJ activity and thus less phosphorylated Ds. There has been limited research on the Fat/Ds pathway in vertebrate models, but there is evidence of regulation of planar polarity through this pathway in mice. *Fat4* mutant mice have several PCP-related phenotypes including decreased migration of kidney ureteric buds, inner ear malformations with misaligned hair cells, and reduced DV axis elongation (Saburi et al. 2012). These defects show that *Fat4* is involved in PCP in mice and in several distinct developmental events, indicating that the Ft/Ds/Fj pathway is likely involved in PCP across vertebrates in various developmental contexts.

Whether the Ft/Ds/Fj pathway is respondent to a morphogen gradient is unclear. During *Drosophila* wing development, the BMP homologue Decapentaplegic (Dpp) appears to influence Ds polarization as Dpp transcriptional repression depolarizes intracellular Ds

polarization (Rogulja et al. 2008). Further, a constitutively active Dpp receptor elevates *fj* expression levels in *Drosophila* wing discs, confirming a regulatory role for Dpp in this polarity pathway. Dpp is expressed in cells along the anterior/posterior (AP) boundary of the wing imaginal disk and produces a morphogen gradient that is greatest at the wing midline and dissipates towards the wing edges. This agrees with the *ft* expression patterns where higher expression is found in the center of the wing disk and decreases toward wing edges. Interestingly, *ds* expression apposes expression of *ft*, with higher expression towards the edge of the wing disk. In the *Drosophila* eye disk *ft* and *ds* show similar opposing expression patterns, with *ft* expression at the equator of the eye disk, and *ds* expression at the poles (Yang et al. 2002). However, Wg appears to modulate the Ft/Ds/Fj pathway in the eye disk. *Wg* overexpressing cells in the eye disk result in ectopic *ds* expression, indicating that Wg regulates *ds*.

It was unclear whether these two polarity pathways are connected or work independently, and early epistasis studies in the *Drosophila* eye showed evidence for interplay between the pathways (Yang et al. 2002). Further experiments have failed to resolve the relationship between the two pathways. Casal et al. (2006) used flies with complete loss of *fz* and *fmi* that have no signalling through the non-canonical Wnt pathway to show that the Fat/Ds pathway is still functional, demonstrating that the Ft/Ds/Fj pathway is not reliant on the core PCP pathway. However, this study did not test whether the core PCP pathway is dependent on the Ft/Ds/Fj pathway.

The initial polarization of microtubules is thought to be set up through Fat/Dsh signalling (Matis et al. 2014). This link between the two PCP pathways suggests that they do not act independently, and pharmacological inhibition of microtubule formation disrupts wing hair orientation in *Drosophila*, indicating that microtubule orientation is essential to polarization of the epithelia. It is likely that there is significant interplay between the pathways even though each is sufficient to polarize a tissue independently. PCP is necessary for proper development of various systems and organs, however the establishment and regulation of PCP proves variable in different contexts. It is thus likely that the two pathways work redundantly to prevent failed development and work cooperatively in some systems.

1.2.5 Planar cell polarity in vertebrate development

Soon after core PCP genes were discovered in *Drosophila*, homologous genes were found in vertebrate models, and it was established that PCP is a conserved mechanism. PCP was found to regulate many developmental processes in vertebrates, and several PCP-loss of function models have been produced to study the role of PCP in vertebrates. The main mouse model for PCP defects is the *Looptail* mouse which was first identified by abnormal tail looping in heterozygous mice (Strong and Hollander 1949). Homozygous *Looptail* mice, however, are not viable due to extreme neural tube defects. The mutation was mapped to the *Vangl2* locus that is homologous to *Drosophila vangl/strabismus* (Kibar et al. 2001). Other PCP mouse models include *Circletail*, which carries an off target *tyrosinase* transgene insertion in *Scrib* (Murdoch et al. 2003), and the *Celsr1* mutants *Spincycle* and *Crash*, which were identified from a ENU screens and exhibit head-shaking phenotype due to inner ear defects (Curtin et al. 2003). These three mutants also exhibit neural tube defects when homozygous. Zebrafish PCP mutants have also been characterized and widely studied to determine the role of PCP in vertebrate development. The main zebrafish PCP mutants originate from an ENU mutation screen and include *trilobite*, *silberblick*, *pipetail*, *landlocked* and *offroad*, which correspond to mutations in *vangl2*, *wnt11, wnt5*, *scribbled* and *celsr* (Heisenberg et al. 2000; Jessen et al. 2002; Westfall et al. 2003; Wada et al. 2005). These PCP loss of function mutants exhibit similar phenotypes with shortened AP axis due to gastrulation defects and are nonviable past 5 days post fertilization (dpf) due to an inability to swim.

As shown in *Drosophila*, PCP is involved in directionality of hair and cellular projections, and this is similarly regulated by PCP during vertebrate development. As with *Drosophila* bristles, mammalian hair grows in specific patterns, with uniform direction on the head, body and extremities, and tufts and whorls on the chest. This patterning results from hair follicle orientation which tilts posteriorly during hair bud formation (Devenport and Fuchs 2008). The mouse mutant, *Looptail*, which carries a deleterious mutation in *Vangl2*, has misalignment of hair follicles, accompanied by several more severe phenotypic consequences of loss of PCP. *Looptail* mice also have inner ear defects due to misorientation

of sensory hair cells (Yin et al. 2012). Inner ear development involves uniform directionality of actin-based stereocilia and kinocilia (reviewed in May-Simera and Kelley 2012), and the organization is similarly regulated by PCP.

PCP controls developmental processes at the single-cell level. For example, PCP is required for oriented cellular division. The involvement of PCP in orientation of mitotic spindles was well characterized in the invertebrate models *Drosophila* and *Caenorhabditis elegans*, but was first identified in vertebrates by Gong et al. (2004). During zebrafish gastrulation, mitotic divisions occur along the animal/vegetal (AV) axis to aid epiboly, however after knockdown of PCP through dominant negative *dsh* mRNA injection, mitotic divisions occur at random angles rather than being oriented along the AV axis (Gong et al. 2004). The mechanism of PCP-controlled mitotic spindle orientation is unclear, but work in *C. elegans* suggests that dynein is a downstream target of non-canonical Wnt signalling (reviewed in Segalen and Bellaïche 2009). Single cell migration, specifically migration of branchiomotor neurons in the hindbrain, is inhibited by loss of PCP. In *vangl2* mutant zebrafish embryos, neurons nVII and nIX fail to migrate posteriorly to their appropriate rhombomeres (Bingham et al. 2002). Through cell-type specific knockout of PCP with dominant negative Dvl, it was established that planar polarization is required in both the neuron and the surrounding neuroepithelial tissue for proper migration (Davey et al. 2016). Planar polarization mediates this migration by regulating filopodia dynamics through antagonistic interacts between Vangl2 and Fzd3a, with Vangl2 causing retraction of filopodia and Fzd3a stabilizing extended filopodia (Davey et al. 2016).

PCP is important for embryonic axis elongation through two mechanisms – oriented cell division and CE cellular movements. Oriented cell division ensures cells divide on the AP axis so that daughter cells do not displace laterally and widen the embryo (Gong et al. 2004). CE behaviour allows cells to intercalate during migration toward the midline, and requires organization through tissue-level planar polarization (Jessen et al. 2002). Convergent behaviour of cells is also required during zebrafish neurulation, where after mitotic division one daughter cell will remain on the originating side of the midline, while the other will intercalate into the neural epithelium on the opposite side of the midline.

Defective PCP, as seen in *vangl2* mutant embryos, disrupts neurulation and forms two parallel midlines separated by a cluster of unorganized cells (Ciruna et al. 2006; Quesada-Hernández et al. 2010). In humans and mice, disrupted midline convergence during gastrulation due to mutations in PCP-core component genes is linked to neural tube defects (Lei et al. 2010; Robinson et al. 2012). PCP is so important for neural tube closure that *Vangl2* and *Scrib* mutations in mice cause craniorachischisis, the most severe form of neural tube defect that prevents closure of the brain and entire spinal neural tube (Murdoch et al. 2003). Loss of PCP results in severe neural tube defects because the widened mediolateral embryonic axis does not allow for meeting of the edges of the neural tube and prevents complete closure.

Organogenesis, which involves complex tissue rearrangements and coordinate cell migrations, requires tissues to be planar polarized in many contexts. During lung development, epithelial tube branching produces a large surface area for oxygen exchange. This process of tube branching is disrupted in *Vangl2* and *Celsr1* mutant mice, resulting in small, misshapen lungs (Yates, Schnatwinkel, et al. 2010). This effect is attributed to disrupted actin cytoskeleton dynamics which prevent normal cellular movements required for branching. Likewise, PCP is required for ureteric bud branching during kidney development, as well as CE behaviours and cellular rearrangements, and mice with *vangl2* loss of function mutations have small, misshapen kidneys with decreased branching (Yates, Papakrivopoulou, et al. 2010). Heart development requires extensive tissue remodelling for heart tube looping, and this tissue remodelling is reliant on planar polarization. Zebrafish embryos carrying loss of function mutations in *wnt5*, *wnt11*, *fzd*, *dvl*, *vangl2* or *pk* have failed heart tube looping (Merks et al. 2018). PCP regulates heart development at the cellular level by promoting dynamic cellular rearrangements through control of the actin cytoskeleton, and at the tissue level produces contractile forces by limiting myosin activation to the apical domain (Merks et al. 2018).

Interestingly, cell differentiation and cell fate decisions can be regulated by non-canonical Wnt signalling. In cultures of human neural progenitor cells, WNT3 regulates neural stem cell differentiation by promoting production of the Cyclic AMP-dependent

transcription factor 2 (ATF2) through the receptors FZD4 and FZD5, and the coreceptors Low density lipoprotein receptor-related protein 6 (LRP6) and ROR1 (Bengoa-Vergniory et al. 2017). This induction was presumed to be regulated by the non-canonical branch of the Wnt signalling pathway because inhibiting downstream targets of the canonical pathway did not affect neural stem cell proliferation. Non-canonical signalling through Wnt11/Fzd7 appears to regulate hematopoietic cell fate in human stem cells (Vijayaragavan et al. 2009). This induction requires additional signalling through the canonical pathway involving Wnt3a stimulation and indicates complicated interactions between these two Wnt pathways branches.

1.2.6 Planar cell polarity in vertebrate eye development

PCP indirectly aids the lateral migration of retinal precursors during evagination of eye field cells and formation of the optic vesicle (Woo and Fraser 1995). As discussed above, CE, which is mediated by planar polarization, drives gastrulation and convergence to the midline (Jessen et al. 2002). The tightly adhered neural plate cells displace cells of the eye field which have down-regulated adhesion (Brown et al. 2010), resulting in lateral movement. Beyond producing physical forces, non-canonical Wnt signalling has molecular roles in eye development, mediating eye field specification and regulating cohesions of retinal precursors.

In *Xenopus*, the optic cup is made up primarily by cells descendent from blastomere D1.1.1 (Moody 1987). Recruitment of these cells to the eye field is dependent upon EphrinB1 interactions that are regulated by PCP (Lee et al. 2006). Failed recruitment of D1.1.1 descendants because of loss of EphrinB1 is rescued by over expression of PCP components such as Dsh, RhoA and JNK. This indicates a mechanism in which Ephrin interactions mediate retinal precursor migrations through non-canonical Wnt signalling where Dsh activates the downstream JNK pathway. This study also indicated non-canonical Wnt11 in morphogenic movements of retinal precursors, although it appears that EphrinB1 and Wnt11 act independently (Lee et al. 2006). This finding corroborated a previous study that similarly found Wnt11 to drive cellular movements of the zebrafish eye field, likely through adhesive forces (Cavodeassi et al. 2005). By examining the effect of transplanted cells that overexpress

canonical or non-canonical Wnts, this study found antagonistic interactions between the two Wnt pathways, in which canonical signalling initiates diencephalic identity and inhibits eye specification, while non-canonical signalling inhibits the canonical pathway to maintain eye field differentiation (Cavodeassi et al. 2005). Non-canonical Wnt11 signalling in the zebrafish eye is likely mediated by the receptor Fzd5, which is highly expressed in the eye field during late gastrulation (Cavodeassi et al. 2005). Loss of *wnt11* and *fzd5* has a synergistic effect on eye field specification defects, indicating a genetic interaction between the receptor and ligand (Cavodeassi et al. 2005).

Wnt4 has been indicated as mediating PCP in early eye development. In *Xenopus*, Wnt4 is expressed is tissues around the eye field and MO knockdown of *Wnt4* prevents expression of eye field markers *Rx* and *Pax6*, causing anophthalmia (Maurus et al. 2005). This effect can be negated by additional injection of Dsh carrying a deletion that makes it specific to the non-canonical Wnt pathway, indicating that Wnt4 acts non-canonically to maintain the eye field (Maurus et al. 2005). Wnt4 was identified to regulate expression of *RNA polymerase II elongation factor-associated factor 2* (*EAF2*), which acts in RNA elongation and regulates expression of *Rx*. The mechanism through which Wnt4 regulates *EAF2* is not known, although non-canonical Wnt signalling has previously been shown to regulate transcription. Loss of *Fzd3* has a similar effect as *Wnt4* abrogation in *Xenopus*, with inhibited expression of eye-field markers *Rx* and *Pax*, and it is possible that Wnt4 signals through Fzd3 to regulate expression of these genes (Rasmussen et al. 2001; Seigfried et al. 2017). Further, non-canonical Fzd3 regulates Activated leukocyte cell adhesion molecule (Alcam) in the *Xenopus* eye field (Seigfried et al. 2017). *Alcam* morphant embryos have microphthalmia and choroidal coloboma, however coloboma can be attributed to defective adhesion between the lobes of the choroid fissure, inhibiting fusion. The microphthalmia phenotype is attributed to loss of eye field markers *Rax* and *Pax6* and suggests a role for adhesive forces in eye field development (Seigfried et al. 2017).

There is little evidence that PCP has a role in ocular development beyond eye field specification and production of motive forces that mediate lateral movement of the eye field cells. During lens formation, cells on the proximal side of the lens vesicle elongate distally

to form lens fibers. This process of elongation is oriented through PCP, and loss of planar polarization results in misalignment of lens fiber cells (Sugiyama et al. 2011). Later in ocular development, retinal ganglion cell axon guidance is mediated in a Vangl2-dependent manner, with *vangl2* knockout causing retinal thickening in mice (Leung et al. 2016). PCP is also involved in post-developmental maintenance of the corneal epithelium by orienting epithelial cells as they migrate across the cornea (Findlay et al. 2016).

1.3 Zebrafish as a model for eye development and planar cell polarity

Both vertebrate eye development and PCP are highly evolutionarily conserved so that experiments in a model system produce results relevant to the human disorders. The work outlined in this thesis was conducted using the model organism *Danio rerio*, which are commonly referred to as zebrafish. As a model organism, zebrafish offer several benefits. Zebrafish produce large clutches allowing for large sample sizes and isolation of compound mutants that are produced at low mendelian ratios. Zebrafish embryos develop at a relatively rapid pace, forming most organs and structures by 5 dpf. This rapid development allows for high turnover of experiments. Zebrafish embryos are transparent, and pigmentation is inhibited by PTU treatment that has little effect on development. Transparency allows for easy observation of external and internal structures, and staging markers such as heartbeat and circulating RBCs. The transparency of zebrafish embryos also enables staining techniques and the use of fluorescent markers.

Zebrafish have been widely used to model eye development and PCP, and thus have reliable readout for both systems. The progression of zebrafish eye development was characterized by Li et al. (2000), bringing new insights into mechanisms of ocular morphogenesis and developing a model with which to study the vertebrate eye. Transgenic strains of zebrafish expressing fluorescent markers under the control of eye-specific promoters, such as *rx3*, have allowed for detailed analysis of eye development from the formation of the eye field to optic cup morphogenesis (Rembold 2006; Heermann et al. 2015). This analysis is aided in part by the transparent nature of zebrafish embryos, which allows fluorescent cell tracking. Zebrafish have large eyes that are easily observed stereomicroscopically allowing for screening of ocular malformations. Because zebrafish

adapt skin pigmentation in response to light stimulus, as characterized by Shiraki et al. (2010), this response can be used to assay vision loss at 5 dpf. As discussed above, several PCP mutant zebrafish lines have been characterized, allowing for well established models with which to study novel roles of PCP. Even though these mutant lines have catastrophic defects, they are viable until 5 dpf which allows evaluation of many aspects of development, including eye development. These catastrophic effects of loss of PCP allow for easy sorting of mutants, and a reliable readout of PCP loss of function.

1.4 Hypothesis

Because superior coloboma has only recently been characterized as a discrete ocular disorder, rather than an atypical form of choroidal coloboma, little is known about the mechanisms involved in the causation of this disorder. Initial investigations by our laboratory and collaborators indicate that superior coloboma is a result of failed closure of the SOS, and because this developmental structure has also been characterized only recently, the regulation of morphogenic events required for proper closure are not well understood. The whole exome sequencing data set that was used to identify a role for BMP signalling in SOS morphogenesis further revealed patient variants in genes involved in AB polarity and PCP. Although the role of PCP in eye development is limited, the finding of these variants led to the hypothesis that PCP regulation of eye development is necessary for SOS closure, and loss of PCP lends to the formation of superior coloboma.

1.5 Figures

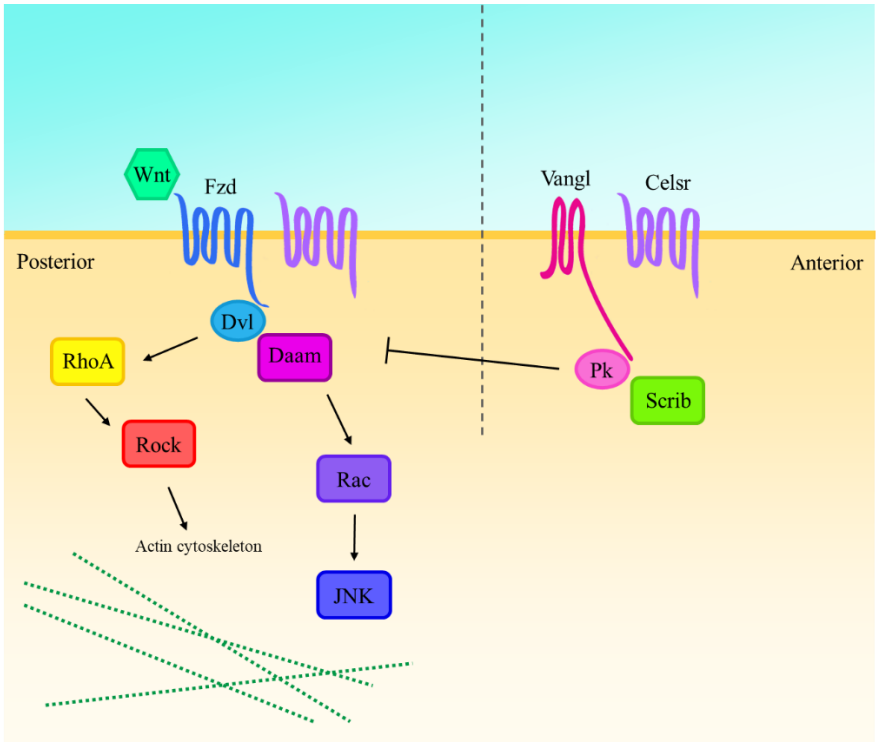

Figure 1.1. Overview of non-canonical Wnt signalling in vertebrates. The signalling pathway is initiated by binding of a Wnt ligand to a Fzd receptor, activating Dvl and Daam and downstream RhoA/Rock or JNK to initiate changes to cytoskeletal dynamics. Binding of Wnt also causes polarization of PCP core component complexes, with Fzd/Dvl localizing to the posterior membrane and Vangl2/Pk localizing to the anterior membrane. The polarized localization of the two complexes is reinforced by negative interactions and binding of Celsr. Figure modified from VanderVorst et al. (2018).

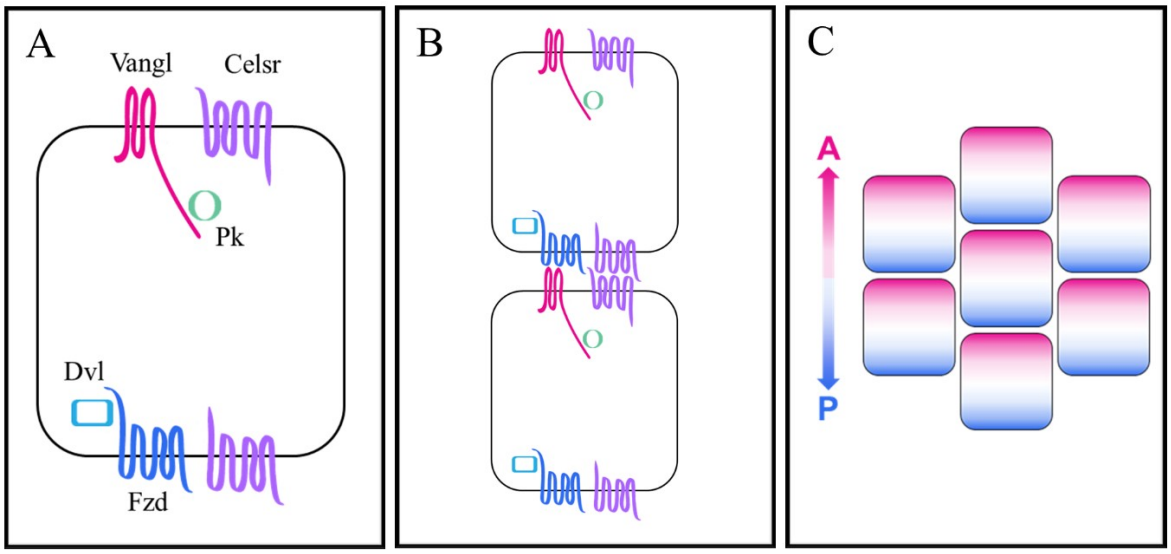

Figure 1.2. Planar polarization in vertebrate cells. A) Following initiation of PCP through binding of a non-canonical Wnt ligand to a Fzd receptor, the PCP complexes Fzd/Dvl and Vangl/Pk localize to the posterior and anterior membranes, respectively. B) These complexes bind to Celsr and form molecular bridges between neighboring cells. C) PCP results in polarization along the anterior/posterior plane of the tissue.

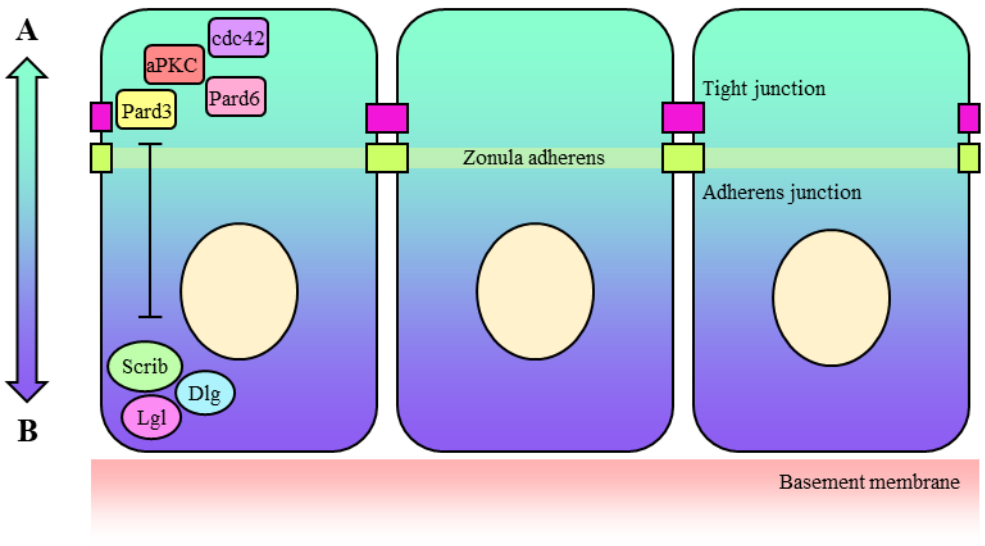

Figure 1.3. Apicobasal polarity in vertebrate cells. AB polarity is initiated through the GTPase Cdc42 activating the apical polarity complex which composed of aPKC, Pard3 and Pard6. The basal complex is composed of Scrib, Lgl, and Dlg. AB polarity is maintained through negative feedback interactions between the apical and basal complexes. The intracellular adhesion complexes, the tight and adherens junctions, aid in maintenance of AB polarity through the zonula adherens which acts as a semi-permeable barrier to keep contents of the apical and basal intercellular domain separate. Figure based on Campanale et al. (2017).

Chapter 2: Materials and Methods

2.1 Zebrafish lines and animal care

Zebrafish work was conducted as outlined in Westerfield (2000) and as approved by the Canadian Council for Animal Care guidelines and the University of Alberta Animal Care and Use Committee for Biosciences. Zebrafish embryos were maintained in E3 medium (15 mM NaCl, 500 nM KCl, 1 mM $CaCl_2$, 150 nM KH_2PO_4, 1 mM $MgSO_4$, 715 nM $NaHCO_3$) supplemented with 10 mL/L penicillin/streptomycin (10,000 U/mL penicillin/10 mg/mL streptomycin, Sigma). If embryos were grown past 22 hpf, media was supplemented with 0.004% phenylthiourea (PTU; Sigma-Aldrich) to prevent pigmentation. Zebrafish were euthanized using 4% Mesab (0.4% tricaine solution).

Morpholino oligo (MO) experiments were performed using AB strain wildtype fish. The *vangl2* mutant strain, *vangl2*^{tk50f}, which carries an uncharacterized deletion within the coding sequence and produces no detectable transcript (Jessen et al. 2002), was obtained from the Ciruna Lab at the University of Toronto. As *vangl2* mutants are not viable past 5 dpf, a heterozygous fish population, which do not show a PCP-related phenotype, was maintained within the aquatics facility and crossed to produce mutant embryos and WT siblings which were used as a control. *Vangl2* heterozygotes were crossed with a transgenic line *Tg[kdrl-mCherry]* to produces a population of *vangl2*$^{+/-}$*;kdrl-mCherry*$^{+/-}$.

2.2 Genotyping of *vangl2*^{tk50f} fish

Adult fish from a tri(tk50f) heterozygote outcross, containing half heterozygotes, were genotyped to give a population of identified heterozygotes. As the *vangl2*^{tk50f} mutation has not been characterized, genotyping using molecular methods was not feasible. Because *vangl2* mutant embryos have a readily apparent phenotype of a shortened AP axis that is easily observed by 20 hpf, testcrosses were used to identify *vangl2*^{tk50f} heterozygous adults. Pairs of fish were crossed and the resulting offspring were screened for the PCP loss of function phenotype. Clutches that contained phenotypically mutant embryos indicate that both parents carry the mutant allele.

2.3 Morpholino injection

MO (**Table 2.1**) were either designed by GeneTools or based on published sequences and all MO were ordered from GeneTools, LLC (Philomath OR, USA). Lyophilized MOs were resuspended to a concentration of 10 mg/mL in autoclaved milli-Q water and incubated at 65°C until the MO had fully dissolved. Working solutions were prepared by further diluting MOs in autoclaved milli-Q water. *Scrib* and *p53* MO were co-injected to reduce necrosis in morphant embryos. The negative control for all MO experiments was an equivalent dose of the standard control oligo produced by GeneTools. MO were incubated at 65°C for five minutes prior to injection to ensure dissolution of secondary structure. Wildtype zebrafish embryos at the one-to-four cell stage were injected with 2 nL of working stock to give the desired dosage (**Table 2.1**). After injection, embryos were transferred to E3 medium supplemented with penicillin/streptomycin and incubated at 28.5°C.

2.4 Laminin immunohistochemistry

Laminin immunohistochemistry (IHC) was used to mark the presence of an open SOS. Embryos were fixed with freshly made 4% paraformaldehyde (PFA) for two hours at room temperature. Embryos were immediately washed four times with phosphate-buffered saline containing 0.1% Tween-20 detergent (PBST) for five minutes each wash and were dechorionated during the third PBST wash. Embryos were then permeabilized with 10 μg/mL proteinase K for one minute, then washed with PBST. Embryos were washed into sterile water with 0.1% Tween, and further permeabilized with acetone for seven minutes at -20°C. After washing out of acetone and into PBST, embryos were incubated for one hour at room temperature in block solution containing 5% goat serum and 2 mg/mL bovine serum albumin (BSA) in PBST. Embryos were incubated overnight at 4°C in rabbit anti-Laminin antibody (1/250 in block solution; L-9393, Sigma-Aldrich), then washed out of primary antibody, and incubated overnight at 4°C in goat anti-rabbit Alexa Fluor 488 or 568 antibody (1/1000 in block solution; A-11008 and A-11011, Invitrogen). Embryos were washed out of secondary antibody with 5 PBST washes and stored in PBST at 4°C.

2.5 Superior ocular sulcus scoring

Scoring of embryos for the presence of an open SOS was conducted as outlined in Yoon et al. (2019) and in Chapter 4 of this thesis. Embryos were grown to 28 hpf in E3 medium at 28.5°C. The time point of 28 hpf was chosen as an ideal stage to screen for SOS closure as the sulcus should no longer be visible under the stereomicroscope by 24 hpf. Embryos were staged based on several morphological features, including somite count, heartbeat, and circulating red blood cells (RBC). When circulating RBC were observed, embryos were staged at 28 hpf. Live embryos were examined on an Olympus stereoscope for the presence of an open SOS, and embryos that showed an open SOS in either one or both eyes were scored as SOS positive (**Figure 4.2**). Where possible, embryo treatment groups were blinded for scoring.

Laminin IHC embryos were washed through 30/70, 50/50, then 70/30 percent glycerol/PBST and both eyes were dissected off and mounted distal-side-up on a microscope slide. Pairs of eyes were examined using a Zeiss Axio Imager Z1, Zeiss LSM700 laser confocal scanner at 20X magnification. Pairs of eyes that showed a well-defined laminin-line fissure in the dorsal optic cup of either one or both eyes were scored as SOS positive.

2.6 *In vitro* mRNA transcription and injection

The pCS2(105):GFP-Pk plasmid (Jenny et al. 2003) was generously provided by the Ciruna Lab at the University of Toronto. The plasmid was linearized through restriction digest using AscI in a reaction volume of 40 µL with 10,000 ng of maxiprep DNA. The pCS2:GFP-CAAX plasmid (Bryan et al. 2016) was generously provided by the Kwan lab at the University of Utah. The plasmid was linearized through restriction digest using NotI in a reaction volume of 40 µL using 9 µg of maxiprep DNA. Complete digest was observed through gel electrophoresis of a 1 µL sample of the restriction digest reaction. The linearized plasmid was purified using phenol/chloroform extraction and ethanol precipitation. Purified, linear plasmid was used as a template to transcribe GFP-Pk mRNA using the mMessage mMachine SP6 kit (Ambion). Approximately 2 µg of linear plasmid was added to the transcription reaction. TurboDNAse (Invitrogen) was used to stop the transcription reaction, and the reaction was cleaned up by ethanol precipitation. mRNA was quantified by

NanoDrop, then diluted to 50 ng/μL with molecular grade water and stored at -80°C. mRNA was thawed on ice immediately prior to injection. 100 pg of mRNA was injected into the cell of one-cell stage WT embryos. After injection, embryos were transferred to E3 medium supplemented with penicillin/streptomycin and incubated at 28.5°C.

2.7 Pharmacological treatments

Zebrafish embryos were treated with DMH1 (Sigma-Aldrich) to inhibit BMP signalling. Groups of 15 embryos at 10 hpf were placed in a 35 mm petri dish with embryo media supplemented with 0.2 μM DMH1 or an equivalent dosage of the vehicle DMSO and incubated until 24 hpf. At 24 hpf, embryos were fixed in 4% PFA and used for *in situ* hybridization.

2.8 Whole embryo RNA extraction and purification

RNA was extracted from whole embryos using the RNAqueous™ Total RNA Isolation kit (Invitrogen). Dechorionated embryos at 24 hpf were added to 350 μL of lysis solution per 50 embryos and vortexed until homogenized. An equal volume of 64% ethanol was added to the mixture and inverted several times to mix. The mixture was transferred to a filter cartridge and centrifuged for one minute at 15,000 g. The flow-through was discarded and the filter washed with 700 μL of wash solution #1, then centrifuged and washed twice with 500 μL of wash solution #2/3. The filter cartridge was transferred to a new RNAse-free tube and the RNA was eluted with 70 μL pre-warmed 70°C elution buffer. The eluted RNA was stored at -80°C.

Extracted RNA was purified using the Qiagen Rneasy Mini kit (Qiagen, 74104). Before purification, 19 μL diethyl pyrocarbonate (DEPC)-treated water, 10 μL DnaseI buffer, and 1 μL DnaseI were added to 100 μL of extracted RNA and the solution was incubated for 30 minutes. In a separate tube, 10 μL β-mercaptoethanol (BME) and 1 mL of buffer RLT were premixed and then 350 μL RLT/BME mixture was added to the RNA sample. The sample was vortexed, and then 250 μL of 100% ethanol was added and the tube was gently inverted to mix. The solution was transferred to a Rneasy spin column and centrifuged for 15 seconds at 8,000 g. After transferring the column to a new tube, it was

washed with 500 µL of RPE buffer and centrifuged for 15 seconds at 8,000 g. The tube was then washed again with 500 µL of RPE buffer and centrifuged for 2 minutes. The tube was centrifuged for 1 minute at max speed to remove any remaining liquid and the column was transferred to a new RNAse-free tube. The RNA was eluted with 10 µL of DEPC-treated water and centrifuged for 1 minute at 8,000 g. The purified RNA sample was stored at 80°C.

2.9 RT-PCR

Purified RNA was used as a template to produce cDNA using the SuperScript™ III One-Step RT-PCR System with Platinum™ Taq DNA Polymerase kit (Invitrogen, 12574026). In an RNAse-free PCR tube, 12.5 µL 2x reaction mix, 1 µL template RNA, 1µL forward primer (10 µM), 1 µL reverse primer (10 µM), 1 µL SuperScript III reverse transcriptase/Platinum Taq mix, and 8.5 µL RNAse-free water was added per reaction. Primers used for RT-PCR are listed in **Table 2.2**. Reverse primers encode the T7 RNA polymerase promoter site. The thermocycler was set to run at 55°C for 15 minutes, then 94°C for 2 minutes before starting 40 cycles of 94°C for 15 seconds, 55-65°C (depending on primers used) for 30 seconds, 68°C for 60 seconds. After 40 cycles, the thermocycler ran one cycle of 68°C for 5 minutes. The reverse-transcribed cDNA was run through a 1% agarose/TAE gel and DNA bands corresponding to the expected amplicon length were excised and gel extracted using the QIAquick Gel Extraction Kit (Qiagen) according to kit instructions.

2.10 *In situ* hybridization riboprobe synthesis

Gel extracted cDNA was used as a template to transcribe digoxigenin (DIG)-labeled probes for whole mount mRNA *in situ* hybridization. For *vax2 in situ* hybridization, the probe was synthesized from linearized plasmid constructed from a pCR4-TOPO vector. The plasmid was linearized using the NotI restriction enzyme. The reaction was assembled with 2 µg cDNA, 2 µL 10X transcription buffer, 2 µL 10 DIG labelling mix, 1 µL T7 RNA polymerase, and 1 µL RNaseOUT, with molecular grade water added to a final volume of 20 µL. For synthesis of the *vax2* probe, T3 RNA polymerase was added to the reaction. The reaction mixture was incubated for 2 hours at 37°C with an additional 1 µL T7 RNA

polymerase added after one hour. 1 μL of RNase-free DNase was added, and the reaction was incubated for 5 minutes at 37°C before addition of 2 μL 0.25M pH 8.0 EDTA. DIG-labeled probe was stored at -80°C.

2.11 mRNA *in situ* hybridization

Whole mount mRNA *in situ* hybridization was performed as outlined in Thisse and Thisse (2008). Embryos were fixed overnight at 4°C in 4% PFA, then washed out of fix with 5 PBST washes and dechorionated. For storage at -20°C, fixed embryos were placed in 100% MeOH. MeOH-treated embryos rehydrated by washing through 75/25, 50/50, and 25/75 percent solutions of MeOH/PBST, then into PBST. Embryos were permeabilized with 10 μg/mL proteinase K for 3-5 minutes and refixed in 4% PFA for 20 minutes, then washed out of fix with 5 washes of PBST. Embryos were prehybridized for 2 hours at 65°C in hybridization mix (50% formamide, 5X SSC, 0.1% Tween 20, 50 mg/mL heparin) with 500 mg/mL Rnase-free tRNA, then incubated in DIG-labelled RNA probe (1:200 in hybridization mix) at 65°C overnight. The next day, embryos were washed in the following solutions, which were prewarmed to 65°C: 5 minutes each in 66% hybridization mix/33% 2X saline-sodium citrate buffer (SSC), 33% hybridization mix/66% 2X SSC, and 2X SSC, then 20 minutes each in 0.2X SSC/0.1% Tween-20 and 0.1X SSC/0.1% Tween-20. Embryos were then washed for 5 minutes each at room temperature in 66% 0.2X SSC/33%PBST, 33% 0.2X SSC/66% PBST, and PBST. Embryos were incubated for 1 hour at room temperature in block solution (2 mg/mL BSA and 20 μL/mL sheep serum in PBST), changed into anti-DIG alkaline phosphatase-conjugated Fab fragments (1:5000 in block solution, Roche) and incubated for 2 hours at room temperature, then washed out of antibody with 5 x 15 minute washes in PBST. Staining was achieved through washing 4 x 5 minutes in colourization buffer (100 mM Tris-HCl pH 9.5, 50 mM MgCl2, 100 mM NaCl, 0.1% Tween-20 in sterile water), then incubating colourization buffer with 0.45 mg/mL nitro-blue tetrazolium chloride (NBT) and 0.175 mg/mL 5-bromo-4-chloro-3-indolyl phosphate (BCIP). Staining was monitored and once satisfactory colour had developed, the colourization reaction was stopped with several 15 minutes washes in MeOH with 0.1% Tween-20. Embryos were

rehydrated with successive washes in 25/75, 50/50, and 25/75 percent MeOH/PBST, then 100% PBST.

Whole embryos were mounted in 3% methyl-cellulose and imaged with a Qimaging camera on an Olympus stereoscope. For imaging of dissected embryos, embryos were first washed through 30/70, 50/50, then 70/30 percent glycerol/PBST, doyolked, and mounted in 70% glycerol on a microscope slide. Embryos were then imaged using a Zeiss AxioImager Z1 compound microscope with an Axiocam HR digital camera (Carl Zeiss Microscopy, LLC).

2.12 Statistical analysis

Each SOS closure delay scoring experiment was run in biological triplicate and bar graphs represent pooled averages of all repeats. Error bars were calculated as the Standard Error of the Mean by calculating [(standard deviation between repeats)/(square root the number of repeats)]. As the data is categorical, the two-tailed Fisher's Exact Test was chosen for statistical analysis of SOS closure delay scoring experiments.

2.13 Tables

Table 2.1. Morpholino oligonucleotides used to knock down gene expression. All MOs used in this project were designed based on published MO sequences with the exception of the *fzd4* MO, which was designed based on the DNA sequence. MOs were titrated through injecting various doses to determine the amount that provides reliable phenotype without producing off target effects. Dosages that are reported here are amounts injected to in SOS closure delay experiment. The standard control oligo was injected at the same dosage as each experimental morpholino.

Target Gene	Type	Sequence (5'-3')	Dosage (ng)	Publication
vangl2	Translation blocking	GTACTGCGACTCGTTATCCATGTC	3	Park and Moon 2002
fzd4	Translation blocking	AGCCATAGCGACACAATCCGATTGA	Up to 12	N/A
scrib	Translation blocking	CCACAGCGGGATACACTTCAGCAT	4	Wada et al. 2005
celsr2	Translation blocking	CAAAGAGCAACAAATCCCCCTTCAT	Ordered, not injected	Witzel et al. 2006
shroom3	Splice blocking	CCTAATAAATTGTTACCTGACTAAC	5	Ernst et al. 2012
p53	Translation blocking	GCGCCATTGCTTTGCAAGAATTG	2	Langheinrich et al. 2002
human *ß-globin* pre-mRNA	Standard control oligo	CCTCTTACCTCAGTTACAATTTATA	N/A	N/A

Table 2.2. Primers used for RT-PCR prior to *in situ* hybridization probe synthesis.

Gene	Forward Primer	Reverse Primer	Amplicon size	T(m) °C
vangl2	CGGAGAAGAGAACAG CACTAATAAC	CATCTCAAAAACATTCA CAACAGA	1066	55.2/53.5
fzd4	TCATCATACTTCATTTC TACTGCAA	TGTAAACCAGCACTGCC AAT	961	52.4/55
tbx5a	GAGGGAAGTTCGCTAT CAACCG	TCCATTGTTTTCATCCGC CTTG	713	52
shroom3	TGAGACGAGAGCGT CAGAGA	CTTCATCGTCCAGGTT GGTT	969	57.2/55

Chapter 3: Results and Discussion

3.1 *In silico* analysis of variants from WES of superior coloboma patients

To explore genetic causation of superior coloboma, whole exome sequencing (WES) of five patients with superior coloboma was used to identify potentially deleterious mutations in genes that may have an important role in early eye development (Hocking et al. 2018). Hocking et al. (2018) narrowed down the variants identified in the initial WES data to non-synonymous or stop-gain/loss mutations with a population frequency less that 1%. These variants were further narrowed by MutationTaster testing, with a score requirement of greater than 0.95. Genes with known roles in ocular development or published ocular expression patterns were prioritized (Hocking et al. 2018).

Several of the candidate genes indicated by WES are involved in AB polarity or PCP (**Table 3.1**), driving the hypothesis that polarization of early ocular tissues is required for SOS closure. To ensure accuracy of predictions, MutationTaster, Polyphen-2 and Sift scores, as well as population frequency from the Exome Aggregation Consortium (ExAC, recently changed to "gnomAD browser") database, of one AB polarity- and six PCP-related genes were recalculated from the initial data collected in 2012 (**Table 3.1**). The MutationTaster algorithm screens for homozygous frequency of variants through the Thousand Genome Project database and accounts for sequence conservation, splice site changes, effects on protein functional domains, and variants linked to known disease states (Schwarz et al. 2014). Because all variants investigated in this project are single nucleotide variants, the simple_aae model was used for MutationTaster analysis. MutationTaster classifies variants as either 'disease causing', 'disease causing automatic', 'polymorphism', or 'polymorphism automatic', with 'polymorphism' indicating that variants are likely benign and 'automatic' designating variants that have been confirmed either deleterious or harmless. The Polyphen-2 algorithm scores variants through sequence-based structure-based predictions and includes analysis of site conservation and distance from nearest evolutionary nucleotide difference at that site (Adzhubei et al. 2010). Polyphen-2 classifies variants as either 'benign', 'possibly damaging', or 'probably damaging'. The Sift algorithm sorts all possible substitutions for each amino acid in a given sequence as either tolerant or intolerant and is based on evolutionary conservation of amino acid sequences (Kumar et al. 2009). Sift classifies

variants as either predicted to affect protein function or tolerated. Because each of these tools have limits, such as MutationTaster being able to only analyse intragenic mutations (Schwarz et al. 2014), the three separate analyses were used for each variant in this study to strengthen predictions of whether the variant is deleterious. The ExAC database is an amalgamation of exome sequencing data from over 60,000 individuals from diverse ethnic backgrounds (Lek et al. 2016). ExAC data comes from multiple sources, including the Thousand Genome Project and several disease-specific genome sequencing projects. The ExAC dataset include over ten million unique sequence variants.

The one variant involved in AB polarity was in the gene *SHROOM3*, which was found in patient #3. This gene encodes a protein that mediates constriction of the apical cell surface. The *Shroom3* variant is predicted to affect protein function (0.00) by Sift analysis, and be disease causing (0.9999998) by MutationTaster analysis and probably damaging (1.000) by Polyphen-2 analysis. This variant has a low ExAC population frequency of 3.499e-04. These analyses indicate that the *SHROOM3* variant is likely deleterious, and this gene was chosen for further investigation.

The patient #1 variant in *FZD4*, which encodes a Wnt receptor that acts noncanonically in some contexts, is predicted to be disease causing (0.99999999) by MutationTaster analysis, possibly damaging (0.568) by Polyphen-2 analysis and tolerated (0.19) by Sift analysis. This variant was not found in the ExAC database, which covers over 60,000 genomes from diverse ethnic backgrounds, indicating an extremely low population frequency. The patient #4 variant in *SCRIB*, which encodes an adaptor protein that acts in vesicular trafficking of Vangl2, is predicted to be disease causing (0.99999999) by MutationTaster analysis, probably damaging (1.000) by Polyphen-2 analysis and tolerated (0.07) by Sift analysis. This variant was found to have a low population frequency (5.9e-05) in the ExAC database. As with the *SHROOM3*, these PCP-related genes were chosen for further investigation because the *in silico* analyses indicate the variants are deleterious.

Patient #5 was found to have variants in two PCP-related genes, *CELSR2*, which encodes an atypical cadherin that mediates intercellular binding of Fzd and Vangl, and *WNT9B*, which encodes a Wnt ligand that has been shown to activate non-canonical Wnt

signalling pathway in some contexts (Karner et al. 2009). The *CELSR2* variant is predicted to be disease causing (0.999947299) by MutationTaster analysis, probably damaging (0.992) by Polyphen-2 analysis and tolerated (0.30) by Sift analysis. This variant has an ExAC population frequency of 8.035e-03, which is just less than 1% of the population and is thus not extremely rare. The *WNT9B* variant is predicted to be disease causing (0.99999807) by MutationTaster analysis, probably damaging (1.000) by Polyphen-2 analysis and tolerated (0.81) by Sift analysis. This variant has an ExAC population frequency of 2.756e-04, indicating that this is a rare variant. Although both *CELSR2* and *WNT9B* variant analyses indicate that these variants may be deleterious, neither gene was investigated further in the course of this project due to time constraints. A translation blocking *celsr2* MO was designed based on a previous publication and ordered (**Table 2.1**), but was not injected.

Variants were found in both *FAT2* (patient #1) and *FAT4* (patient #5), which are involved in the Fat-Dachsous pathway that acts in parallel with the non-canonical Wnt signalling pathway to establish PCP (Matis and Axelrod 2013). The *FAT2* variant is predicted to affect protein function (0.00) by Sift analysis, and be disease causing (0.9999999) by MutationTaster analysis and probably damaging (0.966) by Polyphen-2 analysis. The *FAT4* variant is predicted to affect protein function (0.02) by Sift analysis, and be disease causing (0.98744266) by MutationTaster analysis and probably damaging (0.999) by Polyphen-2 analysis. The *FAT2* variant has an ExAC population frequency of 0.01737, or 1.7%, indicating that this variant is not exceptionally rare. The *FAT4* variant has a much lower ExAC population frequency of 4.252e-03. Although these analyses indicate that both variants may be deleterious, the decision was made to focus on variants in genes associated with the non-canonical Wnt pathway because there is little known about Fat-Dachsous signalling in vertebrate development, and to maintain a clear research direction.

3.2 Loss of *shroom3* does not cause SOS closure delay

The first gene investigated from the WES data set was, *SHROOM3*. This gene encodes an actin binding protein that mediates apical constriction and is part of the AB polarity system. SHROOM3 has three functional domains – an N-terminus PDZ domain and two ASDs (Apx/shroom domain) (Hildebrand and Soriano 1999; Haigo et al. 2003). Human

SHROOM3 has three protein-coding splice variants, with the main transcript containing all three functional domains and encoding 1996 amino acids. One alternate transcript contains both ASDs but not the PDZ domain, while the other alternate transcript encodes only 50 amino acids and does not cover either functional domain. PDZ domains are well characterized protein binding motifs, usually binding cytoplasmic portions of transmembrane receptors. The PDZ domain of SHROOM3 localizes the protein to the apical cell cortex through binding of the adherens junction, where it regulates apical constriction through the ASDs (Hildebrand and Soriano 1999). ASD1 contributes to the actin binding ability of SHROOM3 to form a ring of filamentous actin, while ASD2 mediates constriction of the actin ring, resulting in decreased apical cell surface area (Haigo et al. 2003). The apical constriction function of SHROOM3 allows for bending, folding, and invagination of a tissue, mediating morphogenesis and organogenesis. The variant found in patient #3 is in the ASD1 domain, potentially disrupting the protein's ability to bind actin which would result in a loss of function.

It was hypothesized that a potentially deleterious mutation in *SHROOM3* indicates involvement of AB polarity in closure of the SOS. *In silico* analysis of the variant was updated to reflect current data. *In situ* hybridization of zebrafish embryos shows low levels of ocular expression at 24 hpf, and this expression is likely lens-specific as older embryos show strong staining of the lens but not the surrounding ocular tissue (Ernst et al. 2012). It is reasonable to expect *shroom3* expression in the lens as apical constriction mediates invagination of the lens placode (Plageman et al. 2010). To characterize *shroom3* expression patterns at a time point relevant to SOS closure, *in situ* hybridization was performed using WT zebrafish embryos at 22 hpf (**Figure 3.1)**. These embryos have kidney-specific staining that corresponds to that found in 24 hpf embryos, but also show stronger staining of the optic cup, suggesting that AB polarity may be active in the whole eye during this stage of development, or that higher expression is required for lens pit invagination at this time point. Therefore, it was plausible that Shroom3 may be involved in morphogenic processes required for SOS closure.

To test whether *SHROOM3* is necessary for closure of the SOS, MO was used to knockdown *shroom3* expression in zebrafish. A previously published MO was ordered from GeneTools as this MO has been verified to successfully knockdown *shroom3* expression and results in neuromast defects in the lateral line (Ernst et al. 2012). To determine the proper dosage that results in a loss of function phenotype without causing excessive off-target effects, the MO was titrated prior to scoring *shroom3* morphants for SOS closure defects. Various dosages of *shroom3* MO were given, ranging from 1 ng to 35 ng, but no obvious phenotype was observed beyond tissue necrosis and cardiac edema due to off target effects attributed to high dosages. The highest dosage of 35 ng, which is higher than the maximum 10 ng normally use in our lab, was administered as it reflects the dosage used in Ernst et al. (2012). An attempt was made to verify efficacy of the MO through examination of neuromasts using a Dusp6:GFP line, but rosettes were not visible and no other methods were used to confirm successful knockdown of *shroom3* with this MO. A dosage of 5 ng was used for scoring of SOS delay as this was the highest dosage that did not result in necrosis and edema. These *shroom3* morphants did not show significant SOS closure delays compared to embryos injected with an equal dose of control MO (% SOS positive *shroom3* morphants: 6.1 +/- 0.4, n=130; % SOS positive control morphants: 1.9 +/- 1.4, n=89; p=0.531) (**Figure 3.2**). This negative data indicates that *shroom3* is not required for closure of the SOS. No noticeable eye deformations were observed, even though apical constriction is an important aspect of ocular development through invagination of the optic cup and lens placode. However, it is possible that these events are made robust through redundancies and loss of *shroom3* does not disrupt eye development enough to show defects at 28 hpf, long after formation of the optic cup. Further, because these invagination events occur prior to formation and closure of the SOS, it is unlikely that these events are linked. All together, this experiment did not support the hypothesis that the *SHROOM3* patient variant is causative of superior coloboma. However, because loss of AB polarity was not established, it cannot be concluded whether AB polarity is involved in SOS closure.

3.3 Loss of *fzd4* does not cause SOS closure delay

A previous survey of frizzled gene expression during zebrafish development shows *fzd4* is expressed in ocular tissue at 18 hpf and continues to at least 30 hpf (Nikaido et al. 2013). *FZD4* mutations, among others in Wnt-related genes, are associated with familial exudative vitreoretinopathy (FEVR), which disrupts retinal vascularization and causes retinal detachment (Kondo et al. 2018). Because this gene is expressed during ocular development and has previously been linked to developmental defects in the eye, FZD4 was chosen as a candidate to investigate further for its role in closure of the SOS.

The role of Fzd receptors in canonical and non-canonical Wnt signalling pathways is spatially and temporally dependent and it is unknown whether Fzd4 has a role in PCP during eye development. While Fzd4 is best characterized as using the ligand Norrin to initiate β-catenin dependent Wnt-signalling, there is evidence for interaction with other Wnt ligands. For example, noncanonical WNT3A signalling through FZD4 regulates stem cell differentiation in human neural stem cells through JNK activation (Bengoa-Vergniory et al. 2017). Further, Wnt5a, a normally non-canonical Wnt, has been shown to activate the canonical pathway through binding of Fzd4 in human and mouse cell lines (Mikels and Nusse 2006). A binding affinity assay showed strong Fzd4 binding by both Wnt3a and Wnt5a (Dijksterhuis et al. 2015). Fzd4 has been shown to activate the noncanonical Wnt signalling pathway during angiogenesis. Studies using endothelial cells (EC) from *Fzd4*$^{-/-}$ mice indicate that Fzd4 acts to activate JNK activity showing that Fzd4 is involved in planar polarization required for vascularization (Descamps et al. 2012). Together, previous studies of Fzd4 indicate that, depending on the context, this receptor can regulate planar polarity through non-canonical Wnt signalling, and thus could mediate PCP during eye development.

MO knockdown of *fzd4* expression in zebrafish embryos was used to investigate whether this gene is involved in closure of the SOS and whether the *FZD4* variant is causative of superior coloboma in patient #1. As there are no published zebrafish *fzd4* MOs, I designed a MO that binds around the start codon to prevent translation of *fzd4* transcripts. WT embryos were injected with various doses of *fzd4* MO to titrate the reagent and determine whether *fzd4* morphant embryos have SOS closure defects or other phenotypes. The maximum dose

of 12 ng gave no observable phenotype, including cardiac edema and necrosis normally seen as off target effects of high MO doses. Embryos injected with this maximum dosage were examined at 28 hpf, a time at which the SOS is reliably closed in WT embryos and showed no increase in open SOS compared to the control morphants (% SOS positive *fzd4* morphants: 5.3 +/- 0.8, n=132; % SOS positive control morphants: 2.7 +/- 1.5, n=101; p=0.5205; **Figure 3.5**). These results indicate that loss of *fzd4* is insufficient to disrupt SOS closure. However, it was not determined that the MO was successfully inhibiting translation of *fzd4*, as the embryos showed no obvious phenotype and further tests were not conducted. To confirm that the MO worked as designed, embryos could have been screened for vascularization defects in the kidney and heart, as have been described in *Fzd4*$^{-/-}$ mice, or western blot could be used to detect the presence of Fzd4 in morphant embryos.

While these results do not support a model in which closure of the SOS is dependent on Fzd4-mediated signalling, these data also do not refute the possibility that PCP regulates SOS closure. In both canonical and non-canonical Wnt signalling pathways, Wnt ligands are promiscuous and may bind several different Fzd receptors. It is possible that knockdown of *fzd4* results in Wnts binding other receptors, preventing disruption of the pathway. It is also possible that Fzd4 does not have a role in PCP in ocular development. It is more likely that ocular noncanonical Wnt signalling uses *fzd5*, which is highly expressed during ocular development (Nikaido et al. 2013). It is unknown whether *fzd4* knockdown results in loss of planar polarity as the design of this experiment does not directly test this.

The FZD4 variant found in patient #1 is a non-synonymous mutation and occurs within the Frizzled cysteine-rich domain (CRD) that interacts with Wnt ligands. The current experiment does not investigate the result of this specific mutation, but rather the result of complete loss of function. Mutations that occur in the linker domain that connects the CRD and transmembrane domain have a significant effect on the binding affinity of Norrin by the Fzd4 receptor (Beaven et al. 2018). While the patient #1 variant mutation is in the CRD, it changes the second to last amino acid in this domain before the linker domain. The effect of this mutation on the linker domain is unknown, but the proximity makes it possible that the mutation changes the folding conformation of the linker, and thus the receptor's ability to

bind Norrin. Additionally, another FZD4 mutation, M157V, has been found to cause disorganized ocular vasculature and retinal folding associated with FEVR (Xu et al. 2004). M157 is located at the surface of the CRD and is hypothesized to regulate signal induction through interact with LRP coreceptors or the transmembrane domain. Again, the patient #1 variant in located two amino acids away from M157 and this proximity may relay a similar role to M159. It is possible that the M159I variant is hypermorphic or neomorphic. A hypermorphic mutation that increases binding affinity for norrin/Wnt ligands, and thus upregulates signaling within the cell could have a more severe consequence than loss of a receptor that can be compensated for by other Fzds. Likewise, a neomorphic mutation could be more severe than loss of function, by binding different ligands and thus upregulating intercellular signalling.

All together, the *fzd4* knockdown experiment indicates that this gene is not necessary for regulation of ocular development leading to closure of the SOS but does not rule out the possibility that PCP is involved in this process. Further experiments were implemented to explore genes indicated by the superior coloboma patient WES data to determine whether loss of expression of these genes results in SOS closure defects.

3.4 Loss of *scrib* causes SOS closure delay

While knockdown of *fzd4* did not result in SOS closure delays, it was important to explore other PCP-related genes that were identified through WES of superior coloboma patients. Patient #4 carries a non-synonymous mutation in *SCRIB*. This gene is an ideal target to explore in the link between the WES data and PCP in the causation of superior coloboma as mammalian Scrib acts in the PCP pathway through binding of Vangl2, and is thought to act as an adapter protein as well as facilitate vesicular trafficking of Vangl2 (Montcouquiol et al. 2003; Kallay et al. 2006). The patient #4 *SCRIB* variant results in a D to N change at amino acid 191 within the LRR functional domain. The LRR domain binds Lgl (Kallay et al. 2006) and has a role in membrane localization (Reviewed in Bonello and Peifer 2019). Disruption of the LRR domain therefore may affect the ability of SCRIB to localize properly in the cell and prevent interactions with VANGL2. Zebrafish *scrib* is expressed from the one-cell stage to at least 60 hpf and is present in anterior tissues, including the eyes, during early

development (Thisse and Thisse 2005) While *Circletail* mice, which carry a loss of function *Scrib* mutation, have been studied in conjunction with neural tube defects (Murdoch et al. 2003), and neuronal migration and gastrulation defects have been identified in *scrib* mutant zebrafish (Wada et al. 2005), no ocular defects have been reported in Scribble studies. However, *SCRIB* was an appealing target to study for this project as loss of a core PCP component was sure to disrupt PCP as opposed to the knockdown of *fzd4* in the above experiment.

Although the *landlocked* zebrafish line, which carries a *scrib* loss of function mutation, exists, it was not feasible to obtain these fish due to time restrictions and zebrafish importation laws (Hanwell et al. 2016). Instead, MO knockdown was used to explore whether *scrib* is required for closure of the SOS. Morphant embryos presented with the stereotypical PCP loss of function phenotype of a shortened AP axis (**Figure 3.4**) confirming that the *scrib* MO treatment was sufficient to disrupt PCP. Scoring embryos stereoscopically at 28 hpf showed SOS closure defects in *scrib* morphants but not control morphants (% SOS positive scrib morphants: 28.3 +/- 2.0, n=157; % SOS positive control morphants: 5.8 +/- 1.3, n=106; $p<0.0001$; **Figure 3.5**). Timing of closure was not assayed, but casual observation the day after scoring indicated that embryos no longer had open SOS.

The *scrib* knockdown data indicate that Scrib assists in the closure of the SOS and suggest that the *SCRIB* variant contributes to patient #4's superior coloboma, likely through its role in PCP. However, Scrib is involved in both AB and planar polarity, and due to the design of this experiment, it is unclear which pathway is responsible for delayed closure in the *scrib* morphants. However, knockdown experiments of *shroom3*, an AB polarity protein, did not delay closure of the SOS, suggesting that AB polarity may not be required for this process. Further experiments exploring the role of PCP in SOS closure were required to link the *scrib* morphant SOS closure delay to PCP defects.

3.5 Loss of *vangl2* causes SOS closure delay

To investigate the role of PCP in closure of the SOS, *vangl2* was chosen as a target for subsequent experiments. Vangl2 is a well characterized core PCP component with roles in intracellular polarization and regulation of actomyosin dynamics, and knockdown and

knockout of *vangl2* have been shown to be sufficient for loss of polarization (Bailly et al. 2018). Further, Vangl2 has no known roles outside of PCP, and thus phenotypes in *vangl2* loss of function studies can be directly attributed to disrupted PCP.

To support a model in which PCP regulates closure of the SOS, it was necessary to establish expression patterns of *vangl2*. *In situ* hybridization using a probe for *vangl2* shows ubiquitous expression in whole embryos at 24 hpf as well as expression in ocular tissues (**Figure 3.6**). This result is expected as epithelial tissues are planar polarized and PCP is involved in convergence and extension movements required for elongation of the embryonic axis, and thus *vangl2* expression is required in most tissues at this time point. This data is supported by published *in situ* hybridization data which show similar *vangl2* expression patterns in zebrafish embryos at the 16-somite stage, including strong expression in the optic vesicle (Park and Moon 2002). Similar to zebrafish expression, *Vangl2* is expressed throughout the CNS in mouse embryos and in the optic stalk at E9.5 (Kibar et al. 2001). Given these expression patterns, Vangl2-mediated PCP was a good candidate to further explore the involvement of PCP in ocular development regarding closure of the SOS.

A previously published MO designed to block translation of maternal and zygotic transcripts was used for functional knockdown of *vangl2* (Park and Moon 2002). This study showed CE defects, with zebrafish embryos having somites that are shortened and laterally widened, and loss of *vangl2* expression was confirmed through western blot analysis. In the current study, some embryos that received a high dosage (>5ng) of *vangl2* MO had mild to severe decrease in interocular distance with a few embryos displaying interocular fusion and cyclopia (**Figure 3.8**), although the penetrance of this phenotype was not quantified. This effect of loss of PCP has been reported (Marlow et al. 1998), and is attributed to defective anterior migration of the prechordal plate due to decreased CE during gastrulation. The prechordal plate expresses *shh*, which inhibits eye-specification in the center anterior ectoderm. When the prechordal plate does not migrate sufficiently to contact the ectoderm, the eye field fails to separate into two lobes, resulting in formation of one central eye. The *vangl2* MO was titrated to find an appropriate dose that gives stereotypical PCP defects and reflects published phenotypes of *vangl2* loss of function without inducing the off-target

effects of tissue necrosis or cardiac edema. A dosage of 3 ng satisfied this requirement. Injection of 3 ng of *vangl2* MO resulted in SOS closure delay (27.5 +/- 3.3%, n = 213) compared to control morphants (6.9 +/- 3.2%, n=186; p<0.0001), indicating a role for PCP in closure of the SOS (**Figure 3.7**).

For a more robust model of PCP abrogation, I obtained the *trilobite* (*tri*^{tk50f}) zebrafish line, which originates from an ENU mutagenesis screen (Haffter et al. 1996). This line carries a *vangl2* loss of function mutation that was initially described as a deletion in the coding sequence that results in no detectable transcript, but the exact deletion has not been characterized (Jessen et al. 2002). The deletion was not characterized for this project as this line has been widely used to study the role of PCP in development and has been shown to result in a complete loss of PCP. Further, molecular techniques were not required to genotype this line because homozygous mutant embryos have a striking PCP phenotype, which allows for genotyping of heterozygous adults through test crosses, and sorting of embryos during experiments.

Heterozygous *vangl2* fish were crossed and the resulting clutches were grown to 28 hpf. Because *vangl2* mutant embryos experience developmental delays, this was controlled for by separating mutant embryos from their WT siblings around 22 hpf, once morphological differences allowed for easy sorting (**Figure 3.9**). Both groups of embryos were staged at 28 hpf by the presence of circulating blood cells, rather than by time post fertilization, to account for developmental delays. The *vangl2* mutant embryos had a shortened AP axis (**Figure 3.9**) phenocopied by the *vangl2* morphants. As with the MO knockdown experiment, *vangl2* mutants show SOS closure delays at 28 hpf (*vangl2*$^{-/-}$: 34.5 +/- 5.9%, n=266 ; WT sib: 2.2 +/- 0.5%, n=276; p<0.0001; **Figure 3.10**), supporting the hypothesis that PCP is required for proper SOS closure.

Because PCP is required for embryonic development, *vangl2* morphant and mutant embryos are not viable past five days, which is mostly attributable to an inability to swim. As such, it was not possible to grow mutant fish to adulthood to screen for superior coloboma. However, it was observed that experimental *vangl2* morphants and mutants showed no open SOS after approximately 48 hpf. This calls into question whether the SOS closure delay

phenotype is due to developmental delay rather than disruption to a key developmental process that regulates SOS closure. Although developmental delay was controlled for through careful staging, it is possible that the dramatic loss of PCP phenotype obscured efforts to properly stage embryos at 28 hpf.

3.6 Laminin IHC indicates a higher penetrance of SOS closure delays

The two lobes of the SOS are separated by a lining of laminin when the sulcus is open, and as the sulcus closes through cellular rearrangements the basal lamina is reorganized to be in line with the rest of the ocular cup, appearing as a disappearance of the sulcus (Hocking et al. 2018). Laminin-lining of the open SOS allows for a simple assay to determine closure defects – immunostaining for laminin and examination by confocal microscopy. Although initial scoring of *vangl2* mutants was done by viewing 28 hpf embryos on a stereomicroscope, this method is not completely reliable as the SOS does not always appear as a clear separation in the dorsal optic cup and at times it is necessary to use "best judgement" to score embryos. Laminin IHC was used as a more accurate scoring method for SOS closure delay in *vangl2* mutant embryos. Laminin IHC of *vangl2* mutant embryos at 28 hpf confirmed that embryos scored SOS positive under the stereoscope have open SOS (**Figure 3.11**). Consistent with the above experiments, 28 hpf *vangl2* mutant embryos (67.2 +/- 2.8%, n=73) showed increased incidence of laminin staining in the dorsal optic cup compared to WT siblings (12.8 +/- 6.4%, n=68; $p<0.0001$; **Figure 3.12**), indicating that loss of *vangl2* results in SOS closure defects.

Scoring of SOS through laminin IHC shows a higher proportion of both mutant and WT embryos with open SOS than scoring stereoscopically. This could be due to several factors. Scoring with a stereoscope may not be sensitive enough to detect open SOS unless the embryo has a more severe defect, rather than a simple closure delay. This was the main concern with the stereoscope method that necessitated using laminin IHC to score embryos. While previous characterization indicates that the open SOS is laminin lined, the time course of laminin disappearance due to cellular rearrangements was not examined. It is possible that laminin lining is present in the dorsal eye after closure of the SOS, inflating numbers of SOS positive embryos. It is more likely that this method is more sensitive to closure defects and

is thus gives more accurate data than stereoscopic scoring. However, this method is time consuming and low throughput, and is best implemented after SOS closure delays have been detected through stereoscopic scoring.

3.7 Loss of PCP does not affect dorsal/ventral patterning of the optic cup

Proper eye development requires patterning of the ocular cup. D/V patterning of the optic cup is achieved through a balance of dorsal BMP signalling and ventral Shh signalling. A previous study of the SOS indicated that D/V patterning of the optic cup is required for closure of the sulcus, and that ventralization of the optic cup delays SOS closure (Hocking et al. 2018). Disruption of D/V patterning was hypothesized to be the mechanism through which PCP regulates closure of the SOS. To test this hypothesis, *vangl2* mutant and WT embryos were examined for changes in D/V patterning by in situ hybridization using probes for the dorsal marker, *tbx5a*, and the ventral marker, *vax2*. No differences were observed in the expression boundaries or intensity of either marker (**Figure 3.13**), failing to indicate regulation of optic cup patterning by non-canonical Wnt signalling.

3.8 BMP signalling does not regulate *vangl2* expression

Previous work in our lab investigated the *gdf6a* in DV patterning of the optic cup and in regulation of SOS closure (French et al. 2009; French et al. 2013; Hocking et al. 2018). As part of these investigations, whole 24 hpf *gdf6a* morphant zebrafish embryos were used for microarray analysis of gene expression, although this data remains unpublished. This data showed a two-fold decrease in *vangl2* expression, indicating a link between the regulation of BMP and PCP signalling. This data is significant to the current project because it suggests that the SOS closure delays seen in PCP-morphants and mutants could be recapitulating an effect seen in BMP signalling-deficient embryos. It has been clearly shown that proper D/V patterning is necessary for closure of the SOS, and it is possible that a downstream effect of this patterning is induction of PCP.

To investigate the link indicated by the microarray data, *vangl2* expression patterns were examined in BMP-signalling deficient embryos though *in situ* hybridization. To inhibit BMP signalling, zebrafish embryos were exposed to the dorsomorphin analogue, DMH1.

DMH1 is a specific inhibitor of BMP signalling through binding of BMP Type 1 receptors (Hao et al. 2010). DMH1 treatment causes ventralization of the optic cup and SOS closure defects and is thus an adequate treatment to analyze the effect of loss of BMP signalling on *vangl2* expression. Embryos treated with DMH1 did not show a significant change in *vangl2* expression and had ubiquitous staining as seen in DMSO control embryos (**Figure 3.14**). Further, there was no detectable decrease in staining intensity throughout the DMH1 treated embryos. These data indicate that DMH1 inhibition of BMP signalling does not affect the expression of *vangl2*. However, it is called into question how sensitive *in situ* hybridization is as a measure of gene expression, and whether this method would be able to show a two-fold decrease in whole embryo expression. Another source of error with this experimental design is the method of BMP-inhibition. While DMH1 treatment is well characterized, both in terms of BMP-inhibition and causation of SOS closure defects, the initial data showing decreased *vangl2* expression did not use DMH1 treatment, but rather loss of a BMP ligand. It is possible that Gdf6a signals through several receptors and not just BMP Type 1 receptors. Further, it is possible that the DMH1 treatment was ineffective, as there was no positive control for this experiment. A control that would have helped support the *in situ* hybridization data would be to verify that the DMH1 treatment had effectively inhibited BMP signalling. This would be done by either screening DMH1 treated embryos for open SOS at 28 hpf, or by doing an additional in situ hybridization using a probe for *tbx5a* to verify previous phenotypes associated with DMH1 treatment. As is, this experiment does not indicate that PCP is regulated by BMP signalling during ocular development.

3.9 Tables

Table 3.1. Polarity-related genes identified through WES of Superior Coloboma patients. Variants were rescreened through in silico algorithms to identify mutations that are likely deleterious, and the population frequency of each variant was determined from the ExAC database. This analysis indicates variants one AB polarity gene, and six PCP related genes. From these genes, *SHROOM3, FZD4*, and *SCRIB* were further analysed through MO knockdown experiments to determine whether loss of function results in SOS closure defects.

Patient	Gene	Type	Variant	MutationTaster	Polyphen-2	Sift	ExAC frequency
1	*FZD4*	Nonsynonymous SNV	NM_012193:c.G477A:p.M159I	0.9999999 Disease causing	0.568 Possibly damaging	0.19 Tolerated	Not found in database
1	*FAT2*	Nonsynonymous SNV	NM_001447:c.T1331C:p.V444A	0.9999999 Disease causing	0.966 Probably damaging	0.00 Affect protein function	0.01737
3	*SHROOM3*	Nonsynonymous SNV	NM_020859:c.A2834T:p.D945V	0.99999998 Disease causing	1.000 Probably damaging	0.00 Affect protein function	3.499e-04
4	*SCRIB*	Nonsynonymous SNV	NM_015356:c.G571A:p.D191N	0.999999 Disease causing	1.000 Probably damaging	0.07 Tolerated	5.9e-05
5	*CELSR2*	Nonsynonymous SNV	NM_001408:c.A3800G:p.H1267R	0.999947299 Disease causing	0.992 Probably damaging	0.30 Tolerated	8.036e-03

5	*WNT9B*	Nonsynonymous SNV	NM_003396:c.C555A:p.D185E	0.99999807 Disease causing	1.000 Probably damaging	0.81 Tolerated	2.756e-04
5	*FAT4*	Nonsynonymous SNV	NM_024582:c.C12064T:p.R4022W	0.98744266 Disease causing	0.999 Probably damaging	0.02 Affect protein function	4.252e-03

3.10 Figures

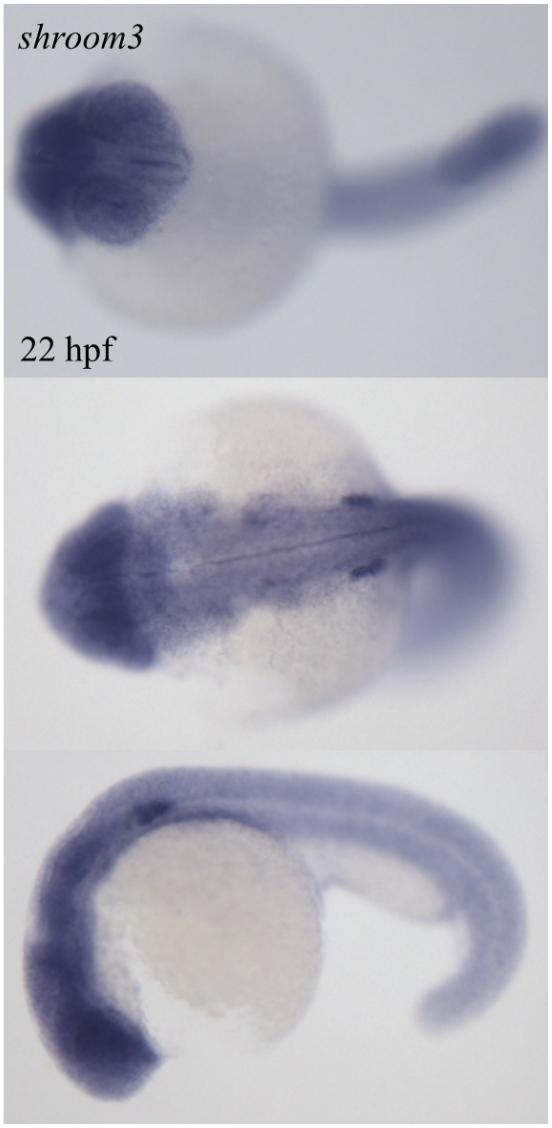

Figure 3.1. *In situ* hybridization of zebrafish embryos using a probe for *shroom3*. Because *SHROOM3* variant analysis indicated a potentially deleterious allele, this gene was further investigated in the causation of superior coloboma. *In situ* hybridization was used to determine whether *shroom3* is expressed in the eye during SOS closure.At 22 hpf, WT embryos were fixed in 4% PFA. After fixation, embryos were stained for *shroom3* expression using *in situ* hybridization. Embryos were mounted in methylcellulose and imaged stereoscopically in anterior, dorsal, and lateral view to examine *shroom3* expression patterns. *shroom3* expression is found in the kidneys and anterior neural tissue, including the eyes.

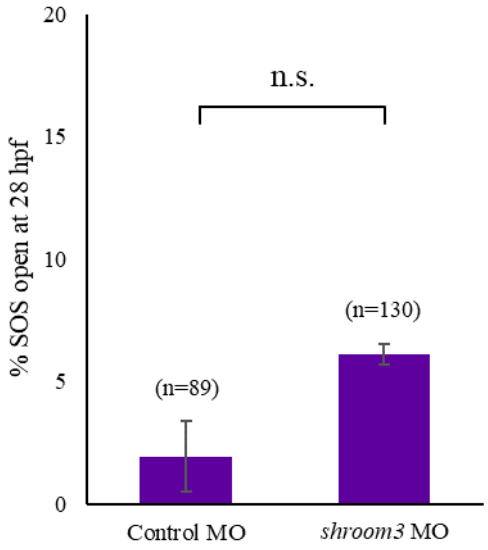

Figure 3.2. Injection of *shroom3* splice blocking MO does not cause significant SOS closure delay. Knockdown of *shroom3* expression was used to determine whether the gene is required for closure of the SOS.WT embryos were injected at the one-cell stage with 5 ng of *shroom3* translation blocking or control MO. At 28 hpf, embryos were examined stereoscopically for the presence of an open SOS. There was no significant increase is SOS closure delays in *shroom3* morphant embryos, indicating that this gene is not required for SOS closure. Data are means ± SEM. N=3 experiments, n = total embryos scored. Statistics are the two-tailed Fisher's Exact Test. n.s., not significant.

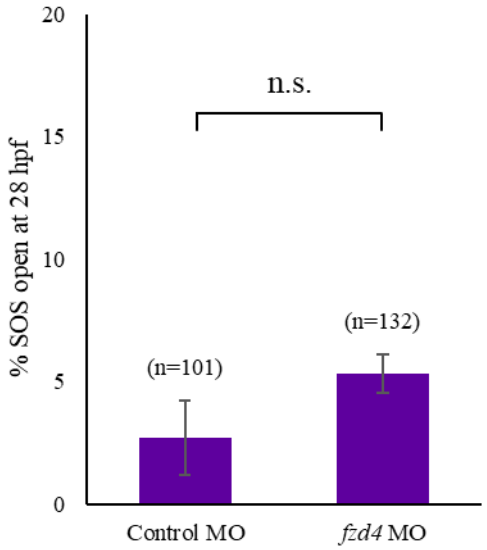

Figure 3.3. Knockdown of *fzd4* expression in zebrafish embryos does not cause significant superior ocular sulcus closure delays. Because *FZD4* variant analysis indicated a potentially deleterious allele, this gene was further investigated in the causation of superior coloboma. Knockdown of *fzd4* expression was used to determine whether the gene is required for closure of the SOS. WT embryos were injected at the one-cell stage with 12 ng of *fzd4* translation blocking or control MO. At 28 hpf, embryos were examined stereoscopically for the presence of an open SOS. There was no significant increase is SOS closure delays in *fzd4* morphant embryos, indicating that this gene is not required for SOS closure. Data are means ± SEM. N=3 experiments, n = total embryos scored. Statistics are the two-tailed Fisher's Exact Test. n.s., not significant.

Figure 3.4. *scrib* morphants show moderate gastrulation defects. Because *SCRIB* variant analysis indicated a potentially deleterious allele, this gene was further investigated in the causation of superior coloboma. Injection of 4 ng of MO was used to knockdown *scrib* expression. At 28 hpf, *scrib* morphants have a shortened A/P axis, as is seen in other PCP morphant and mutant embryos, indicating successful knockdown of *scrib* and abrogation of PCP.

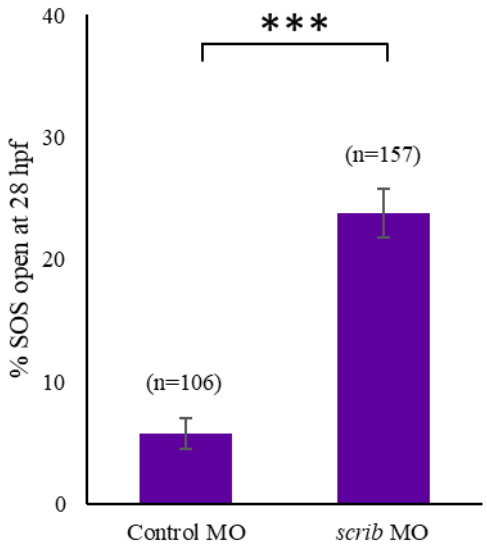

Figure 3.5. Knockdown of *scrib* increases incidence of superior ocular sulcus closure delay. Knockdown of *scrib* expression was used to determine whether the gene is required for closure of the SOS. WT embryos were injected at the one-cell stage with 4 ng of *scrib* translation blocking or control MO. At 28 hpf, embryos were examined stereoscopically for the presence of an open SOS. There was a significant increase is SOS closure delays in *scrib* morphant embryos, indicating that this gene is required for SOS closure, and that PCP may be involved in this process. Data are means ± SEM. N=3 experiments, n = total embryos scored. Statistics are the two-tailed Fisher's Exact Test. ***p>0.001.

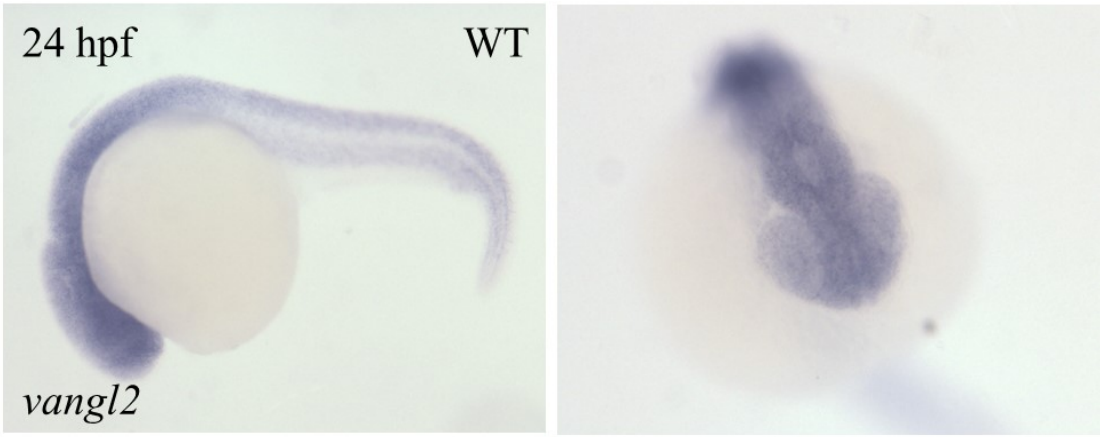

Figure 3.6. *vangl2* is ubiquitously expressed throughout the embryo, with strong staining in the anterior neural tissue. The core PCP component, Vangl2, was used to further investigate the role of PCP in SOS closure. *In situ* hybridization was used to determine expression patterns of *vangl2* in zebrafish embryos. WT embryos were fixed at 24 hpf and *in situ* hybridized using a probe for *vangl2*. After *in situ* hybridization, embryos were mounted in methylcellulose and imaged under a stereoscope in lateral and anterior/dorsal view. *vangl2* is expressed through the whole embryo, with stronger staining in the anterior neural tissue. Importantly, *vangl2* is expressed in the ocular tissues, and may thus be involved in eye development.

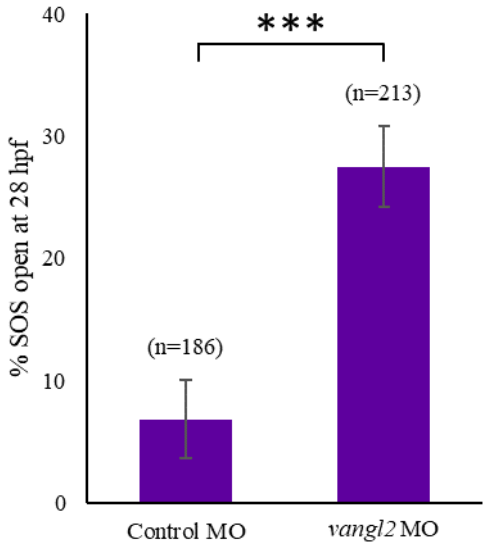

Figure 3.7. Knockdown of *vangl2* increases incidence of superior ocular sulcus closure delay. Knockdown of *vangl2* expression was used to determine whether PCP is required for closure of the SOS. WT embryos were injected at the one-cell stage with 3 ng of *vangl2* translation blocking or control MO. At 28 hpf, embryos were examined stereoscopically for the presence of an open SOS. There was a significant increase is SOS closure delays in *vangl2* morphant embryos, indicating that PCP is required for SOS closure. Data are means ± SEM. N=3 experiments, n = total embryos scored. Statistics are the two-tailed Fisher's Exact Test. ***p>0.001.

Figure 3.8. Embryos injected with high dosages of *vangl2* MO show decreased interocular distance. *vangl2* morphant embryo were examined after injection of 6 ng of MO to screen for PCP-related phenotypes. Some embryos presented with decreased interocular distance, which is a less severe form of cyclopia. This phenotype has been previously characterized in PCP mutant zebrafish embryos and indicates the MO is sufficient to knockdown PCP. Some embryos showed fusion of the optic cup (black arrow). Penetrance of this phenotype was not quantified but the phenotypes appeared in only a few embryos.

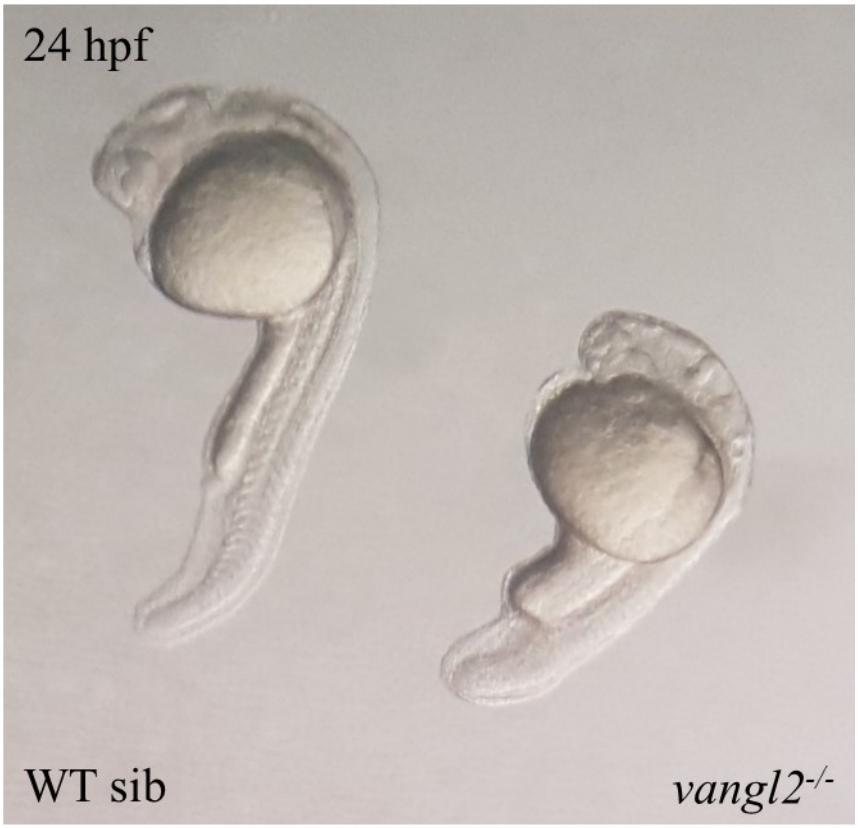

Figure 3.9. *vangl2* mutant embryos have distinct gastrulation defects. To provide a more reliable PCP loss of function model, a well characterized strain of *vangl2* mutant zebrafish was used for further investigations into the role of PCP in SOS closure. Mutants have a shortened AP axis and are widened laterally. This phenotype allows for identification of mutants and WT sibling without using molecular methods to genotype embryos. Embryos from *vangl2* heterozygote incrosses were sorted based on embryo phenotype prior to SOS scoring or laminin IHC.

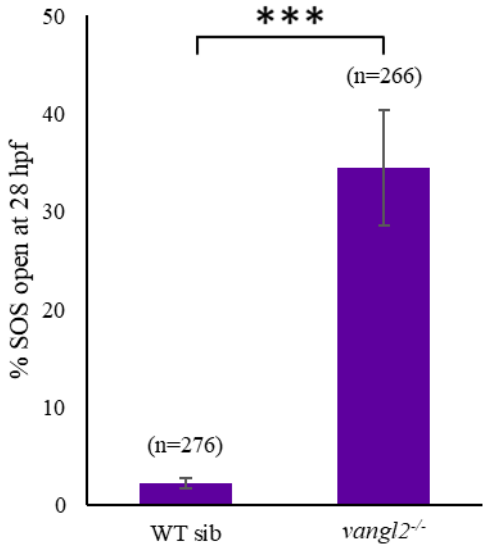

Figure 3.10. Knockout of *vangl2* increases incident of superior ocular sulcus closure delay. Knockout of *vangl2* expression was used to determine whether PCP is required for closure of the SOS. Embryos homozygous for a *vangl2* loss of function allele were examined stereoscopically for the presence of an open SOS at 28 hpf. There was a significant increase is SOS closure delays in *vangl2* mutant embryos, indicating that PCP is required for SOS closure. Data are means ± SEM. N=3 experiments, n = total embryos scored. Statistics are the two-tailed Fisher's Exact Test. ***p>0.001.

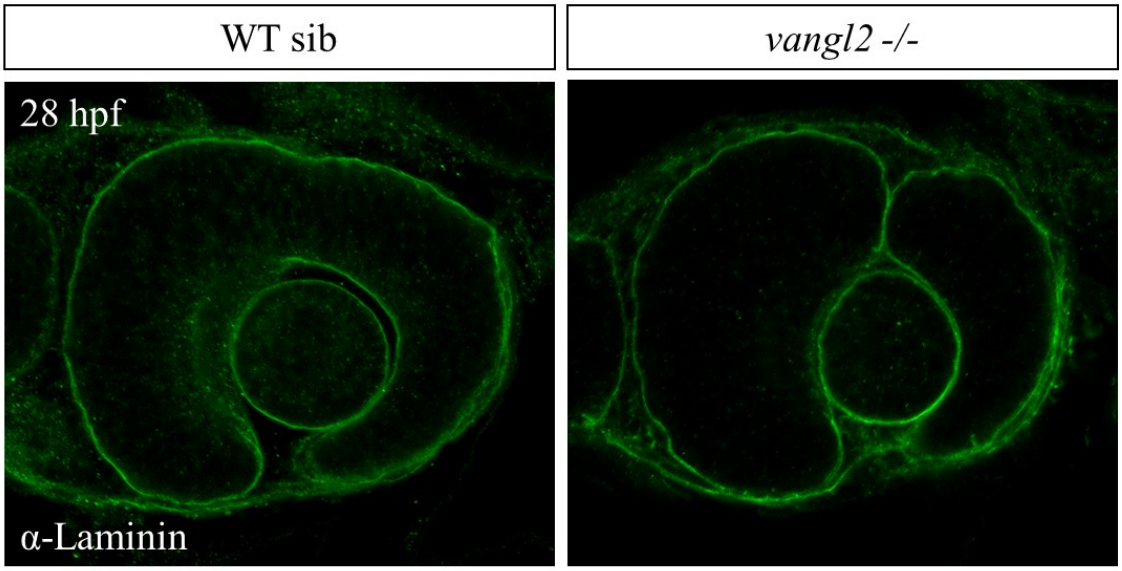

Figure 3.11. Laminin IHC shows staining in the dorsal optic cup of 28 hpf *vangl2* mutant embryos. Laminin staining of *vangl2* mutant embryos was used as a more robust method of screening for SOS closure defect. Embryos homozygous for a *vangl2* loss of function allele and WT embryos were fixed at 28 hpf and IHC was used to fluorescently stain laminin. Eyes were microdissected and mounted in pairs for confocal imaging. SOS were easily identified by staining in the dorsal optic cup.

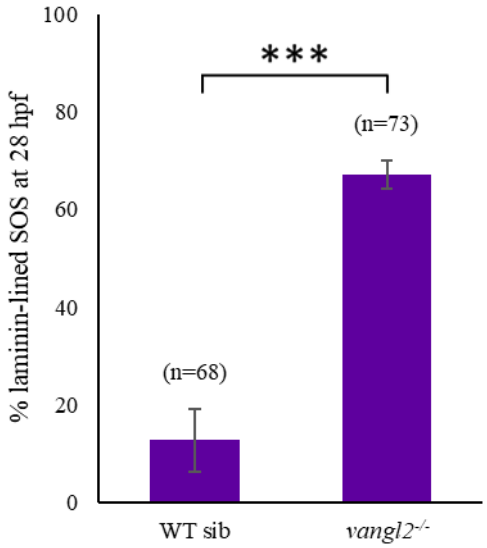

Figure 3.12. Scoring of *vangl2* mutant zebrafish embryos for an open superior ocular sulcus by the presence of laminin indicates higher incidence of closure delay. Laminin IHC was used to provide a more accurate measure of SOS closure delays in *vangl2* mutant embryos. Embryos homozygous for a *vangl2* loss of function allele were fixed at 28 hpf and IHC was used to fluorescently stain laminin. Eyes were microdissected and mounted in pairs for confocal examination. An embryo was scored as SOS positive if one or both eyes presented with clear laminin staining in the dorsal eye. There was a significant increase is SOS closure delays in *vangl2* mutant embryos, indicating that PCP is required for SOS closure. Further the percentage of SOS delays was much higher using laminin IHC than stereoscopic scoring, indicating a higher rate of SOS closure delay than previously measured. Data are means ± SEM. N=3 experiments, n = total embryos scored. Statistics are the two-tailed Fisher's Exact Test. ***p>0.001.

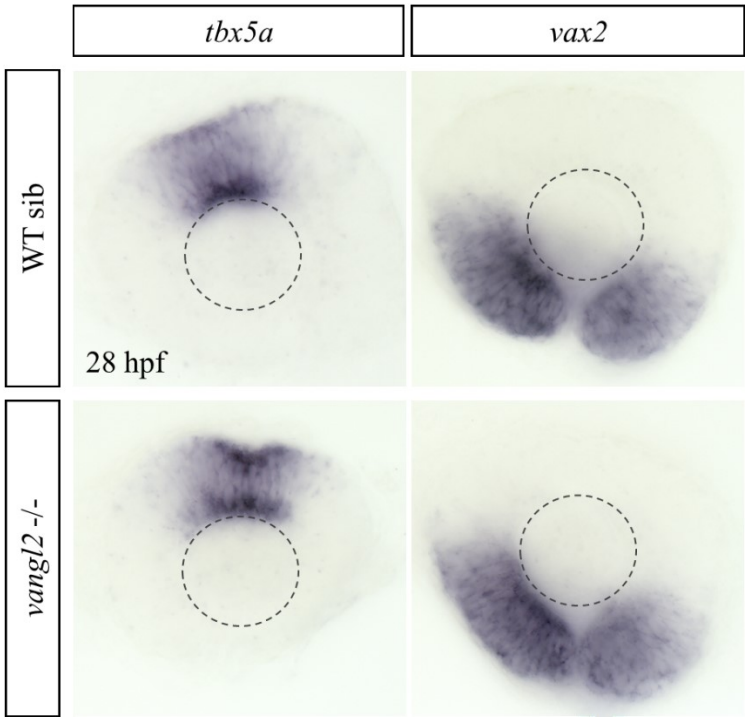

Figure 3.13. Loss of PCP through *vangl2* knockout does not disrupt dorsal/ventral patterning in the optic cup**.** Previous studies in our lab indicate abberant DV patterning as causitive of SOS closure defects. *In situ* hybridization was used to determine whether the *vangl2* mutant embryos have disrupted DV patterning. Embryos homozygous for a *vangl2* loss of function allele and WT embryos were fixed at 28 hpf, then *in situ* hybridized using a probe for either *tbx5a* or *vax2*. After *in situ* hybridization, embryos were sunk through glycerol, and microdissected eyes were mounted for DIC imaging. Mutant and WT embryos show similar expression patterns of the dorsal and ventral markers, indicating that *vangl2* does not regulate DV patterning and that SOS closure delays in these embryos is caused through a different mechanism. Dashed circles outline lenses.

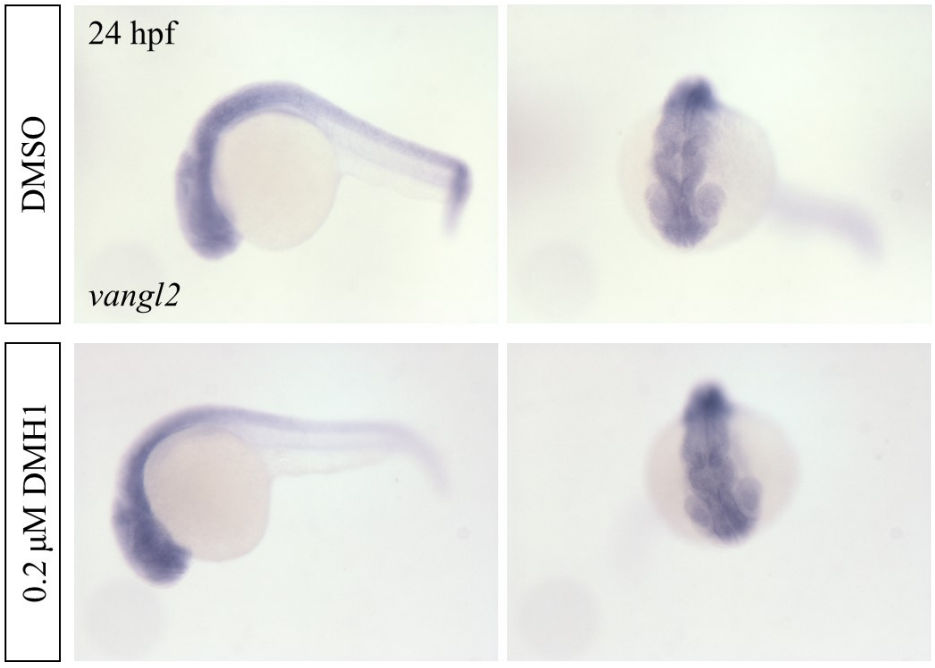

Figure 3.14. Pharmacological inhibition of BMP signalling does not change *vangl2* expression patterns. Previous unpublished microarray data from our lab indicated decreased *vangl2* expression in whole 24 hpf embryos with disrupted BMP signalling. DMH1 treatment was used to pharmacologically inhibit BMP signalling to determine whether BMP signalling regulates *vangl2* expression patterns. WT embryos were treated with the BMP inhibitor DMH1 or DMSO at 10 hpf and fixed at 24 hpf. Embryos were *in situ* hybridized using a probe for *vangl2*. Embryos were placed in methylcellulose and imaged under a stereoscope in lateral and dorsal view. No differences were observed in *vangl2* expression patterns between DMH1-treated and control embryos, indicating that BMP signalling does not regulate *vangl2* expression patterns.

Chapter 4: Visualization of the Superior Ocular Sulcus during *Danio rerio* Embryogenesis

A version of this chapter has been published: Yoon K, Widen S, Wilson M, Hocking JC, Waskiewicz AJ (2019). Visualization of the Superior Ocular Sulcus during *Danio rerio* Embryogenesis. Journal of Visualized Experiments 145: 1-8. https://www.jove.com/video/59259/visualization-superior-ocular-sulcus-during-danio-rerio

4.1 Introduction

The formation of the vertebrate eye is a highly conserved process in which carefully orchestrated intercellular signaling pathways establish tissue types and specify regional identity (Chow and Lang 2001). Perturbations to early eye morphogenesis result in profound defects to the architecture of the eye and are frequently blinding (Slavotinek 2011). One such disease results from the failure to close the choroid ocular fissure in the ventral side of the optic cup (Gregory-Evans 2004). This disorder, known as ocular coloboma, is estimated to occur in 1 out of 4-5000 live births and cause 3-11% of pediatric blindness, commonly manifesting as a keyhole-like structure that protrudes inferiorly from the pupil in the center of the eye (Onwochei et al. 2000; Chang et al. 2006; Williamson and FitzPatrick 2014). The function of the choroid fissure is to provide an entry point for early vasculature growing into the optic cup, after which the sides of the fissure will fuse to enclose the vessels (Kaufman et al. 2015).

While ocular coloboma has been known since ancient times, we have recently identified a novel subset of coloboma patients with tissue loss affecting the superior/dorsal aspect of the eye. Recent work in our lab has led to the discovery of an ocular structure in the zebrafish dorsal eye, which we refer to as the superior ocular sulcus (SOS) or superior fissure (Hocking et al. 2018). It is important to note that the structure has characteristics of both a sulcus and a fissure. Similar to a sulcus, it is a continual tissue layer that spans from the nasal to the temporal retina. In addition, the closure of the structure is not mediated by a fusion of the two opposing basement membrane, and it appears to require a morphogenetic process by which the structure is populated by cells. However, similar to a fissure, it forms a structure that separates the nasal and temporal sides of the dorsal eye with the basement membrane. For consistency, we will refer to it as SOS in this text.

The SOS is evolutionarily conserved across vertebrates, being visible during eye morphogenesis in fish, chick, newt, and mouse (Hocking et al. 2018). In contrast to the choroid fissure, which is present from 20-60 hours post-fertilization (hpf) in zebrafish, the SOS is highly transient, being easily visible from 20-23 hpf and absent by 26 hpf (Hocking et al. 2018). Recent research in our lab has found that, similar to the choroid fissure, the SOS

plays a role in vascular guidance during eye morphogenesis (Hocking et al. 2018). Although the factors that control the formation and closure of the SOS are not yet fully understood, our data did highlight roles for dorsal-ventral eye patterning genes (Hocking et al. 2018).

Zebrafish is an excellent model organism to study the SOS. As a model system, it provides a number of advantages in studying eye development: it is a vertebrate model; each generation exhibits high fecundity (~200 embryos); its genome has been fully sequenced, which facilitates genetic manipulation; and approximately 70% of human genes have at least one zebrafish orthologue, making it an ideal genetics-based model of human disease (Lawson and Wolfe 2011; Howe et al. 2013). Most importantly, its development takes place externally to the mother, and its larvae are transparent, which allows for the visualization of the developing eye with relative ease (Bilotta and Saszik 2001).

In this set of protocols, we describe the techniques through which the SOS can be visualized in zebrafish larvae. The variety of visualization techniques used in this report will allow clear observation of the SOS during normal eye development, as well as the ability to detect SOS closure defects. Our example protocols will feature investigations of Gdf6, a BMP localized to the dorsal eye and known regulator of SOS closure. Further, these techniques can be combined with experimental manipulations to identify genetic factors or pharmacological agents that affect proper SOS formation and closure. In addition, we have included a protocol through which the fluorescent imaging of all cell membranes is possible, allowing the experimenter to observe morphological changes to the cells surrounding the SOS. Our goal is to establish a set of standardized protocols that can be used throughout the scientific community to offer new insights into this novel structure of the developing eye.

4.2 Protocols

Protocol 1: **Visualization of SOS using stereomicroscopy and differential interference contrast (DIC) imaging**

1. Embryo collection
    1. In a tank of dechlorinated water, prepare crosses of *gdf6a*$^{+/-}$ zebrafish in the evening by pairing a male zebrafish with a female zebrafish. Be sure to

separate the male from the female by using a divider to ensure that the embryos are born within a small range of time.

2. The following morning, pull the divider and allow the zebrafish to breed for no longer than 30 min. Collect the embryos in Petri dishes with E3 media, described in The Zebrafish Book (Westerfield 2000), and place them in a 28.5 °C incubator.
3. Remove any unfertilized eggs or dead embryos, which will appear white and opaque.

2. Preparation and live-imaging of zebrafish embryos
    1. At 20 hpf, replace the E3 media with E3 media containing 0.004% 1-phenyl 2-thiourea (PTU) to prevent pigment production. NOTE: Addition of PTU at a slightly later timepoint, such as 22-24 hpf, is unlikely to interfere with the experiment due to the early age of the embryos at the time of imaging. However, it is recommended to treat the embryos early to completely prevent pigmentation as there is a band of pigmentation that appears in the dorsal eye, which can interfere with the imaging of the SOS.
    2. Ensure that all embryos are at the correct developmental stages at various points leading up to the time of observation. It is recommended that this is done at the stages at which somite number is clearly visible as outlined by Kimmel et al. (1995). Remove those that are developmentally immature.
    3. Place the embryos under a dissecting microscope, and dechorionate the embryos by gently pulling apart the chorion using fine forceps. Visualize the SOS in the dorsal eye. The SOS may appear as an indentation at the dorsal margin of the eye, and a line should be visible across the dorsal eye. For normal SOS closure, observe the embryos at around 20-23 hpf. For examination of delayed SOS closure phenotypes, observe the embryos at 28 hpf or later.
    4. Sort the embryos that show SOS closure delay from those that do not.
    5. To photograph these embryos using a dissecting microscope, prepare a Petri dish containing 1% agarose in E3. Lightly prick the center of the agarose to

create a shallow hole in which the yolk of the embryo can sit when the embryo is placed on the agarose. This will ensure that the embryo is not at an oblique angle when being photographed.

6. Anesthetize embryos with 0.003% tricaine in E3 and place laterally on the agarose.
7. To image the embryos using a compound or confocal microscope, transfer the embryo into 35 mm Petri dish containing a small bolus of non-gelled 1% low-melting point agarose in E3 (w/v). Quickly position the embryo laterally using a fine fishing line or an eyelash and wait for the agarose to cool. Once the agarose is firm, pour enough E3 into the dish to cover the agarose. For more details, see Distel and Köster (2007). NOTE: If using an inverted microscope, the embryo can be placed against the glass of a glass-coverslip-bottom dish and imaged with a standard 20X objective lens.
8. Use a water immersion 20x objective lens to visualize the SOS with a compound microscope. Following visualization, gently pull the agarose from the embryos and fix in 4% paraformaldehyde (PFA) or allow to continue their development.

Protocol 2: **Whole-mount immunofluorescent staining of laminin**

1. Whole-mount immunofluorescent staining of laminin: Day 1
    1. Dechorionate embryos as described in Step 1.2.3, if not already done. Fix embryos in a microcentrifuge tube at the desired timepoint in freshly made 4% PFA for 2 h on a room temperature (22-25 °C) shaker. Wash in 1x PBST for 5 min, four times. NOTE: Following gastrulation, embryos may fix better after dechorionation.
    2. Permeabilize embryos in 10 mg/mL proteinase K at room temperature for 5 min. Incubation time will depend on the developmental stage at which the embryos are fixed (see Thisse and Thisse, 2005).
    3. Wash in 1x PBST for 5 min, four times.

4. Block embryos in a solution of 5% goat serum and 2 mg/mL bovine serum albumin (BSA) in 1xPBST for 1-2 h on a room temperature shaker.
5. Prepare primary antibody solution by diluting rabbit anti-laminin antibody in block solution at a 1:200 dilution.
6. Incubate the embryos in anti-laminin primary antibody overnight on a 4 °C shaker.

2. Whole-mount immunofluorescent staining of laminin: Day 2
    1. Wash in 1x PBST for 15 min, five times.
    2. Prepare secondary antibody solution by diluting goat anti-rabbit Alexa Fluor 488 antibody in 1x PBST to a dilution of 1:1000. NOTE: It is possible to adapt this step to suit the resources available to the experimenter by using a different secondary antibody.
    3. Incubate the embryos in secondary antibody overnight on a 4 °C shaker. Shield from light as much as possible from this step onwards.
    4. Wash in 1x PBST for 15 min, four times. The embryos can be stored at 4 °C for up to a week, if necessary.
3. Dissection and mounting of embryonic eyes
    1. If desired, place the embryos in a small Petri dish and deyolk the embryos in 1x PBST. Do this by gently disrupting the yolk with fine forceps and removing the yolk cells through mild scraping of the yolk sac.
    2. Prepare the following concentrations of PBS-glycerol series solutions in microcentrifuge tubes: 30%, 50%, and 70% glycerol in PBS. Transfer embryos into 30% glycerol/PBS, making sure to place the embryos on top of the solution and transferring as little of the previous solution as possible. Wait for the embryos to sink to the bottom of the tube.
    3. When embryos have sunk to the bottom, transfer them to 50% glycerol/PBS. Repeat and transfer to 70% glycerol/PBS.
    4. Once the embryos have sunk in 70% glycerol/PBS, move them to a small plastic dish for dissections.

5. Sever the embryo posterior to the hindbrain, and use the posterior tissue for genotyping, if necessary.
6. Move the head to a glass slide, transferring as little glycerol as possible. Use forceps or other fine dissection tools to hold onto the posterior end to keep the head stationary. Use a fine minutien pin or other fine dissection tools to gently insert into the forebrain ventricle from the anterior and push downward to separate the right and left halves of the head from each other. Repeat this while moving posteriorly through the midbrain and into the hindbrain ventricle, essentially fileting the head down the midline. This minimizes manual manipulation of the eye and surrounding tissue, thereby leaving the SOS undamaged.
7. Mount each side of the head midline down, eye up. Position four posts of vacuum grease at the corners (an appropriate distance apart for the coverslip being used) and cover with a glass coverslip, pushing down sequentially on each post until the coverslip makes contact with the samples. Pipette 70% glycerol at the edge of the coverslip so that the glycerol is pulled underneath, filling the space between the coverslip and the slide.
8. Image samples within a day, or seal around the coverslip with nail polish and image samples only after the nail polish has dried. Store in the dark at 4 °C.

Protocol 3: **Visualization of SOS using eGFP-CAAX mRNA**

1. Synthesis of eGFP-CAAX mRNA
    1. Linearize 1 mg of pCS2-eGFP-CAAX plasmid (Kwan et al. 2012) with NotI in a reaction volume of 40 mL for 4 hours at 37 °C.
    2. To stop the restriction digest reaction, add 10 mL RNase-free water, 2.5 mL 10% SDS and 2.0 mL 10 mg/mL Proteinase K.
    3. Incubate 1 hour at 50 °C.
    4. Add the following to the reaction (total volume 200 mL) and proceed to next step: 50 mL RNase-free water, 20 mL 3 M sodium acetate pH 5.2 and 75.5

mL RNase-free water. NOTE: RNase-free water is added in two separate occasions to prevent excessive dilution of the sodium acetate.

2. Purification of DNA through phenol/chloroform extraction and ethanol precipitation
    1. Add 200 mL phenol:chloroform:isoamyl alcohol and vortex for 20 s. Separate the aqueous and organic phases through centrifugation at 18,000 x g for 5 min.
    2. Transfer the upper aqueous layer to a new microcentrifuge tube, making sure to avoid the transfer of the bottom organic layer. Add an equal volume of chloroform to the new tube.NOTE: Addition of chloroform is optional, but it is recommended to ensure complete removal of phenol from the sample.
    3. Vortex for 20 s. Separate the aqueous and organic phases through centrifugation at 18,000 x g for 5 min.
    4. As before, transfer the upper aqueous layer to a new microcentrifuge tube, making sure to avoid the transfer of the bottom organic layer.
    5. Add 1/10 volume of 3 M sodium acetate pH 5.2.
    6. Precipitate DNA by adding 3 volumes of 100% RNase-free ethanol and chill at -20 °C for 15 min. Centrifuge at 18,000 x g for 20 min at 4 °C. A pellet should be visible. Decant the supernatant.
    7. Wash the pellet with 100 mL of cold 70% ethanol/RNase-free water. After gently mixing to break the pellet loose, centrifuge at 18,000 x g for 15 min at 4 °C. A pellet should be visible. Decant the supernatant.
    8. Air-dry the pellet for 5 min and resuspend the DNA in 7 mL water. NOTE: The pellet may need to be dried for longer than 5 min depending on the airflow available.
3. Transcription and purification of eGFP-CAAX mRNA
    1. In an RNase-free manner, prepare an in vitro transcription reaction with a commercially available Sp6 RNA polymerase kit, using about 1 mg of purified linearized plasmid DNA obtained in Step 3.2. Incubate for 2 h at 37 °C. NOTE: Sp6 RNA polymerase must be used for the production of capped mRNA.
    2. Add 1 mL of DNase (2 U/mL; RNase free) and incubate for 30 min at 37 °C.

3. Purify the mRNA with any commercially available RNA purification kit. Aliquot the mRNA to avoid repeated freeze-thaw, and store at -80 °C.

4. Injection and visualization
    1. Obtain embryos as outlined in Protocol 1.1.
    2. Using a microinjection apparatus, inject 300 pg of eGFP-CAAX mRNA at the 1-cell stage.
    3. Screen for embryos with the bright expression of eGFP in the eyes using a fluorescence stereoscope.
    4. Image the embryos as described in Protocol 1.2.
    5. Alternatively, dechorionate and fix the embryos at the desired timepoint in 4% PFA for 4 hours at room temperature or overnight at 4°C. Wash the embryos in 1x PBST for 5 min, four times, and dechorionate, if not previously done. Dissect the eyes and mount them on slides as described in Protocol 2.3.

4.3 Representative Results

The zebrafish SOS appears at 20 hpf in the presumptive dorsal retina (Hocking et al. 2018). By 23 hpf the SOS transitions from its initial narrow architecture to a wide indentation and by 26 hpf it is no longer visible (Hocking et al. 2018). Therefore, to examine the SOS during normal zebrafish eye development, the embryos must be observed between 20-23 hpf. During this period, the SOS is observable through the dissecting microscope and via DIC imaging as a thin line in the dorsal eye that separates the nasal and temporal halves of the developing retina (**Figure 4.1**). In addition, a subtle indentation may be visible in the dorsal boundary of the eye (**Figure 4.1**). Following immunofluorescent staining of laminin, the thin line can be confirmed to be the basement membrane (**Figure 4.1**).

To examine molecular pathways resulting in delayed SOS closure, we chose to observe the embryos at 28 hpf as this is a timepoint that is sufficiently removed from the time of normal SOS closure and is, therefore, a reliable marker of SOS closure delay due to experimental manipulations. Through direct visualization of 28 hpf zebrafish under the dissecting microscope, it is possible to evaluate SOS closure delay due to experimental manipulation. When SOS closure is delayed, its prolonged presence can be seen as a

pronounced cleft in the dorsal side of the eye under the dissecting microscope (**Figure 4.2**). When observed under the compound microscope using DIC or Nomarski optics, this feature is even more prominent, and the nasal and temporal sides of the eye are separated by the SOS, which is clearly visible as a line in the dorsal eye (**Figure 4.3**).

The SOS is lined with basal lamina components, including laminin. Therefore, immunofluorescent staining provides a complementary method of evaluating SOS closure in fixed embryos. When imaging the embryonic eye from a lateral view, the basal lamina demarcates the outside margin of the eye, both ocular fissures, and the border between the lens and the retina (**Figure 4.4**). The SOS is oriented directly opposite to the choroid fissure in the dorsal aspect of the eye. Whole embryos can be mounted laterally, with somewhat better optical clarity achieved if eyes are previously microdissected. By 28 hpf, in wildtype zebrafish, laminin staining demonstrates clearly that the SOS is completely closed, which makes this the ideal stage for monitoring delays in fissure closure.

Injection of eGFP-CAAX mRNA allows visualization of the cell membranes of a live or fixed embryo (**Figure 4.5**). Successful one-cell stage injection is sufficient to produce embryos with complete cell membrane fluorescence. In the lateral view, all cellular boundaries should be marked by GFP fluorescence, and as such, cell morphology is also clearly observed. This allows the visualization of the morphological changes to the cells that lead to SOS closure.

4.4 Discussion

Here, we present a standardized series of protocols to observe the SOS in the developing zebrafish embryo. To determine closure delay phenotypes, our protocols have focused on the ability to distinguish the separation of two discrete lobes of the dorsal-nasal and dorsal-temporal sides of the eye, similar to techniques used to visualize choroid fissure closure delay phenotypes in the ventral eye.

These visualization techniques can be used in conjunction with a variety of genetic manipulation techniques to study the effects of inhibiting or inducing expression of certain genes to study their roles in the closure of the SOS. We have chosen to demonstrate these

protocols using *gdf6a*$^{-/-}$ embryos as we have previously shown that its loss can affect proper closure of the SOS, but the protocols can be used to study the effects of manipulating the expression of any gene as required. It is recommended that any morphological changes to the dorsal eye are studied preliminarily with observations using the dissecting microscope. The other techniques should be used once an initial link is established definitively, as they are more time-consuming and lower throughput.

While the protocols can be easily modified to suit the needs of the experimenter, there are several aspects that must be followed carefully. Because of the transient nature of this structure, it is imperative to ensure that all observed embryos are of the same developmental stage. For our work, we find it important to allow only a small window of breeding time and to periodically sort the embryos throughout early development. The most important step of equalizing stages is at 20 hpf, when you can still accurately count somites (24) (Kimmel et al. 1995), and we find this much more reliable than the staging hallmarks that delineate time at 28 hpf. In addition, pigmentation must be inhibited or removed to ensure successful visualization of the structure. We have observed the pigmentation in the eye begins to start around 22 hpf, and there is a pattern of pigmentation in the dorsal eye that can interfere with proper visualization of the SOS. Therefore, it is highly recommended to treat the embryos with PTU prior to pigmentation to ensure successful visualization. Additionally, dissection of the embryonic eye prior to slide mounting without causing damage requires some practice. It is also imperative to laterally mount the eyes as parallel as possible to the slide. It is recommended that the experimenter practices these techniques with extra embryos prior to the experiment.

With the exception of the immunofluorescent staining of the basal lamina, all of the protocols described here can be completed using live embryos. This allows continual visualization of the SOS throughout early embryogenesis, allowing the experimenter to conduct time-lapse studies of the morphological changes involved in the closure of the SOS. In the past, we have used retina-specific transgenes, such as *Tg(rx3:eGFP)*, which marks the neural retina during early development. Although it lacks the ability to visualize cell membranes, the use of *Tg(rx3:eGFP)* has the advantage of not requiring microinjections and

has been our primary method of visualizing gross morphological changes to SOS architecture in real-time. That protocol has not been included here, as similar methods have been discussed previously in this journal (Gfrerer et al. 2013; Percival and Parant 2016). However, investigation of cell biological basis of SOS formation and closure will require membrane fluorescent proteins. Specifically, the injection of eGFP-CAAX mRNA allows visualization of the cell membranes around the SOS as seen in **Figure 4.5**, which allows us to study the dynamics of cell shape changes in the dorsal eye that are required for proper SOS closure. While eGFP-CAAX can be useful for performing live- imaging of SOS closure, it is made difficult by the presence of the enveloping layer in zebrafish. In addition, care must be taken when analyzing results from mRNA injections because it can result in mosaicism, making it difficult to directly compare embryos based on quantification of eGFP expression strength. This could be ameliorated through the use of transgenic zebrafish lines that fluorescently label cell membranes specifically in the developing retina, such as *Tg(vsx2.2:GFP-caax)*.

4.5 Figures

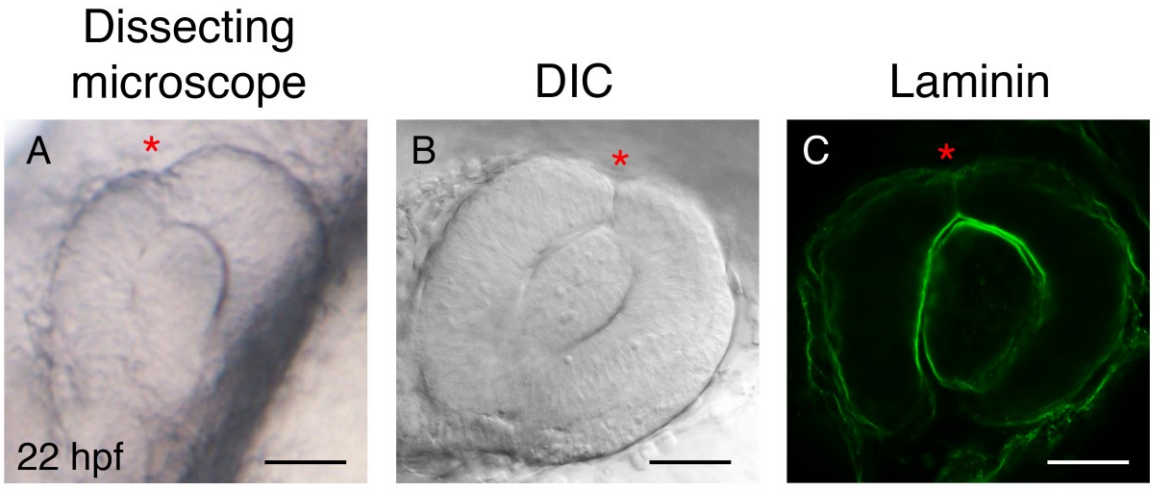

Figure 4.1. Observation of SOS during normal zebrafish eye development. Zebrafish embryos were collected and imaged at 22 hpf. A-B) Lateral view of 22 hpf embryos live-imaged with the dissecting microscope (A) and via DIC imaging (B), respectively. The SOS is marked by a red asterisk. C) Laminin immunofluorescent staining of a 22 hpf embryo. Embryos were fixed in 4% PFA and obtained for whole-mount immunofluorescent staining of laminin. The embryos were fileted and mounted in 70% glycerol/PBS. Single slice images were obtained through confocal imaging with a software. The SOS is marked by a white asterisk. All figures were annotated and assembled using Adobe Illustrator software. Scale bars represent 50 mm.

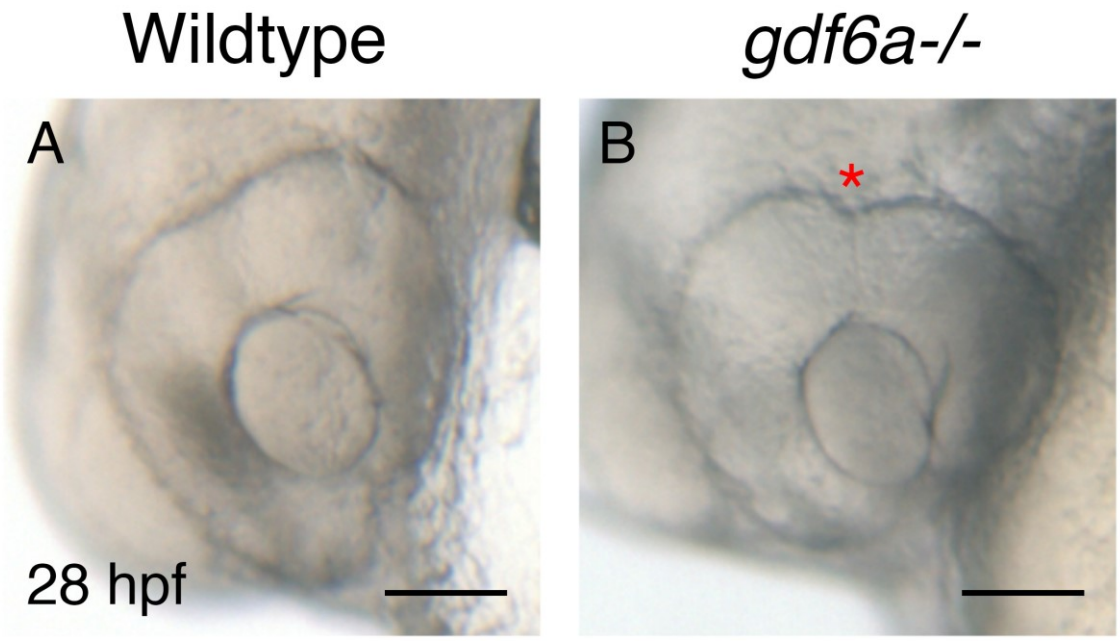

Figure 4.2. Dissecting microscope images of SOS closure delay in zebrafish larvae. Wildtype and *gdf6a*$^{-/-}$ embryos were collected and live-imaged at 28 hpf. A) Lateral view of a wildtype embryo with a closed SOS. B) Lateral view of a *gdf6a*$^{-/-}$ embryo with an SOS closure delay (asterisk). A sharp depression is observable in the dorsal aspect of the eye due to the failure of the SOS to close appropriately. Scale bars represent 50 mm.

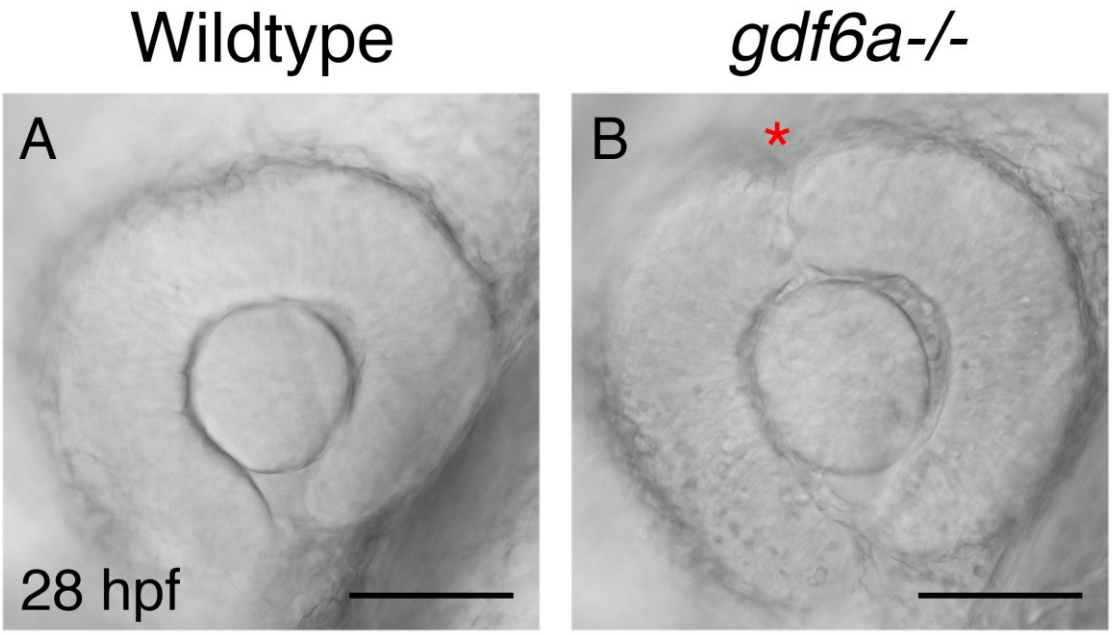

Figure 4.3. Representative DIC images of the SOS in the zebrafish embryonic eye. Wildtype and *gdf6a*$^{-/-}$ embryos were collected, anesthetized, and placed laterally in 1% Ultrapure low-melting point agarose in E3 on a 35 mm Petri dish. The dish was filled with E3, and a compound microscope with a 20x water-dipping objective was used for DIC imaging. A) Lateral view of a wildtype embryo with a closed SOS. B) Lateral view of a *gdf6a*$^{-/-}$ embryo with an SOS closure delay (asterisk). The SOS is observable as a thin line in the dorsal aspect of the eye. Scale bars represent 50 mm.

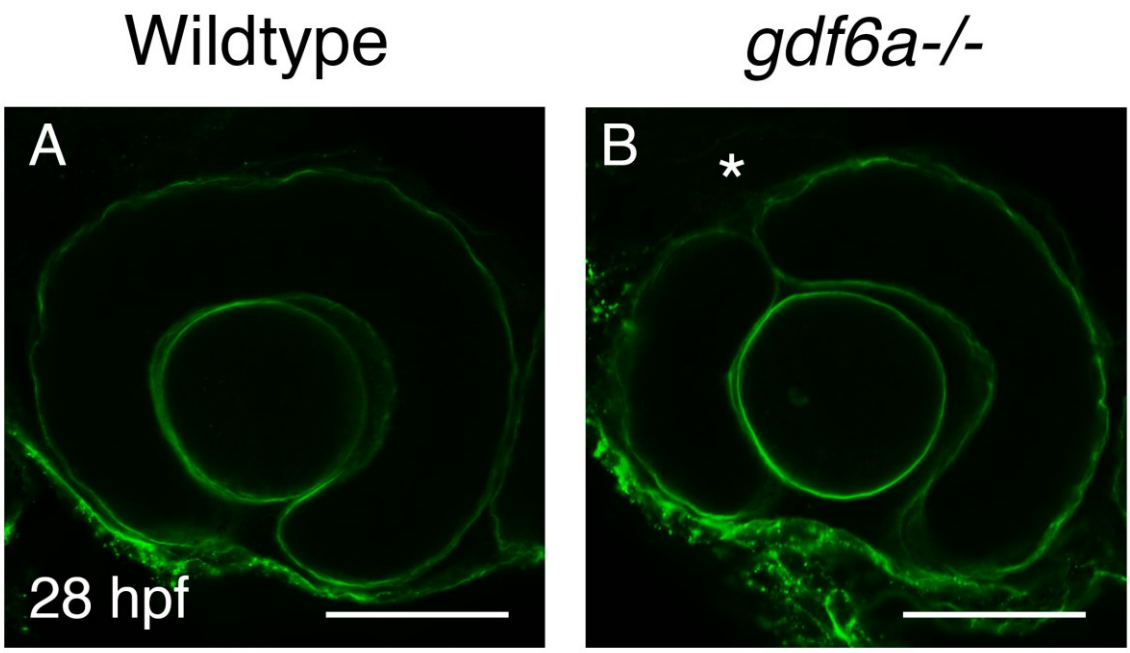

Figure 4.4. Representative images of laminin immunofluorescent staining in embryonic zebrafish eye. Wildtype and *gdf6a*$^{-/-}$ embryos were collected and fixed in 4% PFA at 28 hpf. The basal lamina was immunostained, and the embryos were fileted and mounted in 70% glycerol/PBS for confocal imaging. Single slice images were obtained using ZEN software. A) Lateral view of a wildtype embryo with a closed SOS. B) Lateral view of a *gdf6a*$^{-/-}$ embryo with an SOS closure delay (asterisk). The basal lamina is shown outlining the eye in green, with the SOS visible in the dorsal part of the eye in *gdf6a*$^{-/-}$ embryos. Scale bars represent 50 mm.

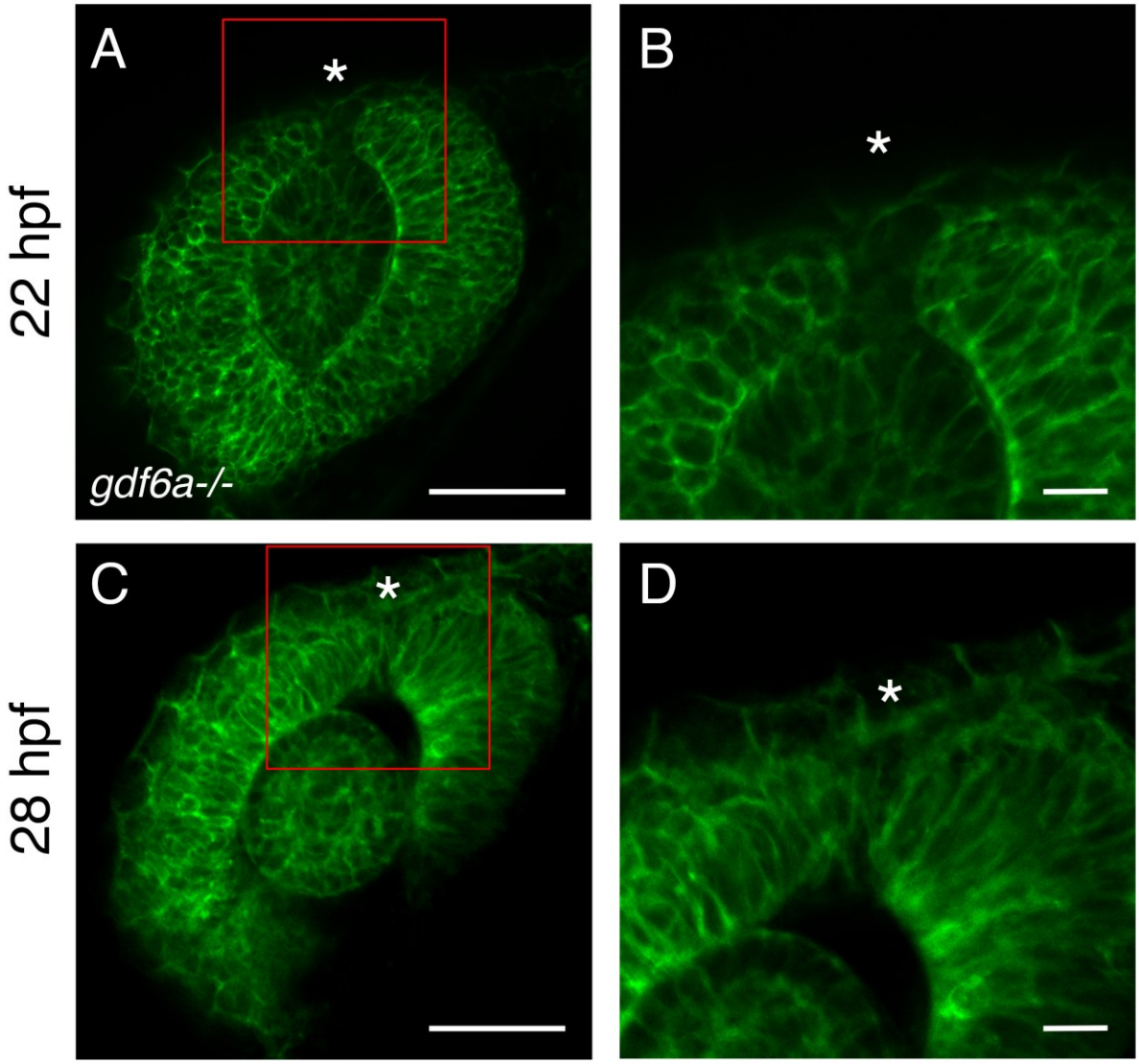

Figure 4.5. Imaging of the zebrafish embryonic eye following eGFP-caax mRNA injection. Wildtype embryos were injected with 300 pg of eGFP-caax mRNA at 1-cell stage. At 22 hpf and 28 hpf, respectively, the embryos were anesthetized and mounted laterally in 1% Ultrapure low-melting point agarose in E3 on a 35 mm Petri dish. A confocal microscope with a 20x water-dipping objective was used for imaging, and single slice images were obtained using a software. A) Lateral view of a *gdf6a*$^{-/-}$ embryo at 22 hpf with a visible open SOS (asterisk). B) Enlarged panels of a *gdf6a*$^{-/-}$ embryo at 22 hpf. C) Lateral view of a *gdf6a*$^{-/-}$ embryo at 28 hpf with a SOS closure delay. D) Enlarged panels of a *gdf6a*$^{-/-}$ embryo at 28 hpf. Scale bars represent 50 mm and 10 mm in Panels A and C, and B and D, respectively.

Chapter 5: Conclusion

5.1 PCP may have a role in eye development

The results of this project are suggestive of a role for PCP, but not AB polarity, in eye development, although the mechanism of PCP regulation of SOS closure is unclear. *In silico* analysis of one variant in an AB polarity-related gene and six variants in PCP-related genes, indicated potentially deleterious alleles that could be responsible for the causation of superior coloboma in the patients. To test whether cell polarity is required for SOS closure, expression of three genes from the *in silico* analysis was knocked down using MO treatment. Although *shroom3* was found to be expressed in ocular tissues during the time point of SOS closure, no closure delays were observed, and no evidence was collected to indicate a role for AB polarity in SOS closure.

The decision was made to focus on investigating PCP in the SOS closure. The first PCP gene investigated was *fzd4* through a MO knockdown experiment. Although no closure delays were observed in this experiment, it was not concluded that PCP has no role in eye development, as it was possible that the Fzd4 receptor does not have a noncanonical role in the eye, or that redundancies through other Fzd receptors make up for loss of Fzd4. To further investigate PCP in SOS closure, *scrib* expression was knocked down using MO treatment. *scrib* morphant embryos showed SOS closure delays, indicating a possible link between PCP and SOS closure. Further, this data is integral to the project because it incorporates the superior coloboma patient WES data into the link between PCP and SOS closure. However, a problem with Scrib is that the protein is involved in both AB polarity and PCP. To determine whether loss of its role in PCP is responsible for the SOS closure delay, the core PCP component, Vangl2¸ was investigated next. *vangl2* morphant and mutant embryos showed SOS closure delays, firmly linking the phenotype to loss of PCP.

The mechanism of how PCP regulates eye development and SOS closure was not discovered through the course of this project. It was hypothesized that loss of PCP affects optic cup DV patterning, perhaps by interfering with the maintenance stage of dorsalization, would result in SOS closure delays. However, *vangl2* mutants have normal expression patterns of DV markers, indicating that PCP regulates SOS closure through another mechanism. Another possibility investigated was that BMP signalling involved in optic cup

morphogenesis may influence PCP. However, pharmacological inhibition of BMP signalling did not affect *vangl2* expression patterns.

Little is known about PCP in eye development beyond a role in specification of the eye field and a hypothesized role in contributing motive forces that aid lateral migration of the eye field. This leaves the question of why disruption of PCP delays closure of the SOS. Because PCP mutants do not have anophthalmia, loss of PCP is not sufficient to completely inhibit eye specification. This is reasonable as eye specification is a carefully controlled process, as reviewed earlier, and involvement of PCP comes after the eye field cells have become specified through Pax6 and Rax. Further, the genes investigated, *vangl2* and *scrib*, do not appear to have roles in eye-field specification, but more so a role in planar polarization of cells. Therefore, anophthalmia, as seen in *Xenopus* with *Wnt4* knockdown, would not be expected in the current experiments.

It is likely that the role for PCP in eye development that results in proper SOS closure is linked to its function of maintaining the eye field boundary and coordinating cellular movements during evagination of the optic vesicle. Loss of PCP could allow slight intermixing of retinal precursors with cells of the telencephalon and diencephalon, although this has not been tested in PCP loss of function studies. Further, loss of PCP inhibits midline convergence, and this would reduce the amount of displacement of eye field cells that adds to lateral movements. More importantly, retinal precursors are likely to be planar polarized during coordinated cell migration as the optic vesicle forms and migrates laterally. As well, migration of cells during optic cup migration may require planar polarization. Altogether, loss of these functions of PCP in eye development would slow lateral movements of the optic cup. This could have a general effect of delaying eye development relative to whole embryo development. Because the SOS eventually closes in *scrib* and *vangl2* morphant/mutant embryos, it can be assumed that the developmental processes required for closure eventually occur. In this model of delayed retinal precursor migration, eventually the cells will migrate far enough, and the eye will form correctly.

Another explanation for SOS closure delays is that PCP acts locally to regulate closure of the SOS. Hocking et al. (2018) described SOS closure as a gradual filling-in of the

sulcus, rather than the fusion of two lobes as is seen in closure of the choroid fissure. This filling-in would require cell shape changes or cellular rearrangements, activities which PCP has been shown to mediate. Therefore, loss of PCP may delay the morphogenesis of cells around the sulcus and prevent timely closure. However, there is no data on whether the retinal cells lining the SOS are planar polarized. Similarly, the role of PCP in movements of retinal precursors during optic vesicle migration has not been directly established. Therefore, to determine the validity of either hypothesis requires further studies.

5.2 Drawbacks to the current study design

A complicating factor in studies of superior coloboma is that this disorder is likely multifactorial, as are most congenital ocular disorders. That is, several developmental processes and many genes regulate eye development, and for an individual to present with the ocular disorder they must accumulate enough deleterious mutations. Multifactorial inheritance is difficult to study because even when investigating a factor that lends to the causation of the disorder, there may be no phenotype as the model organism does not have other background mutations. Such may have been the case with both *shroom3* and *fzd4* knockdown experiments, where loss of either gene on its own is insufficient to cause SOS closure defects even if apical constriction or Fzd4-mediated PCP have a role in SOS morphogenesis. Multifactorial inheritance is further complicated by environmental factors, where a disorder may only present when sufficient genetic and environmental stressors are present. Ocular coloboma is known to be affected by environmental factors, and superior coloboma appears to be similar, as exposing *gdf6a-/-* zebrafish embryos to suboptimal temperatures increases incidence of SOS closure defects (unpublished observation). While multifactorial disorders are more difficult to study, there is still much to be gained from studying these disorders. As genetic networks are characterized, new factors become easier to discover, as sensitized models can be produced.

To discover these genetic networks, mass data sets are often helpful but can have their own complicating factors. Our lab's current approach to discovering genetic factors involved in SOS closure is dependant on clues found in the superior coloboma WES data set. Several hundred variants filtered through the *in silico* testing and were classified as rare and likely to

affect protein function. Although this approach is necessary when working with large data sets, *in silico* testing may filter out variants that contribute to the causation of the disease. After establishing the requirement of a process, such as PCP, in a disorder, it is worthwhile to sort through the variants that missed the statistical cut off to determine whether further disease-causing variants exist in the WES data set. While having so much data leaves room for forming hypotheses and conducting more studies, large data sets are often full of false leads and can be difficult to analyze. The approach in the current project was to identify many variants in genes involved in the same process across several patients. This approach strengthens the possibility of correctly identifying lines of inquiry, as if a particular process is integral to SOS closure, it is reasonable to expect variants in related genes in several patients.

5.3 Future studies

The data presented here show a tantalizing link between PCP and SOS closure, however the data do not explain how PCP is involved and why loss of planar polarization causes such a specific ocular phenotype. The logical next step in this project would be to examine the role of PCP in vertebrate eye development, as little research has been done in this area. I attemped to do this through examination of GFP-Pk localization during several stages of eye development, however this experiment was not completed due to time restraints and no conclusive results were obtained. However, Pk puncti, which are indicative of planar polarized localization, were observed in the optic cup around 20 hpf, a developmental stage which is relevant to SOS closure. This lends to the possibility that PCP is involved in ocular morphogenesis. Further inquiry would examine Pk localization in cells lining the SOS at 20 to 22 hpf to determine whether these cells are planar polarized during SOS closure.

The PCP component, CELSR2, was not investigated in this work despite being indicated by the WES data set. A MO was designed to perform knockdown experiments, but these experiments were not run due time constrictions. A strength of the data collected in this study is that PCP-related SOS closure delay was linked to superior coloboma by investigating *SCRIB*, as a patient had a potentially deleterious mutation in this gene. Examination of more patient variants would strengthen this link, and thus it is important to complete *celsr2*

knockdown experiments in zebrafish embryos to produce stronger evidence for PCP-regulated SOS closure defects. Scrib was investigated before Celsr2 because there was more evidence that loss of Scrib would result in loss of PCP. Although Celsr is a main component of PCP, previous studies have indicated that Celsr1has a strong functional roles in PCP (Curtin et al. 2003; Robinson et al. 2012), but not Celsr2. Therefore, it is likely that knockdown of *celsr2* may not result in loss of PCP due to functionality of Celsr1.

A question that comes to mind is why complete loss of PCP, as has previously been established in *vangl2* mutant embryos, does not have more severe effects on eye development. Beyond SOS closure delay and low penetrance of cyclopia due to inhibited prechordal plate migration, no drastic ocular phenotypes were observed in this study. In fact, it is impressive that despite how integral PCP is to vertebrate development, in the initial stages of development as seen through gastrulation, and later in development as seen through organogenesis, that *vangl2* embryos with complete loss of PCP can still develop to 5 days post fertilization. As discussed earlier, there are two separate planar polarity pathways, the Fzd/Dvl or "core" pathway, and the Ft/Ds pathway. It is unclear how independent these pathways are and it is likely that their intersection varies by context, depending on spatial and temporal context as well as species. There is evidence for genetic interactions between Vangl2 and Fat4 in mice during kidney, inner ear and neural tube development, indicating that the two pathways are interconnected rather than being independent (Saburi et al. 2012). Redundancy in these pathways may allow for loss of one pathway while maintaining sufficient polarization for proper development. This hypothesized redundancy may be responsible for why loss of non-canonical Wnt-derived PCP only results in a delay of SOS closure, rather than preventing closure all together. It would be worthwhile to investigate *FAT2* and *FAT4* in the causation of SOS, as variants were found in these two genes in the WES data of superior coloboma patients. If functional redundancy between these two pathways regulate eye development, then loss of both pathways would result in more severe ocular phenotype than a delay in SOS closure. However, there is no data to suggest involvement of Ft/Ds in vertebrate eye development and because little is known about the amount of overlap between these two parallel pathways, more research on the Ft/Ds pathway

in vertebrate development is required to determine this. Double knockout of a core component in each PCP pathway would determine whether there is a synergistic effect that indicates interactions between the two pathways in eye development.

Looking at a broader scope, much is left to understand about eye development as it pertains to the function and development of the SOS. To date, we have ascertained that it is evolutionarily conserved amongst vertebrates, functions to guide blood vessel migration in the dorsal eye and is reliant on DV patterning signals to close properly. Our lab continues to focus much of our research on the causation of superior coloboma, investigating genetic factors indicating by the WES data set. Our lab has published an extensive study characterizing the SOS and investigating mechanisms of closure. We have further published a paper outlining our main methodology for investigating SOS closure defects. The publications may lead to research by other groups, which would indicate further factors that regulate SOS closure, and in turn indicate further directions of study.

References

Abouzeid H, Meire FM, Osman I, ElShakankiri N, Bolay S, Munier FL, Schorderet DF. 2009. A New Locus for Congenital Cataract, Microcornea, Microphthalmia, and Atypical Iris Coloboma Maps to Chromosome 2. Ophthalmology 116:154-162.e1. doi:10.1016/j.ophtha.2008.08.044.

Adler PN, Charlton J, Liu J. 1998. Mutations in the cadherin superfamily member gene dachsous cause a tissue polarity phenotype by altering frizzled signaling. Development 125:959–968.

Adzhubei IA, Schmidt S, Peshkin L, Ramensky VE, Gerasimova A, Bork P, Kondrashov AS, Sunyaev SR. 2010. A method and server for predicting damaging missense mutations. Nat. Methods 7:248–249. doi:10.1038/nmeth0410-248.

Bailly E, Walton A, Borg JP. 2018. The planar cell polarity Vangl2 protein: From genetics to cellular and molecular functions. Semin. Cell Dev. Biol. 81:62–70. doi:10.1016/j.semcdb.2017.10.030.

Beaven AH, Kim J, Ko S, Rie G, Lee H, Im W, Seok C, Chung KY, Bang I, Ryung H, et al. 2018. Biophysical and functional characterization of Norrin signaling through Frizzled4. Proc. Natl. Acad. Sci. 115:E10807–E10807. doi:10.1073/pnas.1817333115.

Bengoa-Vergniory N, Gorroño-Etxebarria I, López-Sánchez I, Marra M, Di Chiaro P, Kypta R. 2017. Identification of Noncanonical Wnt Receptors Required for Wnt-3a-Induced Early Differentiation of Human Neural Stem Cells. Mol. Neurobiol. 54:6213–6224. doi:10.1007/s12035-016-0151-5.

Bilder D, Li M, Perrimon N. 2000. Cooperative regulation of cell polarity and growth by Drosophila tumor suppressors. Science (80-.). 289:113–116. doi:10.1126/science.289.5476.113.

Bilotta J, Saszik S. 2001. The zebrafish as a model visual system. Int. J. Dev. Neurosci.

19:621–629. doi:10.1016/S0736-5748(01)00050-8.

Bingham S, Higashijima S ichi, Okamoto H, Chandrasekhar A. 2002. The zebrafish trilobite gene is essential for tangential migration of branchiomotor neurons. Dev. Biol. 242:149–160. doi:10.1006/dbio.2001.0532.

Bonello TT, Peifer M. 2019. Scribble: A master scaffold in polarity, adhesion, synaptogenesis, and proliferation. J. Cell Biol. 218:742–756. doi:10.1083/jcb.201810103.

Brown KE, Keller PJ, Ramialison M, Rembold M, Stelzer EHK, Loosli F, Wittbrodt Joachim J. 2010. Nlcam modulates midline convergence during anterior neural plate morphogenesis. Dev. Biol. 339:14–25. doi:10.1016/j.ydbio.2009.12.003.

Bryan CD, Chien C, Kwan KM. 2016. Loss of laminin alpha 1 results in multiple structural defects and divergent effects on adhesion during vertebrate optic cup morphogenesis. Dev. Biol. 416:324–337. doi:10.1016/j.ydbio.2016.06.025.

Bryant PJ, Huettner B, Held LI, Ryerse J, Szidonya J. 1988. Mutations at the fat locus interfere with cell proliferation control and epithelial morphogenesis in Drosophila. Dev. Biol. 129:541–554. doi:10.1016/0012-1606(88)90399-5.

Campanale JP, Sun TY, Montell DJ. 2017. Development and dynamics of cell polarity at a glance. J. Cell Sci. 130:1201–1207. doi:10.1242/jcs.188599.

Cao M, Ouyang J, Guo J, Lin S, Chen S. 2018. Metalloproteinase adamts16 is required for proper closure of the optic fissure. Investig. Ophthalmol. Vis. Sci. 59:1167–1177. doi:10.1167/iovs.17-22827.

Casal J, Lawrence PA, Struhl G. 2006. Two separate molecular systems, Dachsous/Fat and Starry night/Frizzled, act independently to confer planar cell polarity. Development 133:4561–4572. doi:10.1242/dev.02641.

Cavodeassi F, Carreira-Barbosa F, Young RM, Concha ML, Allende ML, Houart C, Tada M, Wilson SW. 2005. Early stages of zebrafish eye formation require the coordinated

activity of Wnt11, Fz5, and the Wnt/β-catenin pathway. Neuron 47:43–56. doi:10.1016/j.neuron.2005.05.026.

Cavodeassi F, Ivanovitch K, Wilson SW. 2013. Eph/Ephrin signalling maintains eye field segregation from adjacent neural plate territories during forebrain morphogenesis. Development 140:4193–4202. doi:10.1242/dev.097048.

Chang L, Blain D, Bertuzzi S, Brooks BP. 2006. Uveal coloboma: Clinical and basic science update. Curr. Opin. Ophthalmol. 17:447–470. doi:10.1097/01.icu.0000243020.82380.f6.

Chen W, Ten Berge D, Brown J, Ahn S, Hu LA, Miller WE, Caron MG, Barak LS, Nusse R, Lefkowitz RJ. 2003. Dishevelled 2 recruits β-arrestin 2 to mediate Wnt5A-stimulated endocytosis of frizzled 4. Science (80-.). 301:1391–1394. doi:10.1126/science.1082808.

Chow RL, Altmann CR, Lang RA, Hemmati-Brivanlou A. 1999. Pax6 induces ectopic eyes in a vertebrate. Development 126:4213–4222.

Chow RL, Lang RA. 2001. Early Eye Development in Vertebrates. Annu. Rev. Cell Dev. Biol. 17:255–296. doi:10.1146/annurev.cellbio.17.1.255.

Ciruna B, Jenny A, Lee D, Mlodzik M, Schier AF. 2006. Planar cell polarity signalling couples cell division and morphogenesis during neurulation. Nature 439:220–224. doi:10.1038/nature04375.

Curtin JA, Quint E, Tsipouri V, Arkell RM, Cattanach B, Copp AJ, Henderson DJ, Spurr N, Stanier P, Fisher EM, et al. 2003. Mutation of Celsr1 Disrupts Planar Polarity of Inner Ear Hair Cells and Causes Severe Neural Tube Defects in the Mouse. Curr. Biol. 13:1129–1133. doi:10.1016/S0960-9822(03)00374-9.

Davey CF, Mathewson AW, Moens CB. 2016. PCP Signaling between Migrating Neurons and their Planar-Polarized Neuroepithelial Environment Controls Filopodial Dynamics and Directional Migration. Lu X, editor. PLOS Genet. 12:e1005934. doi:10.1371/journal.pgen.1005934.

Deml B, Reis LM, Lemyre E, Clark RD, Kariminejad A, Semina E V. 2016. Novel mutations in PAX6, OTX2 and NDP in anophthalmia, microphthalmia and coloboma. Eur. J. Hum. Genet. 24:535–541. doi:10.1038/ejhg.2015.155.

Descamps B, Sewduth R, Ferreira Tojais N, Jaspard B, Reynaud A, Sohet F, Lacolley P, Allières C, Lamazière JMD, Moreau C, et al. 2012. Frizzled 4 regulates arterial network organization through noncanonical Wnt/planar cell polarity signaling. Circ. Res. 110:47–58. doi:10.1161/CIRCRESAHA.111.250936.

Devenport D, Fuchs E. 2008. Planar polarization in embryonic epidermis orchestrates global asymmetric morphogenesis of hair follicles. Nat. Cell Biol. 10:1257–1268. doi:10.1038/ncb1784.

Dijksterhuis JP, Baljinnyam B, Stanger K, Sercan HO, Ji Y, Andres O, Rubin JS, Hannoush RN, Schulte G. 2015. Systematic mapping of WNT-FZD protein interactions reveals functional selectivity by distinct WNT-FZD pairs. J. Biol. Chem. 290:6789–6798. doi:10.1074/jbc.M114.612648.

Distel M, Koster RW. 2007. In Vivo Time-Lapse Imaging of Zebrafish Embryonic Development. Cold Spring Harb. Protoc.:4816. doi:10.1101/pdb.prot4816.

Ernst S, Liu K, Agarwala S, Moratscheck N, Avci ME, Nogare DD, Chitnis AB, Ronneberger O, Lecaudey V. 2012. Shroom3 is required downstream of FGF signalling to mediate proneuromast assembly in zebrafish. Development 139:4571–4581. doi:10.1242/dev.083253.

Findlay AS, Panzica DA, Walczysko P, Holt AB, Henderson DJ, West JD, Rajnicek AM, Collinson JM. 2016. The core planar cell polarity gene, Vangl2, directs adult corneal epithelial cell alignment and migration. R. Soc. Open Sci. 3:160658. doi:10.1098/rsos.160658.

Fisher KH, Strutt D. 2019. A theoretical framework for planar polarity establishment through interpretation of graded cues by molecular bridges. Development 146:dev168955. doi:10.1242/dev.168955.

French CR, Erickson T, French D V., Pilgrim DB, Waskiewicz AJ. 2009. Gdf6a is required for the initiation of dorsal-ventral retinal patterning and lens development. Dev. Biol. 333:37–47. doi:10.1016/j.ydbio.2009.06.018.

French CR, Stach TR, March LD, Lehmann OJ, Waskiewicz AJ. 2013. Apoptotic and proliferative defects characterize ocular development in a microphthalmic BMP model. Investig. Ophthalmol. Vis. Sci. 54:4636–4647. doi:10.1167/iovs.13-11674.

Fujimura N, Taketo MM, Mori M, Korinek V, Kozmik Z. 2009. Spatial and temporal regulation of Wnt/β-catenin signaling is essential for development of the retinal pigment epithelium. Dev. Biol. 334:31–45. doi:10.1016/j.ydbio.2009.07.002.

Gao B, Song H, Bishop K, Elliot G, Garrett L, English MA, Andre P, Robinson J, Sood R, Minami Y, et al. 2011. Wnt Signaling Gradients Establish Planar Cell Polarity by Inducing Vangl2 Phosphorylation through Ror2. Dev. Cell 20:163–176. doi:10.1016/j.devcel.2011.01.001.

Gfrerer L, Dougherty M, Liao EC. 2013. Visualization of craniofacial development in the sox10: kaede transgenic zebrafish line using time-lapse confocal microscopy. J. Vis. Exp.:1–5. doi:10.3791/50525.

Gombos R, Migh E, Antal O, Mukherjee A, Jenny A, Mihály J. 2015. The formin DAAM functions as molecular effector of the planar cell polarity pathway during axonal development in Drosophila. J. Neurosci. 35:10154–10167. doi:10.1523/JNEUROSCI.3708-14.2015.

Gong Y, Mo C, Fraser SE. 2004. Planar cell polarity signalling controls cell division orientation during zebrafish gastrulation. Nature 430:689–693. doi:10.1038/nature02796.

Green JL, Inoue T, Sternberg PW. 2008. Opposing Wnt Pathways Orient Cell Polarity during Organogenesis. Cell 134:646–656. doi:10.1016/j.cell.2008.06.026.

Gregory-Evans CY. 2004. Ocular coloboma: a reassessment in the age of molecular neuroscience. J. Med. Genet. 41:881–891. doi:10.1136/jmg.2004.025494.

Gubb D, Garcia-Bellido. 1982. A genetic analysis of the determination of cuticular polarity during development in Drosophila melanogaster. J. Embryol. Exp. Morphol. Vol. 68:37–57.

Habas R, Kato Y, He X. 2001. Wnt/Frizzled activation of Rho regulates vertebrate gastrulation and requires a novel formin homology protein Daam1. Cell 107:843–854. doi:10.1016/S0092-8674(01)00614-6.

Haffter P, Granato M, Brand M, Mullins MC, Hammerschmidt M, Kane DA, Odenthal J, Van Eeden FJM, Jiang YJ, Heisenberg CP, et al. 1996. The identification of genes with unique and essential functions in the development of the zebrafish, Danio rerio. Development 123:1–36.

Haigo SL, Hildebrand JD, Harland RM, Wallingford JB. 2003. Shroom Induces Apical Constriction and Is Required for Hingepoint Formation during Neural Tube Closure. Curr. Biol. 13:2125–2137. doi:10.1016/j.cub.2003.11.054.

Halder G, Johnson RL. 2011. Hippo signaling: Growth control and beyond. Development 138:9–22. doi:10.1242/dev.045500.

Hale R, Brittle AL, Fisher KH, Monk NAM, Strutt D. 2015. Cellular interpretation of the long-range gradient of Four-jointed activity in the Drosophila wing. Elife 2015:1–21. doi:10.7554/eLife.05789.

Hanwell D, Hutchinson SA, Collymore C, Bruce AE, Louis R, Ghalami A, Allison WT, Ekker M, Eames BF, Childs S, et al. 2016. Restrictions on the Importation of Zebrafish into Canada Associated with Spring Viremia of Carp Virus. Zebrafish 13:S153–S163. doi:10.1089/zeb.2016.1286.

Hao J, Ho JN, Lewis JA, Karim KA, Daniels RN, Gentry PR, Hopkins CR, Lindsley CW, Hong CC. 2010. In Vivo Structure−Activity Relationship Study of Dorsomorphin Analogues Identifies Selective VEGF and BMP Inhibitors. ACS Chem. Biol. 5:245–253. doi:10.1021/cb9002865.

Heermann S, Schütz L, Lemke S, Krieglstein K, Wittbrodt J. 2015. Eye morphogenesis

driven by epithelial flow into the optic cup facilitated by modulation of bone morphogenetic protein. Elife 2015:1–17. doi:10.7554/eLife.05216.

Heisenberg C, Tada M, Rauch G-J, Saúde L, Concha ML, Geisler R, Stemple DL, Smith JC, Wilson SW. 2000. Silberblick/Wnt11 mediates convergent extension movements during zebrafish gastrulation. Nature 405:76–81. doi:10.1038/35011068.

Hildebrand JD, Soriano P. 1999. Shroom, a PDZ domain-containing actin-binding protein, is required for neural tube morphogenesis in mice. Cell 99:485–497. doi:10.1016/S0092-8674(00)81537-8.

Hocking JC, Famulski JK, Yoon KH, Widen SA, Bernstein CS, Koch S, Weiss O, Agarwala S, Inbal A, Lehmann OJ, et al. 2018. Morphogenetic defects underlie Superior Coloboma, a newly identified closure disorder of the dorsal eye. PLoS Genet. 14:1–28. doi:10.1371/journal.pgen.1007246.

Hornby SJ, Gilbert CE, Rahi JK, Sil AK, Xiao Y, Dandona L, Foster A. 2000. Regional variation in blindness in children due to microphthalmos, anophthalmos and coloboma. Ophthalmic Epidemiol. 7:127–38. doi:10.1076/0928-6586(200006)721-ZFT127.

Hornby SJ, Ward SJ, Gilbert CE, Dandona L, Foster A, Jones RB. 2002. Environmental risk factors in congenital malformations of the eye. Ann. Trop. Paediatr. 22:67–77. doi:10.1179/027249302125000193.

Howe K, Clark MD, Torroja CF, Torrance J, Berthelot C, Muffato M, Collins JE, Humphray S, McLaren K, Matthews L, et al. 2013. The zebrafish reference genome sequence and its relationship to the human genome. Nature 496:498–503. doi:10.1038/nature12111.

Huang J, Rajagopal R, Liu Y, Dattilo LK, Shaham O, Ashery-Padan R, Beebe DC. 2011. The mechanism of lens placode formation: A case of matrix-mediated morphogenesis. Dev. Biol. 355:32–42. doi:10.1016/j.ydbio.2011.04.008.

Ishikawa HO, Takeuchi H, Haltiwanger RS, Irvine KD. 2008. Four-jointed is a Golgi kinase

that phosphorylates a subset of cadherin domains. Science (80-.). 321:401–404. doi:10.1126/science.1158159.

Islam N, Best J, Mehta JS, Sivakumar S, Plant GT, Hoyt WF. 2005. Optic disc duplication or coloboma? Br. J. Ophthalmol. 89:26–29. doi:10.1136/bjo.2004.049122.

Ivanovitch K, Cavodeassi F, Wilson SW. 2013. Precocious Acquisition of Neuroepithelial Character in the Eye Field Underlies the Onset of Eye Morphogenesis. Dev. Cell 27:293–305. doi:10.1016/j.devcel.2013.09.023.

Jain A, Ranjan R, Manayath G. 2018. Atypical superior iris and retinochoroidal coloboma. Indian J. Ophthalmol. 66:1474. doi:10.4103/ijo.IJO_531_18.

James A, Lee C, Williams AM, Angileri K, Lathrop KL, Gross JM. 2016. The hyaloid vasculature facilitates basement membrane breakdown during choroid fissure closure in the zebrafish eye. Dev. Biol. 419:262–272. doi:10.1016/j.ydbio.2016.09.008.

Jenny A. 2010. Planar Cell Polarity Signaling in the Drosophila Eye. Curr. Top. Dev. Biol. 93:189–227. doi:10.1016/B978-0-12-385044-7.00007-2.

Jenny A, Darken RS, Wilson PA, Mlodzik M. 2003. Prickle and strabismus form a functional complex to generate a correct axis during planar cell polarity signaling. EMBO J. 22:4409–4420. doi:10.1093/emboj/cdg424.

Jessen JR, Topczewski J, Bingham S, Sepich DS, Marlow F, Chandrasekhar A, Solnica-krezel L. 2002. Zebrafish trilobite identifies new roles for Strabismus in gastrulation and neuronal movements. Nat. Cell Biol. 4:610–5. doi:10.1038/ncb828.

Jethani J, Sharma VR, Marwah K. 2009. Superior lens coloboma with superior rectus palsy and congenital ptosis. J. Optom. 2:67–69. doi:10.3921/joptom.2009.67.

Kallay LM, McNickle A, Brennwald PJ, Hubbard AL, Braiterman LT. 2006. Scribble associates with two polarity proteins, Lgl2 and Vangl2, via distinct molecular domains. J. Cell. Biochem. 99:647–664. doi:10.1002/jcb.20992.

Karner C, Wharton KA, Carroll TJ. 2006. Apical-basal polarity, Wnt signaling and vertebrate

organogenesis. Semin. Cell Dev. Biol. 17:214–222. doi:10.1016/j.semcdb.2006.05.007.

Karner CM, Chirumamilla R, Aoki S, Igarashi P, Wallingford JB, Carroll TJ. 2009. Wnt9b signaling regulates planar cell polarity and kidney tubule morphogenesis. Nat. Genet. 41:793–799. doi:10.1038/ng.400.

Kaufman R, Weiss O, Sebbagh M, Ravid R, Gibbs-Bar L, Yaniv K, Inbal A. 2015. Development and origins of Zebrafish ocular vasculature. BMC Dev. Biol. 15:18. doi:10.1186/s12861-015-0066-9.

Kibar Z, Vogan KJ, Groulx N, Justice MJ, Underhill DA, Gros P. 2001. Ltap, a mammalian homolog of Drosophila Strabismus/Van Gogh, is altered in the mouse neural tube mutant Loop-tail. Nat. Genet. 28:251–255. doi:10.1038/90081.

Kikuchi A, Yamamoto H, Kishida S. 2007. Multiplicity of the interactions of Wnt proteins and their receptors. Cell. Signal. 19:659–671. doi:10.1016/j.cellsig.2006.11.001.

Kimmel CB, Ballard WW, Kimmel SR, Ullmann B, Schilling TF. 1995. Stages of embryonic development of the zebrafish. Dev. Dyn. 203:253–310. doi:10.1002/aja.1002030302.

Kolte D, McClung JA, Aronow WS. 2016. Vasculogenesis and Angiogenesis. In: Translational Research in Coronary Artery Disease. Elsevier. p. 49–65.

Kondo H, Uchio E, Kusaka S, Higasa K. 2018. Risk allele of the FZD4 gene for familial exudative vitreoretinopathy. Ophthalmic Genet. 39:405–406. doi:10.1080/13816810.2017.1401090.

Kozmik Z. 2005. Pax genes in eye development and evolution. Curr. Opin. Genet. Dev. 15:430–438. doi:10.1016/j.gde.2005.05.001.

Kruse-Bend R, Rosenthal J, Quist TS, Veien ES, Fuhrmann S, Dorsky RI, Chien C Bin. 2012. Extraocular ectoderm triggers dorsal retinal fate during optic vesicle evagination in zebrafish. Dev. Biol. 371:57–65. doi:10.1016/j.ydbio.2012.08.004.

Kumar P, Henikoff S, Ng PC. 2009. Predicting the effects of coding non-synonymous

variants on protein function using the SIFT algorithm. Nat. Protoc. 4:1073–1082. doi:10.1038/nprot.2009.86.

Kwan KM, Otsuna H, Kidokoro H, Carney KR, Saijoh Y, Chien C Bin. 2012. A complex choreography of cell movements shapes the vertebrate eye. Development 139:359–372. doi:10.1242/dev.071407.

Langheinrich U, Hennen E, Stott G, Vacun G. 2002. Zebrafish as a model organism for the identification and characterization of drugs and genes affecting p53 signaling. Curr. Biol. 12:2023–2028. doi:10.1016/S0960-9822(02)01319-2.

Lavery DL, Martin J, Turnbull YD, Hoppler S. 2008. Wnt6 signaling regulates heart muscle development during organogenesis. Dev. Biol. 323:177–188. doi:10.1016/j.ydbio.2008.08.032.

Lawson ND, Wolfe SA. 2011. Forward and Reverse Genetic Approaches for the Analysis of Vertebrate Development in the Zebrafish. Dev. Cell 21:48–64. doi:10.1016/j.devcel.2011.06.007.

Lee HS, Bong YS, Moore KB, Soria K, Moody SA, Daar IO. 2006. Dishevelled mediates ephrinB1 signalling in the eye field through the planar cell polarity pathway. Nat. Cell Biol. 8:55–63. doi:10.1038/ncb1344.

Lei YP, Zhang T, Li H, Wu BL, Jin L, Wang HY. 2010. VANGL2 mutations in human cranial neural-tube defects. N. Engl. J. Med. 362:2232–2235. doi:10.1056/NEJMc0910820.

Lek M, Karczewski KJ, Minikel E V., Samocha KE, Banks E, Fennell T, O'Donnell-Luria AH, Ware JS, Hill AJ, Cummings BB, et al. 2016. Analysis of protein-coding genetic variation in 60,706 humans. Nature 536:285–291. doi:10.1038/nature19057.

Leung V, Iliescu A, Jolicoeur C, Gravel M, Apuzzo S, Torban E, Cayouette M, Gros P. 2016. The planar cell polarity protein Vangl2 is required for retinal axon guidance. Dev. Neurobiol. 76:150–165. doi:10.1002/dneu.22305.

Li Z, Joseph NM, Easter SS. 2000. The morphogenesis of the zebrafish eye, including a fate map of the optic vesicle. Dev. Dyn. 218:175–88. doi:10.1002/(SICI)1097-0177(200005)218:1<175::AID-DVDY15>3.0.CO;2-K.

Loosli F, Staub W, Finger-Baier KC, Ober EA, Verkade H, Wittbrodt J, Baier H. 2003. Loss of eyes in zebrafish caused by mutation of chokh/rx 3. EMBO Rep. 4:894–899. doi:10.1038/sj.embor.embor919.

Mann IDA, Ross JA. 1927. Atypical Coloboma with Abnormal Retial Vessels. Br. J. Ophthalmol.:608–612.

Marlow F, Topczewski J, Sepich D, Solnica-Krezel L. 2002. Zebrafish Rho kinase 2 acts downstream of Wnt11 to mediate cell polarity and effective convergence and extension movements. Curr. Biol. 12:876–884. doi:10.1016/S0960-9822(02)00864-3.

Marlow F, Zwartkruis F, Malicki J, Neuhauss SCF, Abbas L, Weaver M, Driever W, Solnica-Krezel L. 1998. Functional interactions of genes mediating convergent extension, knypek and trilobite, during the partitioning of the eye primordium in zebrafish. Dev. Biol. 203:382–399. doi:10.1006/dbio.1998.9032.

Matis M, Axelrod JD. 2013. Regulation of PCP by the fat signaling pathway. Genes Dev. 27:2207–2220. doi:10.1101/gad.228098.113.

Matis M, Russler-Germain DA, Hu Q, Tomlin CJ, Axelrod JD. 2014. Microtubules provide directional information for core PCP function. Elife 3:1–17. doi:10.7554/eLife.02893.

Maurus D, Héligon C, Bürger-Schwärzler A, Brändli AW, Kühl M. 2005. Noncanonical Wnt-4 signaling and EAF2 are required for eye development in Xenopus laevis. EMBO J. 24:1181–1191. doi:10.1038/sj.emboj.7600603.

May-Simera H, Kelley MW. 2012. Planar Cell Polarity in the Inner Ear. 1st ed. Elsevier Inc.

Merks AM, Swinarski M, Meyer AM, Müller NV, Özcan I, Donat S, Burger A, Gilbert S,

Mosimann C, Abdelilah-Seyfried S, et al. 2018. Planar cell polarity signalling coordinates heart tube remodelling through tissue-scale polarisation of actomyosin activity. Nat. Commun. 9:2161. doi:10.1038/s41467-018-04566-1.

Mikels AJ, Nusse R. 2006. Purified Wnt5a protein activates or inhibits β-catenin-TCF signaling depending on receptor context. PLoS Biol. 4:570–582. doi:10.1371/journal.pbio.0040115.

Montcouquiol M, Rachel RA, Lanford PJ, Copeland NG, Jenkins NA, Kelley MW. 2003. Identification of Vangl2 and Scrb1 as planar polarity genes in mammals. Nature 423:173–177. doi:10.1038/nature01618.

Moody SA. 1987. Fates of the blastomeres of the 32-cell-stage Xenopus embryo. Dev. Biol. 122:300–319. doi:10.1016/0012-1606(87)90296-X.

Murdoch JN, Henderson DJ, Doudney K, Gaston-Massuet C, Phillips HM, Paternotte C, Arkell R, Stanier P, Copp AJ. 2003. Disruption of scribble (Scrb1) causes severe neural tube defects in the circletail mouse. Hum. Mol. Genet. 12:87–98. doi:10.1093/hmg/ddg014.

Nguyen MTT, Arnheiter H. 2000. Signaling and transcriptional regulation in early mammalian eye development: A link between FGF and MITF. Development 127:3581–3591.

Nikaido M, Law EWP, Kelsh RN. 2013. A Systematic Survey of Expression and Function of Zebrafish frizzled Genes. PLoS One 8. doi:10.1371/journal.pone.0054833.

Onwochei BC, Simon JW, Bateman JB, Couture KC, Mir E. 2000. Ocular Colobomata. Surv. Ophthalmol. 45:175–194. doi:10.1016/S0039-6257(00)00151-X.

Park M, Moon RT. 2002. The planar cell-polarity gene stbm regulates cell behaviour and cell fate in vertebrate embryos. Nat. Cell Biol. 4:20–25. doi:10.1038/ncb716.

Percival SM, Parant JM. 2016. Observing mitotic division and dynamics in a live zebrafish embryo. J. Vis. Exp. 2016:1–13. doi:10.3791/54218.

Person AD, Beiraghi S, Sieben CM, Hermanson S, Neumann AN, Robu ME, Schleiffarth JR, Billington CJ, Van Bokhoven H, Hoogeboom JM, et al. 2010. WNT5A mutations in patients with autosomal dominant Robinow syndrome. Dev. Dyn. 239:327–337. doi:10.1002/dvdy.22156.

Plageman TF, Chung M-I, Lou M, Smith AN, Hildebrand JD, Wallingford JB, Lang RA. 2010. Pax6-dependent Shroom3 expression regulates apical constriction during lens placode invagination. Development 137:405–415. doi:10.1242/dev.045369.

Quesada-Hernández E, Caneparo L, Schneider S, Winkler S, Liebling M, Fraser SE, Heisenberg CP. 2010. Stereotypical cell division orientation controls neural rod midline formation in zebrafish. Curr. Biol. 20:1966–1972. doi:10.1016/j.cub.2010.10.009.

Rasmussen JT, Deardorff MA, Tan C, Rao MS, Klein PS, Vetter ML. 2001. Regulation of eye development by frizzled signaling in Xenopus. Proc. Natl. Acad. Sci. U. S. A. 98:3861–3866. doi:10.1073/pnas.071586298.

Rembold M. 2006. Individual Cell Migration Serves as the Driving Force for Optic Vesicle Evagination. Science (80-.). 313:1130–1134. doi:10.1126/science.1127144.

Robinson A, Escuin S, Vekemans KD, Stevenson RE, Greene NDE, Copp AJ, Stanier P. 2012. Mutations in the planar cell polarity genes CELSR1 and SCRIB are associated with the severe neural tube defect craniorachischisis. Hum. Mutat. 33:440–447. doi:10.1002/humu.21662.

Rogulja D, Rauskolb C, Irvine KD. 2008. Morphogen Control of Wing Growth through the Fat Signaling Pathway. Dev. Cell 15:309–321. doi:10.1016/j.devcel.2008.06.003.

Rosso SB, Sussman D, Wynshaw-Boris A, Salinas PC. 2005. Wnt signaling through Dishevelled, Rac and JNK regulates dendritic development. Nat. Neurosci. 8:34–42. doi:10.1038/nn1374.

Rousseau B, Larrieu-Lahargue F, Bikfalvi A, Javerzat S. 2003. Involvement of fibroblast growth factors in choroidal angiogenesis and retinal vascularization. Exp. Eye Res.

77:147–156. doi:10.1016/S0014-4835(03)00127-1.

Saburi S, Hester I, Goodrich L, McNeill H. 2012. Functional interactions between Fat family cadherins in tissue morphogenesis and planar polarity. Development 139:1806–1820. doi:10.1242/dev.077461.

Saint-Geniez M, D'Amore PA. 2004. Development and pathology of the hyaloid, choroidal and retinal vasculature. Int. J. Dev. Biol. 48:1045–1058. doi:10.1387/ijdb.041895ms.

Schmidt C, McGonnell IM, Allen S, Otto A, Patel K. 2007. Wnt6 controls amniote neural crest induction through the non-canonical signaling pathway. Dev. Dyn. 236:2502–2511. doi:10.1002/dvdy.21260.

Schwarz JM, Cooper DN, Schuelke M, Seelow D. 2014. Mutationtaster2: Mutation prediction for the deep-sequencing age. Nat. Methods 11:361–362. doi:10.1038/nmeth.2890.

Segalen M, Bellaïche Y. 2009. Cell division orientation and planar cell polarity pathways. Semin. Cell Dev. Biol. 20:972–977. doi:10.1016/j.semcdb.2009.03.018.

Seigfried FA, Cizelsky W, Pfister AS, Dietmann P, Walther P, Kühl M, Kühl SJ. 2017. Frizzled 3 acts upstream of Alcam during embryonic eye development. Dev. Biol. 426:69–83. doi:10.1016/j.ydbio.2017.04.004.

Seo HS, Habas R, Chang C, Wang J. 2017. Bimodal regulation of Dishevelled function by Vangl2 during morphogenesis. Hum. Mol. Genet. 26:2053–2061. doi:10.1093/hmg/ddx095.

Shah SP, Taylor AE, Sowden JC, Ragge NK, Russell-Eggitt I, Rahi JS, Gilbert CE. 2011. Anophthalmos, microphthalmos, and typical Coloboma in the United Kingdom: A prospective study of incidence and risk. Investig. Ophthalmol. Vis. Sci. 52:558–564. doi:10.1167/iovs.10-5263.

Shimada Y, Yonemura S, Ohkura H, Strutt D, Uemura T. 2006. Polarized transport of Frizzled along the planar microtubule arrays in Drosophila wing epithelium. Dev.

Cell 10:209–222. doi:10.1016/j.devcel.2005.11.016.

Shiraki T, Kojima D, Fukada Y. 2010. Light-induced body color change in developing zebrafish. Photochem. Photobiol. Sci. 9:1498. doi:10.1039/c0pp00199f.

Slavotinek AM. 2011. Eye development genes and known syndromes. Mol. Genet. Metab. 104:448–456. doi:10.1016/j.ymgme.2011.09.029.

Stone J, Itin A, Alon T, Pe'er J, Gnessin H, Chan-Ling T, Keshet E. 1995. Development of retinal vasculature is mediated by hypoxia-induced vascular endothelial growth factor (VEGF) expression by neuroglia. J. Neurosci. 15:4738–4747. doi:10.1523/jneurosci.15-07-04738.1995.

Strigini M, Cohen SM. 2000. Wingless gradient formation in the Drosophila wing. Curr. Biol. 10:293–300. doi:10.1016/S0960-9822(00)00378-X.

Strong LC, Hollander WF. 1949. Hereditary loop-tail in the house mouse. J. Hered. 40:329–334. doi:10.1093/oxfordjournals.jhered.a105976.

Strutt H, Strutt D. 2008. Differential Stability of Flamingo Protein Complexes Underlies the Establishment of Planar Polarity. Curr. Biol. 18:1555–1564. doi:10.1016/j.cub.2008.08.063.

Sugiyama Y, Lovicu FJ, McAvoy JW. 2011. Planar cell polarity in the mammalian eye lens. Organogenesis 7:191–201. doi:10.4161/org.7.3.18421.

Take-uchi M, Clarke JDW, Wilson SW. 2003. Hedgehog signalling maintains the optic stalk-retinal interface through the regulation of Vax gene activity. Development 130:955–968. doi:10.1242/dev.00305.

Tanentzapf G, Tepass U. 2003. Interactions between the crumbs, lethal giant larvae and bazooka pathways in epithelial polarization. Nat. Cell Biol. 5:46–52. doi:10.1038/ncb896.

Taylor J, Abramova N, Charlton J, Adler PN. 1998. Van Gogh: A new Drosophila tissue polarity gene. Genetics 150:199–210.

Theisen H, Purcell J, Bennett M, Kansagara D, Syed A, Marsh JL. 1994. Dishevelled is required during wingless signaling to establish both cell polarity and cell identity. Development 120:347–360.

Thisse C, Thisse B. 2005. High Throughput Expression Analysis of ZF-Models Consortium Clones. ZFIN Direct Data Submiss.

Thisse C, Thisse B. 2008. High-resolution in situ hybridization to whole-mount zebrafish embryos. Nat. Protoc. 3:59–69. doi:10.1038/nprot.2007.514.

Usui T, Shima Y, Shimada Y, Hirano S, Burgess RW, Schwarz TL, Takeichi M, Uemura T. 1999. Flamingo, a seven-pass transmembrane cadherin, regulates planar cell polarity under the control of Frizzled. Cell 98:585–595. doi:10.1016/S0092-8674(00)80046-X.

VanderVorst K, Hatakeyama J, Berg A, Lee H, Carraway KL. 2018. Cellular and molecular mechanisms underlying planar cell polarity pathway contributions to cancer malignancy. Semin. Cell Dev. Biol. 81:78–87. doi:10.1016/j.semcdb.2017.09.026.

Veien ES, Rosenthal JS, Kruse-Bend RC, Chien C-B, Dorsky RI. 2008. Canonical Wnt signaling is required for the maintenance of dorsal retinal identity. Development 135:4101–4111. doi:10.1242/dev.027367.

Vijayaragavan K, Szabo E, Bossé M, Ramos-Mejia V, Moon RT, Bhatia M. 2009. Noncanonical Wnt Signaling Orchestrates Early Developmental Events toward Hematopoietic Cell Fate from Human Embryonic Stem Cells. Cell Stem Cell 4:248–262. doi:10.1016/j.stem.2008.12.011.

Villarroel CE, Villanueva-Mendoza C, Orozco L, Alcántara-Ortigoza MA, Jiménez DF, Ordaz JC, González-del Angel A. 2008. Molecular analysis of the PAX6 gene in Mexican patients with congenital aniridia: report of four novel mutations. Mol. Vis. 14:1650–1658.

Wada H, Iwasaki M, Sato T, Masai I, Nishiwaki Y, Tanaka H, Sato A, Nojima Y, Okamoto H. 2005. Dual roles of zygotic and maternal Scribble1 in neural migration and

convergent extension movements in zebrafish embryos. Development 132:2273–2285. doi:10.1242/dev.01810.

Wansleeben C, Feitsma H, Montcouquiol M, Kroon C, Cuppen E, Meijlink F. 2010. Planar cell polarity defects and defective Vangl2 trafficking in mutants for the COPII gene Sec24b. Development 137:1067–1073. doi:10.1242/dev.041434.

Westerfield M. 2000. The zebrafish book. A guide for the laboratory use of zebrafish (Danio rerio). 4th ed. Eugene: University of Oregon Press.

Westfall TA, Brimeyer R, Twedt J, Gladon J, Olberding A, Furutani-Seiki M, Slusarski DC. 2003. Wnt-5/pipetail functions in vertebrate axis formation as a negative regulator of Wnt/β-catenin activity. J. Cell Biol. 162:889–898. doi:10.1083/jcb.200303107.

Williamson KA, FitzPatrick DR. 2014. The genetic architecture of microphthalmia, anophthalmia and coloboma. Eur. J. Med. Genet. 57:369–380. doi:10.1016/j.ejmg.2014.05.002.

Winter CG, Wang B, Ballew A, Royou A, Karess R, Axelrod JD, Luo L. 2001. Drosophila Rho-associated kinase (Drok) links Frizzled-mediated planar cell polarity signaling to the actin cytoskeleton. Cell 105:81–91. doi:10.1016/S0092-8674(01)00298-7.

Witzel S, Zimyanin V, Carreira-barbosa F, Tada M, Heisenberg C. 2006. Wnt11 controls cell contact persistence by local accumulation of Frizzled 7 at the plasma membrane. J. Cell Biol. 175:791–802. doi:10.1083/jcb.200606017.

Woo K, Fraser SE. 1995. Order and coherence in the fate map of the zebrafish nervous system. Development 121:2595–2609.

Wu J, Roman AC, Carvajal-Gonzalez JM, Mlodzik M. 2013. Wg and Wnt4 provide long-range directional input to planar cell polarity orientation in Drosophila. Nat. Cell Biol. 15:1045–1055. doi:10.1038/ncb2806.

Xu Q, Wang Y, Dabdoub A, Smallwood PM, Williams J, Woods C, Kelley MW, Jiang L, Tasman W, Zhang K, et al. 2004. Vascular Development in the Retina and Inner Ear:

Control by Norrin and Frizzled-4, a High-Affinity Ligand-Receptor Pair. Cell 116:883–895. doi:10.1016/s0092-8674(04)00216-8.

Yamamoto H, Komekado H, Kikuchi A. 2006. Caveolin Is Necessary for Wnt-3a-Dependent Internalization of LRP6 and Accumulation of β-Catenin. Dev. Cell 11:213–223. doi:10.1016/j.devcel.2006.07.003.

Yamanaka H, Moriguchi T, Masuyama N, Kusakabe M, Hanafusa H, Takada R, Takada S, Nishida E. 2002. JNK functions in the non-canonical Wnt pathway to regulate convergent extension movements in vertebrates. EMBO Rep. 3:69–75. doi:10.1093/embo-reports/kvf008.

Yang CH, Axelrod JD, Simon MA. 2002. Regulation of Frizzled by Fat-like cadherins during planar polarity signaling in the Drosophila compound eye. Cell 108:675–688. doi:10.1016/S0092-8674(02)00658-X.

Yates LL, Papakrivopoulou J, Long DA, Goggolidou P, Connolly JO, Woolf AS, Dean CH. 2010. The planar cell polarity gene Vangl2 is required for mammalian kidney-branching morphogenesis and glomerular maturation. Hum. Mol. Genet. 19:4663–4676. doi:10.1093/hmg/ddq397.

Yates LL, Schnatwinkel C, Murdoch JN, Bogani D, Formstone CJ, Townsend S, Greenfield A, Niswander LA, Dean CH. 2010. The PCP genes Celsr1 and Vangl2 are required for normal lung branching morphogenesis. Hum. Mol. Genet. 19:2251–2267. doi:10.1093/hmg/ddq104.

Yin H, Copley CO, Goodrich L V., Deans MR. 2012. Comparison of phenotypes between different vangl2 mutants demonstrates dominant effects of the looptail mutation during hair cell development. PLoS One 7. doi:10.1371/journal.pone.0031988.

Yoon KH, Widen SA, Wilson MM, Hocking JC, Waskiewicz AJ. 2019. Visualization of the Superior Ocular Sulcus during Danio rerio Embryogenesis. J. Vis. Exp.:e59259. doi:10.3791/59259.

Zeidler MP, Perrimon N, Strutt DI. 1999. The four-jointed gene is required in the Drosophila

eye for ommatidial polarity specification. Curr. Biol. 9:1363–1372. doi:10.1016/S0960-9822(00)80081-0.

Zeke A, Misheva M, Reményi A, Bogoyevitch MA. 2016. JNK Signaling: Regulation and Functions Based on Complex Protein-Protein Partnerships. Microbiol. Mol. Biol. Rev. 80:793–835. doi:10.1128/mmbr.00043-14.

Zhao L, Saitsu H, Sun X, Shiota K, Ishibashi M. 2010. Sonic hedgehog is involved in formation of the ventral optic cup by limiting Bmp4 expression to the dorsal domain. Mech. Dev. 127:62–72. doi:10.1016/j.mod.2009.10.006.

Zuber ME, Gestri G, Viczian AS, Barsacchi G, Harris WA. 2003. Specification of the vertebrate eye by a network of eye field transcription factors. Development 130:5155–5167. doi:10.1242/dev.00723.

Appendix: Visualization of PCP during ocular development

7.1 Introduction

The experiments described in this work indicate a role for PCP in SOS closure, but do not indicate a mechanism by which PCP regulates this event. I attempted to develop a method to characterize the dynamics of PCP during eye development. Previous studies have used fluorescent-tagged *Drosophila* Pk as a readout of planar polarization (Ciruna et al. 2006). When cells become planar polarized, Pk complexes with Vangl on the anterior membrane, forming puncta when viewed fluorescently, and thus the presence of GFP puncta indicates that cells are planar polarized. It was hypothesized that PCP mediates migration of retinal precursors during evagination of the optic vesicle and formation of the optic cup. To test this hypothesis, GFP-Pk mRNA injection was used to examine the developing ocular tissue for puncta to identify cells that were planar polarization.

7.2 Results and Discussion

To investigate the presence of planar polarized cells during eye development, GFP-Pk was injected into WT embryos at the one-cell stage. The plasmid encoding GFP-Pk was obtained from the Ciruna lab at the University of Toronto. To confirm plasmid identity, the plasmid was sequenced and aligned with the *pk* sequence of *Drosophila*. After injection, embryos were examined with fluorescent stereomicroscope to confirm successful injection and expression of GFP-Pk mRNA. Embryos at the 5 somite stage (ss) showed strong whole-embryo GFP expression (**Figure 7.1**), indicating proper injection and successful expression of the injected mRNA. At 20 hpf, the optic cup was examined confocally for the presence of GFP-Pk puncta. Puncta are visible around proximal edge (lens apposing layer) of the optic cup both at the dorsal pole and in more ventral z-slices, indicating planar polarization of the presumptive RPE cells (**Figure 7.2**).

During invagination of the optic cup, cells from the lens-apposing layer migrate around the nasal and temporal sides of the optic cup to increase surface area of the neural retina (Heermann et al. 2015). The movement of lens averted cells to the lens facing surface of the optic cup is dependent on proper DV patterning as BMP signalling prevents epithelial flow (Heermann et al. 2015). Other mechanisms that regulate this movement of cells are unknown. Based on the presence of GFP-Pk puncta in the lens averted cells, it is possible

that planar polarization of cells in the optic cup regulates their morphogenic movements. If PCP mediates cellular movements during optic cup formation, inhibition of PCP would prevent proper ocular development. Because the SOS closes due to a filling-in mechanism rather than fusion of the lobes (Hocking et al. 2018), misregulation of epithelial flow into the dorsal optic cup could delay SOS closure.

Although these data suggest PCP involvement in optic cup formation, only preliminary experiments have been conducted. GFP-Pk embryos have not been examined at time points other than 20 hpf. Examination during eye field specification or early evagination of the optic vesicle would indicate whether PCP is involved in the initial lateral movement of the eye field cells. Further, examination of the SOS in lateral view during closure would indicate whether local PCP is involved in cell shape changes that fill in the sulcus or migration of cells into the SOS. Time lapse imaging of GFP-Pk dynamics during eye development would give further insight into the special and temporal activity of PCP.

A challenge experienced with this experiment is reduction in fluorescence intensity after 22 hpf. Embryos show minimal GFP signal at 22 hpf, and fluorescence is quickly lost subsequently due to degradation of mRNA. This drawback prevented attempts at examining GFP-Pk around the open SOS at 22 hpf to determine if localized PCP regulates filling of the SOS. Injection of mRNA at the 16-cell stage would delay degradation of mRNA by a couple hours and may allow examination during SOS closure. However, this design would result in mosaic expression, which would give an incomplete picture of planar polarized cells.

7.3 Figures

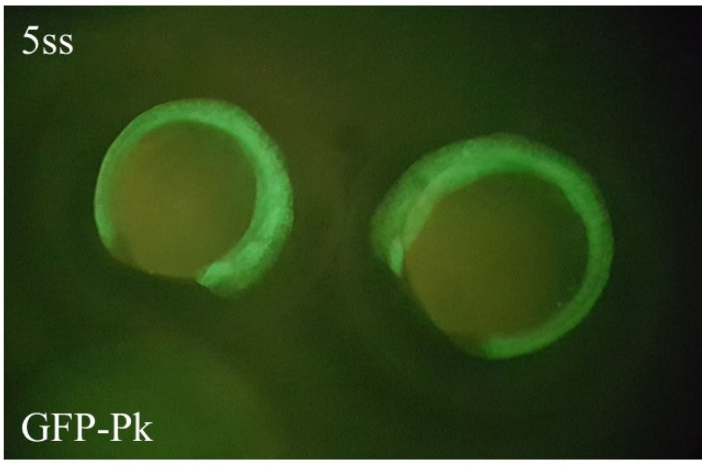

Figure 7.1. GFP-Pk mRNA injection in WT embryos shows whole embryo expression at the 5ss. WT embryos were injected with 100 pg of GFP-Pk mRNA at the one-cell stage, then examined under a fluorescent stereoscope to confirm GFP-Pk expression.

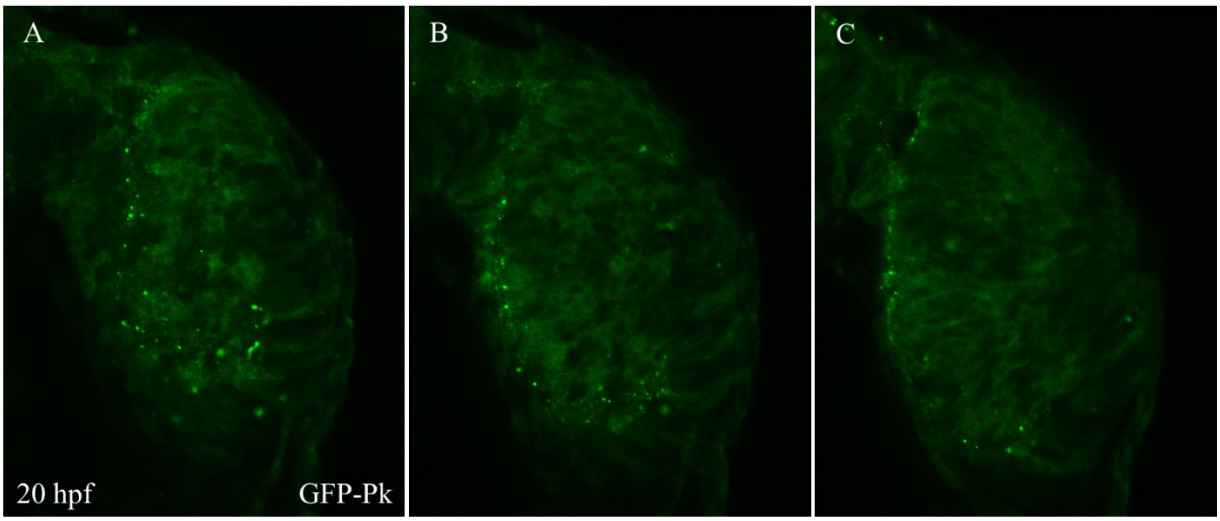

Figure 7.2. GFP-Pk mRNA injection in WT embryos shows Pk puncta along the lens averted layer in the early optic cup. WT embryos were injected with 100 pg of GFP-Pk mRNA at the one-cell stage. Embryos were fixed at 20 hpf, washed into 70% glycerol, deyolked, and mounted in dorsal view for confocal examination. Images show three z-slices of the optic cup in dorsal view. A represents the most dorsal slice, and B and C are progressively ventral slices.